Doctoral Dissertation
Doctoral Program in Civil Engineering (35th Cycle)

The fire resistance of curvilinear masonry structures

By

Nicholas Sergio Burello

******

Supervisors:

Prof. B.M. Chiaia
Prof. A. P. Fantilli

Doctoral Examination Committee:

Prof. K. Nemati, Referee, State University of New York
Prof. T. Nishiwaki , Referee, Tohoku University

Politecnico di Torino
2023

Declaration

I hereby declare that, the contents and organization of this dissertation constitute my own original work and do not compromise in any way the rights of third parties, including those relating to the security of personal data.

Nicholas Sergio Burello

2023

I would like to dedicate this thesis to my father because he has been able to be the point of reference for all these years, despite the life's adversities.

Acknowledgment

Abstract

Arches, vaults and domes constitute a milestone for the transition from the older method of construction, using masonry, to the modern one, based on concrete and steel. The arched masonry structures are still recurring within our architectural heritage, ranging from historic constructions to common residential buildings.

Although high efforts have been employed to assess the structural response, with and without reinforcements, the issue of fire resistance has remained unaddressed for masonry curvilinear structures. In particular, the assessment by direct tests is not feasible, exhaustive experimental campaigns have never been undertaken, and simplified tabulated methods are not applicable.

In the event of fire, a certain level of performance is required to meet the new needs, and the new use of these buildings. Thus, structural engineers and architects are often called to assess arches and vaults, even if no numerical model has been developed so far.

Hence, the aim of this thesis is to give a contribution to the assessment of masonry arched structures subjected to elevated temperatures under the most common fire scenario, in addition to the self-weight and external loads. It consists of full-scale experimental analyses conducted on masonry barrel vaults subjected to fire and numerical models as well. More specifically, with the aim of providing a practical tool for existing curvilinear masonry structures under fire, a simplified numerical method is firstly introduced. It is based on the well-known Heyman's Safe Theorem combined with the residual cross-section method, currently used for walls and columns.

Furthermore, an advanced numerical model have been also developed and presented in this thesis. It is able to take into account the actual degradation of the material and the thermal expansion by means of the Colonnetti's Theory of the elastic coactions.

Both the models have been validated by the comparison of the predicted numerical results and those experimentally measured with the tests.

Finally, the simplified model has been applied to assess the fire resistance of an historic structure, extending the applicability to cross-vaults reinforced with concrete shell. The calculations have been performed according to the Italian code rules and the recommendations of the Italian fire brigade. Results shown that, from a practical point of view, only a low level of knowledge can be sufficient to correctly assess the masonry existing structures.

Contents

List of Figures

List of Tables

Chapter 1

Introduction

1.1 Background

Among the most recurring structures in our architectural heritage, pyramids, churches, cathedrals, castles and palaces are certainly important. Even if not considering only symbolic structures, most of the historical existing constructions have in common that they are made of masonry.

Natural stone, brick or marble blocks, often stacked with mortars of various types, are the most commonly used materials for structural purposes in antiquity. Until the advent of reinforced concrete and steel, architects and master builders had usually chosen masonry (and timber). The reasons certainly include the natural availability, the overall satisfactory mechanical, acoustic and thermal properties, as well as the high durability of the constituent materials. In fact, despite the slow deterioration of materials, the actions of wind and temperature, as well as the damage caused by applied loads, masonry structures still stand out among the existing structures.

However, during the decades many of the existing structures have collapsed under the action of exceptional loads, such as fires (and earthquakes). Hence, to ensure that existing structures are suitable for new purposes, studies on one of the oldest building technologies, as well as on the materials used, have become one of the most complex tasks for engineers and architects.

Among the most recurring problems, especially in arched structures, there is certainly lack of knowledge on the actual geometry and on the material properties, as well as on numerical tools dedicated to analyzing these ancient building systems under accidental loads. Furthermore, limited resources are dedicated to non-destructive in-situ experimental investigations and only few full-scale laboratory tests have been performed in the last decades. To exacerbate the situation, the mechanical characterization of materials is often difficult to perform, in addition to being very expensive. Moreover, due to the wide variety of workmanship and natural materials used, a large variability of mechanical performances is often observed also under ordinary environmental conditions. As result, the current structural codes are often not applicable to a various range of existing structures as masonry arches, vaults and domes, despite a certain level of fire performance is still required by other regulations.

As shown in following chapters, in the international literature the topic of curvilinear masonry structures under fire action has remained almost unaddressed so far, and current regulations do not even consider them.

1.2 Literature review

1.2.1 Fire performance requirements

Due to the wide use of these structures in Europe, much of the work in this thesis has been developed with respect to the current standards, namely the Eurocode 6 1-2 [1] "*Design of masonry structures. General rules - Structural fire design*".

In the event of a fire, all constructions must contain the generation and spread of fire and combustion smoke, making it possible for occupants to evacuate and for firefighting teams to intervene. Fire performance requirements are some of the fire protection measures to be pursued in order to ensure an adequate level of safety and should be guaranteed by each structure under the risk of fire exposure. Generally, the performances required to masonry structural members under fire action concerns the mechanical resistance (indicated by the symbol R), the integrity (E) and the thermal insulation (I). These criteria are expressed in minutes and are satisfied when the structures guarantees the following principles:

- R: load-bearing function is maintained throughout the required time of fire exposure;

- *E*: the passage of flames and hot gases through the member is avoided. Namely, the separating function is satisfied if it is not possible to cause the ignition of a cotton pad, the penetration of a gap gauge or resulting in sustained flames;
- *I*: mean temperature of the unexposed face does not rise by more than 140 ℃, and the maximum temperature rise at any point of that surface does not exceed 180 ℃.

For instance, not load-bearing walls must satisfy the *EI* requirement (membrane that performs the separating function), while the *REI* is required for membrane fulfilling the criterion of the separating and load-bearing functions. In some cases, it is also necessary to comply with an impact resistance requirement [2], also known as criterion *M*.

1.2.2 Fire resistance assessment methods

The current structural code (Eurocode 6 Part 1-2 [1]) describes the general rules for design in case of fire and provides precise guidance on the requirements for masonry. It recognizes different methods for evaluating the fire resistance of masonry, which can be summarized as follows:
- direct testing the structure (Annex A)
- tabulated data based on extensive experimental campaigns (Annex B)
- simplified calculation method (Annex C)
- guidelines for the development of advanced calculation models (Annex D)

Obviously, when dealing with existing historical structures, the assessment of fire resistance by means of direct tests on is inconceivable. Furthermore, arched structures such as vaults and domes are characterized by unique geometric and material properties. Thus, the direct testing remains a procedure generally applicable only for new modular construction technologies (generally walls), for which a direct certification is undoubtedly one of the most effective methods.

1.2.2.1 Tabulated fire resistance

As an alternative to design by calculation, the tabulated method was introduced as a result of extensive experimental campaigns carried out to assess the fire resistance of masonry walls, both in the case of separation-only and load-bearing functions. This method is contained in the Annex B of Eurocode 6 Part 1-2 [1], and is based on the use of tables. Through them, having a basic level of knowledge of the masonry, it is possible to directly estimate the time for which the structural

element is able to meet the requirements. The use of tables is undoubtedly the quickest approach to assess the fire resistance, but it can be done when one of the following materials is used:

- Clay masonry
- Calcium silicate masonry
- Dense and lightweight aggregate concrete masonry
- Autoclaved aerated concrete masonry
- Manufactured stone masonry

Depending on the required criteria (*R, EI, REI, REI-M*), type of masonry, function, finish and joint thickness, each table provides the minimum thickness of the masonry that ensures the required level of safety (namely to withstand to fire action for a limited period of exposure). For instance, according to Table 1, the minimum wall thickness to guarantee a fire resistance *REI* of 90 minutes is 100 mm in the case of a single-leaf clay masonry loadbearing wall made with units having a mean compressive strength $5 \leq f_b \leq 75$ MPa, general purpose mortar and a gross density $\rho = 1000 \div 2000$ kg/m^3 ([1]).

The application of this approach is severely limited due to the high degree of conservatism, which often may lead to do not meet requirements, in addition to the scope of applicability which is limited to vertical structures that comply with predetermined geometric and material conditions.

Table 1: Excerpt from Eurocode 6 1-2 [1]: Minimum thickness of separating loadbearing single-leaf walls (Criteria REI) made with clay units for fire resistance classifications.

Row No.	Material properties: unit strength fb [MPa] gross density [kg/m³] combined thickness *ct* % of wall thickness	Minimum wall thickness (mm) for fire resistance classification REI for time (minutes)						
		30	45	60	90	120	180	240
1S	Group 1S units							
1S.1	$5 \leq f_b \leq 75$ general purpose mortar or $5 \leq f_b \leq 50$ thin layer mortar $1000 \leq \rho \leq 2000$							
1S.1.1 1S.1.2	$\alpha \leq 1.0$	90 (70/90)	90 (70/90)	90 (70/90)	100 (70/90)	100/140 (90/140)	170/190 (110/140)	170/190 (170/190)
1S.1.3 1S.1.4	$\alpha \leq 0.6$					100/140 (100/140)	170 (110/140)	170 (140/170)

1.2.2.2 Simplified calculation method

The design by calculation is the alternative to either direct tests or tabulated methods, to numerically obtain R. Two approaches are permitted: the simplified or the advanced calculation methods, and the guidelines of these approaches are respectively contained in Annexes C and D [1].

The simplified calculation method is actually the only numerical method that allows a direct assessment of fire resistance R, for which more conservative assumptions must be made. It is applicable to vertical masonry members exposed, on one or more sides, to fire action. This approach is based on the method of reduced cross-sections, and the verification is conducted on one or more sections of masonry element. For a given period of fire exposure, the vertical loadbearing capacity is verified when the following inequality is satisfied:

$$N_{Ed} \leq N_{Rd,fi(\theta)} \tag{1}$$

where:

- N_{Ed} = design value of normal stress calculated by combining acting loads under room temperature (also known as cold condition) according to the exceptional combination [4];
- $N_{Rd,fi(\theta)}$ = design value of normal resistant stress, calculated as a function of the reached temperature and the properties of the material itself, at a given period of fire exposure (subscript "fi").

The calculation of $N_{Rd,fi(\theta)}$ shall consider the degradation of the material due to the fire exposure. The level of degradation is determined by defining the temperature distributions within the masonry, in order to identify three different zones within the cross-section (see Fig.1). The three zones are distinguished on base of preestablished temperature limit values (namely θ_1 and θ_2). According to these temperatures, the ineffective (A_{ineff}), damaged (A_{red}) and residual zones (A_{res}) are identified, as depicted in Fig. 1b. The limit temperatures θ_1 and θ_2 are themselves depending on the type of masonry and, as shown in Table 1, in the case of masonry made with clay units and general purpose mortar, they can be assumed $\theta_1 = 100°C$ and $\theta_2 = 600 °C$. For each type of masonry, a reductive factor, c, obtained from stress-strain tests at elevated temperature shall also be defined. As shown in Fig.1c, c is used to characterize the compressive strength in the damaged zone as $f_{d\theta2} = f_{d\theta1} \times c$, where $f_{d\theta1}$ is the design value of the compressive strength (i.e., f_m) measured in cold condition and assumed in within the residual cross-section (A_{res}).

In this way, A_{ineff} (i.e., where $T > \theta_2$) provides no contribution to the load-bearing capacity of the structure, whereas A_{red} (i.e., where $\theta_1 < T < \theta_2$) is characterized by the reduced strength $f_{d\theta2}$, and A_{res} is characterized by the so-called cold strength $f_{d\theta1}$.

Table 2: Values of constant c, temperature θ_1 and θ_2 by masonry material. [1]

Masonry units and mortar (surface unprotected)	Value of constant c	Temperature [°C]	
		θ_2	θ_1
Clay units with general purpose mortar	c_{cl}	600	100
Calcium silicate units with thin layer mortar	c_{cs}	500	100
Lightweight concrete units (pumice) with general purpose mortar	c_{la}	400	100
Dense aggregate units with general purpose mortar	c_{da}	500	100
Autoclaved aerated units with thin layer mortar	c_{aac}	700	200

(a)   (b)   (c)
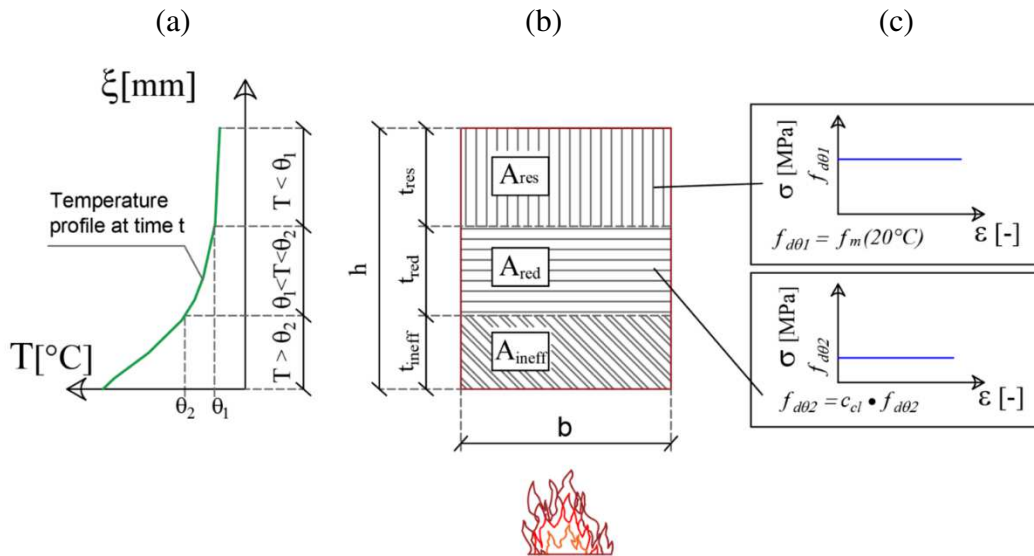
Figure 1 - (a) The temperature profile at time *t* through (b) the cross-section in which different resisting zones are defined (Please note: res = residual; red = reduced; ineff = ineffective); (c) Rigid-plastic constitutive laws adopted in residual cold-strength zone (t_{res}) and reduced-strength zones (t_{red})

Referring to Fig.1, the load-bearing capacity of a generic cross-section $b \times h$, after a period t of fire exposure, can be calculated according to Eq.2:

$$N_{Rd,fi(\theta)} = \varphi(A_{res} \cdot f_{d\theta1} + A_{red} \cdot f_{d\theta2})$$ (2)

where:

φ = capacity reduction factor in the middle of the wall, according to Eurocode 6 1-1 [3].

By applying this approach, Eurocode 6 1-2 [1] also requires: "*The temperature distribution across a masonry section and the temperature at which the masonry becomes ineffective, as a function of the time of fire exposure, should be obtained from the results of tests or from a data base of test results. In the absence of test results or a database the Figures C.3(a) to (d) may be used.*"

For completeness of information, the temperature profiles related to the case of brick masonry structure made with generic purpose mortar is reported in Fig. 2. As shown, it is possible to use temperature profiles at t = 30, 60, 90 and 120 min and, as a consequence, determine ineffective and damaged thicknesses within the masonry. ξ is the coordinate measured from the exposed surface.
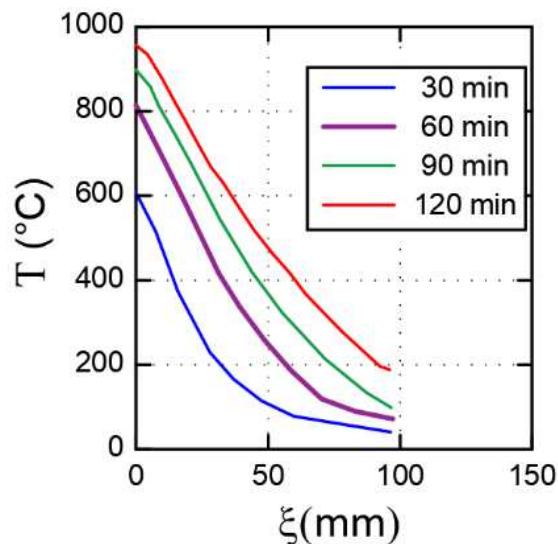
Figure 2 - Excerpt redrawn from [1]: Temperature distributions in the case of "clay units with general purpose".

1.2.2.3 Advanced calculation method

Eurocode 6 1-2 [1] provides the basis for a more rigorous calculation, in order to obtain a more accurate structural response of a generic masonry member subject to fire. In fact, this calculation method can be adopted to analyze, in addition to walls and columns, masonry arches and vaults. As prescribed, an advanced assessment of the fire resistance should include the so-called thermal and mechanical response models.

The thermal response model should be based on the theory of heat transfer [4] and shall provide the temperature distributions as a function of a predetermined heating curves [5-6]. A natural fire model [5, 7] is also allowed as alternative. Those models are able to take into account how the environment, the density of combustible materials and the ventilation will affect the development of the fire. Furthermore, the thermal response model shall consider the temperature-dependent material properties, as shown in Fig.3a, where the behavior at different temperatures of density $\rho(T)$, thermal conductivity $\lambda_a(T)$, and specific heat $c_a(T)$ for clay masonry are illustrated.

Therefore, due to the increase in temperature and its distribution within the structures, the mechanical response model must consider the effects these phenomena entail. This is of particular importance in statically indeterminate structures, in which restrained thermal expansion induces non-negligible additional stresses. For this reason, it is necessary to know the thermal expansion $\varepsilon_T(T)$ which, in turn, is a parameter influenced by the temperature, as illustrated in Fig.3b.

Finally, as a consequence of the exposure to high temperatures, the mechanical response model shall be based on the assumptions of the theory of structural mechanic combined with the degradation of the mechanical properties (i.e., Young Modulus and compressive strength, as shown Fig.3c).

Thus, the annex D is dedicated to provide general guidelines for the development of numerical model for masonry structures under fire. Unfortunately, to date, computational models based on these guidelines have not yet been developed for the purpose of analyzing horizontal curved elements.

(a)

(b)   (c)
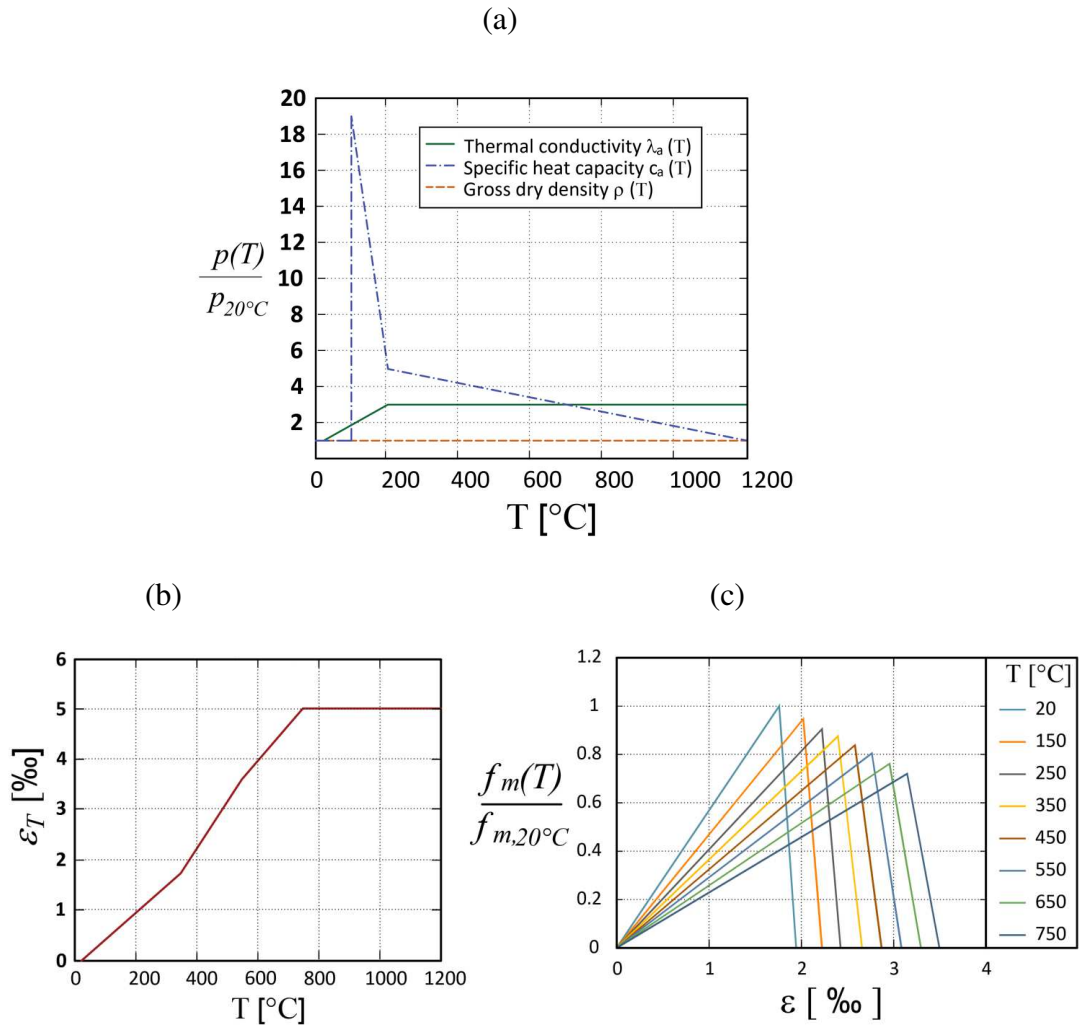
Figure 3 - Figures redrawn from [1]: clay units (group 1) with unit strength $12 \div 20$ N/mm² and with a density range of $900 \div 1\,200$ kg/ m³. Values of (a) temperature-dependent material properties; (b) thermal strain ε_T ; and (c) temperature-dependent stress-strain diagrams (i.e., normalized compressive strength).

1.2.3 Mechanical characterization of masonry

This section presents an overview of research activities conducted in the last decades on masonry exposed to high temperatures. All the research activities related to masonry are considered, including those focused on the local level (i.e., mechanical characterization) and on the structural level, either small-scale and/or full-scale experimental analyses.

It is worth noting that, in the case of references to third-party work or structural code recommendations, because of the nature of the experimental investigations conducted and described in this thesis, special attention is given to masonry made of clay units and cement-lime based mortar.

1.2.3.1 Mechanical characterization of masonry at room temperature

As previously stated, a variety of masonry types have been built over the centuries. In particular, various thickness of the mortar-joints, the irregular or squared shape of the blocks, as well as the nature of the materials has undergone significant changes depending on local resources and available technologies [8]. In all the cases, masonry is generally characterized by an overall good compressive strength, almost negligible, even if not null, tensile and shear strengths affected by the weak brick-mortar interface. Due to the scopes of this work, literature review of research studies carried out mostly for determining the compressive strength of masonry materials are taken into consideration.

From the design point of view, the mechanical characterization of newly built masonry under room temperature can be analytically determined by means of initial tests on its constituent materials. The tests are usually carried out for evaluating the flexural and compressive strengths of the mortar [9-11] and of the individual units [12,13]. According to the Eurocode 6 1-1 [3], the compressive strength of masonry can be calculated according to the following equation:

$$f_k = K \cdot f_{bl}^{\alpha} \cdot f_{mor}^{\beta} \tag{3}$$

where:

– f_k = characteristic compressive strength of the masonry;
– f_{bl} = normalized compressive strength of the unit in the direction of the load;
– f_{mor} = compressive strength of the mortar;
– K = reductive factor modified according to the type of units and of the thickness of the joint (e.g., $K = 0.55$ if clay units of Group 1 are used);
– $\alpha = 0.7$ and $\beta = 0.3$ in case of general purpose mortar.

In the absence of experimental analyzes [14-15] directly performed on assembled masonry samples with one row of stacked bricks (see Fig.4a), the Young's Modulus can be calculated according to eq.4.

$$E = K_E \cdot f_k \tag{4}$$

where:

– K_E = multiplication factor (where K_E = 1000 or determined according to National Annexes of the Eurocode 6 1-2 [1]).

In the last decades, these correlations were studied by several researchers [16-22], who focused on a better evaluation of α, β, K, and K_E on the base of local raw materials, and to propose new formulations based on experimental results of different types of masonry. Readers may also refer to [23], where an overview of prediction models for the mechanical behavior of unreinforced masonry with lime-based mortar is proposed. In general, it is possible to observe that these studies show a high variability of coefficients, depending on the raw materials, as well as on the size of the joints. This is particularly evident in the evaluation of the coefficient K_E, which can take values even much lower than those proposed by current standards [1] (for example, K_E = 85 in the case of masonry with mortar having low strengths [23]).

An important benchmark is the work conducted in 1981 by Page [25], who analyzed the failure mechanism and the compressive strength of masonry subjected to biaxial compression tests (see Fig.4c). The analyses showed that the masonry is characterized by distinct directional mechanical properties due to the brick-mortar interface, which constitutes a plane of weakness. As depicted Fig.4b, recent tests [26] considered the influence of the inclination of bed-joints with respect to the direction of uniaxial compression, in which a clear decrease in compressive strength of the unconfined masonry (up to 76% in the case of $\phi = 67.5°$) was observed.

Relevant research [27-31] was also conducted to determine the bond strength of the unit/mortar composite through direct tensile testing. Moreover, although the materials showed non-negligible tensile strengths, masonry is characterized by a tensile strength at the interface varying from 0.05 to 0.3 MPa, in the case of brick units and cement-lime based mortars.

(a)   (b)   (c)
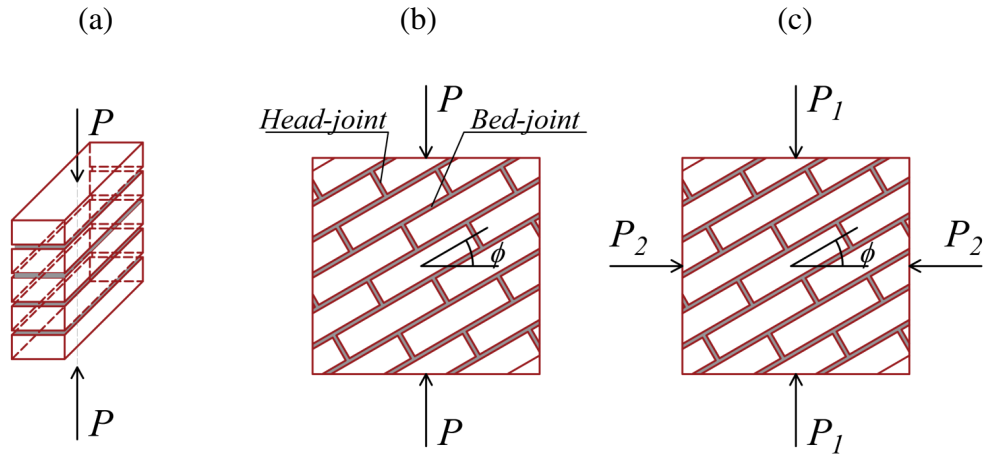
Figure 4 - Test setup for (a) uniaxial compression test with the application of load orthogonal to the bed-joints (on stacked bricks); (b) uniaxial [26] and (c) biaxial [25] compression tests with various inclinations with respect to the bed-joints (on small-scale masonry walls).

It is worth mentioning that, especially for certain types of analysis (e.g., in seismic conditions) the shear strength [32] of masonry composites plays an important role. Since it is out of the scope of this thesis, readers may refer to the studies [33, 34] for further information.

1.2.3.2   Mechanical characterization of masonry at elevated temperatures

 According to European standards [1], the analysis of main masonry structures under fire shall be performed assuming proper constitutive laws, characterised by the absence of tensile strength and a variable compressive strength, as depicted in Fig.3c. The variation factors of the compressive strength and of the deformability in the elastic stage, namely the Young's Modulus, must be defined as a function of the temperature.

In the last decades, a high level of effort was required for the study of the main materials used in masonry structures, such as clay, aerated-autoclaved concrete (AAC), light-weight concrete (LWC), and cement-lime based mortar.

In addition to the so-called "cold mechanical characterization" (CMC) at room temperature and humidity conditions, the aims of such research activities can be distinguished into two main groups: the so-called "hot mechanical charaicterization" (HMC) and the "residual mechanical characterization" (RMC).

The procedure to perform the HMC was similar to that followed for the analysis of concrete [35-36], when samples were heated in a furnace up to a predetermined temperature. Once the target temperatures were reached, the samples were subjected to the distructive test during which the compressive stress-strain curves up to collapse were measured.

Andreini et al. [37-38] minimized the temperature loss on the lateral surfaces (declared to be in average less then 5% from target temperature) by means of a mineral whool coating applied on each specimen. Thus, samples were placed into a muffle furnace and heated up to 100°C with a temperature ratio of 2.67°C/min, at which they where kept for 2 hours before to heat again up to the prescibed temperature (at a new temperature ratio of 1.1÷6.6 °C/min). Once reached a uniform temperature distribution (roughly an hold time of 2.5 h), the samples were extracted and inserted in a "thermally insulated thermos" made of AAC (which in turn was pre-heated at 200°C), ah shown in Fig.5. Then the specimens were tested under uniaxial compression.

A slightly different preparation was instead followed by Khaliq and Bashir [39]. In accordance with the Rilem test procedures [40], they applied a heating rate of 2°C/min up to the target temperature at which the furnace chamber was mainteined for 60 minutes in order to achieve the steady state (namely the thermal equilibrium). At the end of the hold time, specimens were taken out from the furnace and covered with a proper thermal jacket. Subsequently, mechanical tests were performed.

The results of these experiments are depicted in Fig.6a, where the compressive strengths are normalised with respect to that obtained in room conditions. Additional results obtained by testing hollow-clay bricks [41] and high-strength cement-based mortar [42], besides the current standard prescriptions [1], are also reported.

(a)   (b)

(c)
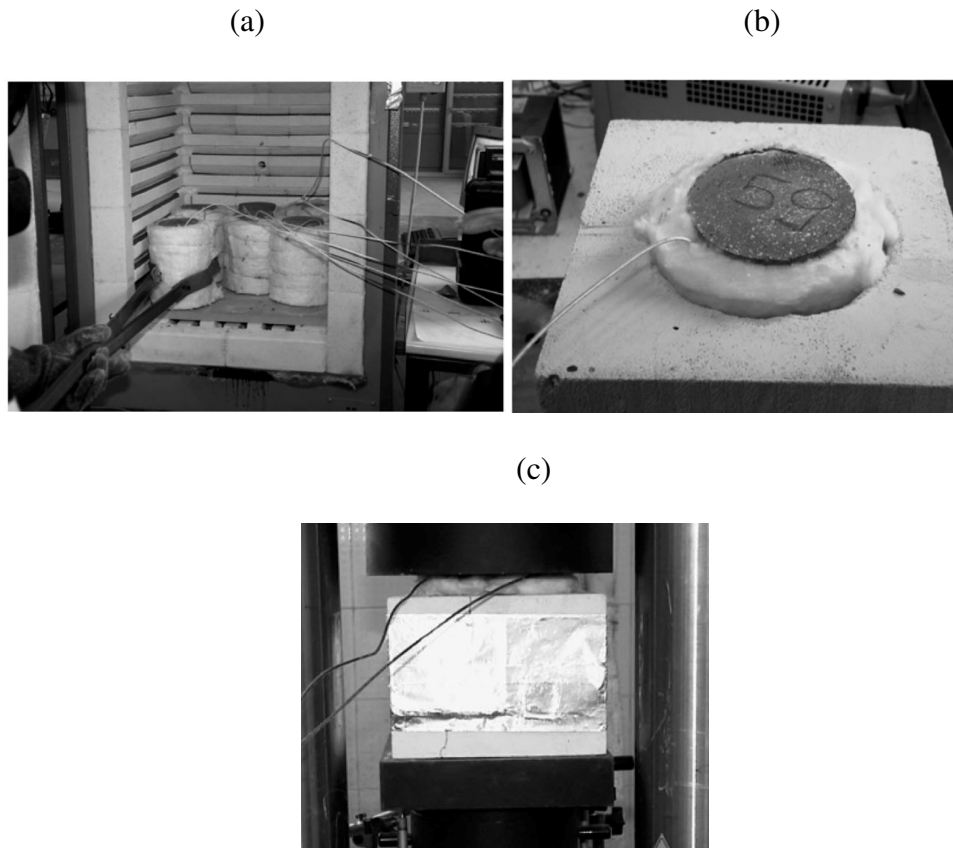
Figure 5 - Main phases of testing procedure for the HMC adopted from Andreini et al. [38]: (a) extraction from furnace after reaching the prescribed temperature; (b) insertion of the cylinder in the thermally insulated thermos made of AAC; (c) uniaxial compressive test at high temperatures.

In spite of HMC, where the specimen is directly tested once a predetermined temperature is reached (i.e., without theoretically loss of heat), in the case of RMC the specimen is subjected to destructive tests only after a cooling phase at the end of which the sample has came back to the room temperature. Also in this case, the followed heating schemes were sligthly different. In the studies currently available in literature, a heating rate of 1÷10 °C/min was applied to the specimens up to the desired temperature, at which they remained for a prefixed exposure time, with a range of 1÷2 hours, before to be subjected to the cooling phase. These tests were originally performed to evaluate the residual properties of the material, after being exposed to a certain range of temperatures. A further purpose of these studies [43]

was to compare the numerical response, by means of current available method, to the actual performance of masonry structures collapsed after the fire exposure.

(a)

(b)
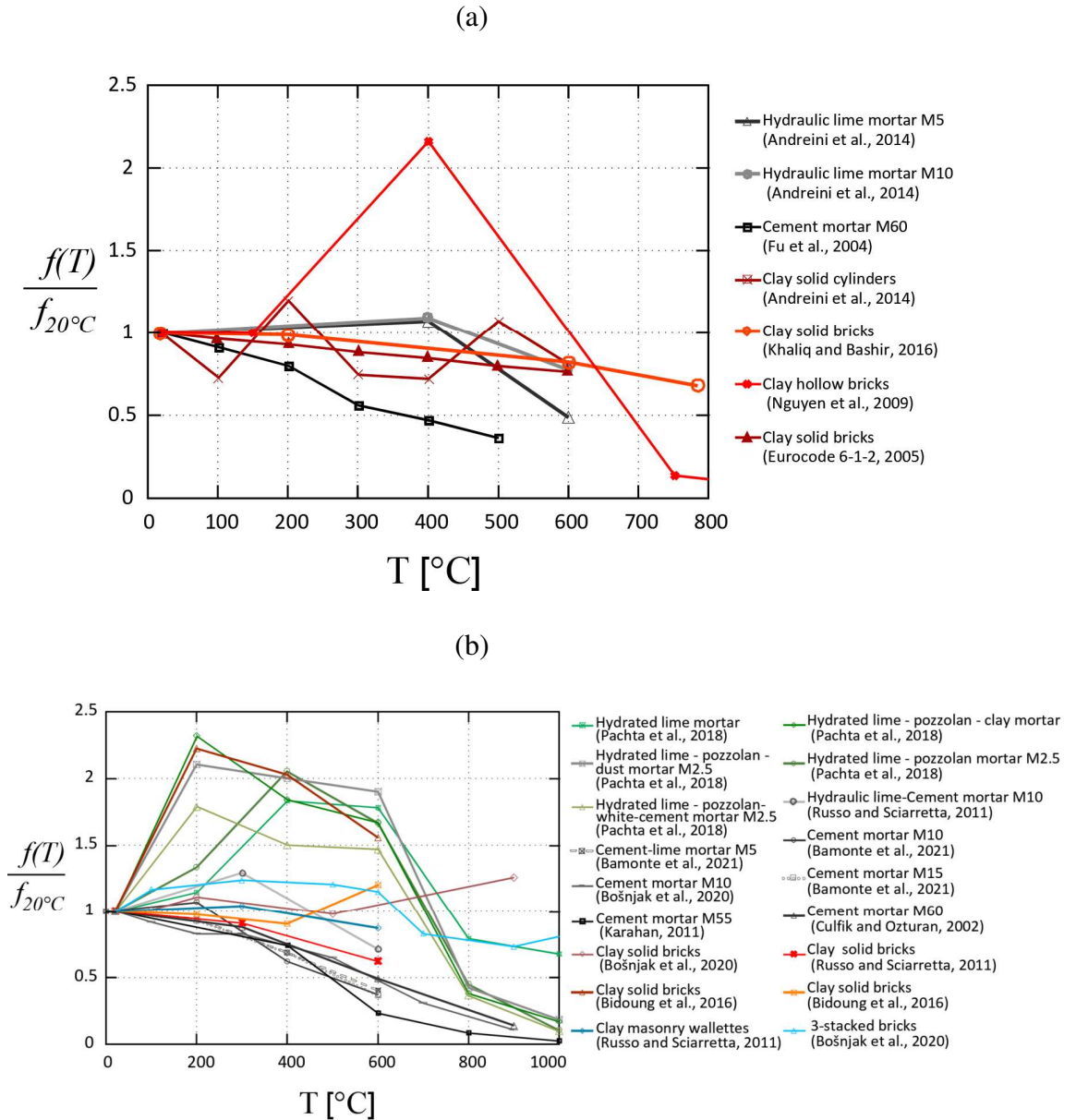
Figure 6 - Overview of mechanical characterization of clay masonry materials (a) under the fire exposure (HMC) and (b) after the cooling phase (RMC).

In Fig.6b the results of several studies are compiled; they were obtained from on clay units [44-46], lime-cement based mortars [47-50], small clay masonry walls [46] or prisms [45] constructed from clay units and general purpose mortars.

Similar analyses and reviewes of test results were previously proposed by Russo and Sciarretta [51] and by Daware and Naser [52]. It is worth mentioning Daware and Naser [53] applied the artificial neural networks to derive generalized temperature-dependent model for determining the compressive strength of masonry under high temperatures.

1.2.4 Fire investigations on masonry walls

Over the past 50 years, several research studies have been conducted on masonry structures at elevated temperature, with a general focus on masonry vertical structures made with modern constituent materials. These studies were generally limited to assess the stability of walls having only one side exposed to fire, because it represents the most common scenario for these structures.

From the structural point of view, because of vertical loadbearing structures are mainly subjected to axial loads, the compressive strength has always been considered as a key parameter for the evaluation of the residual load-bearing capacity when exposed to fire, even if shear and tensile strengths are also involved, especially when lateral forces are applied.

As previously stated, the mechanical characterization of masonry materials is based on a steady state test in which the sample is heated up to reaching a specified temperature, without any application of any load. Then the specimen is loaded at a constant rate and the stress-strain properties are measured.

In the cases of analyses at a structural level, a transient state test is generally adopted. Namely, the load is applied to the structure and kept constant for the whole duration of the fire exposure. During the test, special fire resistance devices are used, and the strains and temperatures are measured. The aim is to analyze the failure mechanisms of the walls, often affected by the so-called "thermal bowing" due to the temperature gradient within the masonry. As known, this phenomenon is affected by many intrinsic material properties which, in turn, are temperature-dependent and it is recurring in the case of clay masonry due to its low thermal conductivity.

Thus, the structure is characterized by an increasing bowing towards the fire, due to the greater thermal expansion of the exposed surface, which is also affected by the larger degradation of the mechanical properties than the unexposed surface.

Among the earliest studies carried out in this field, the work by Byrne [54] on the evaluation of the load-bearing capacity of a series of 14 walls, made of clay brick masonry under the effect of fire, is recognized. The impact of thermo-physical properties (i.e., thermal conductivity and thermal expansion) were the main focus of study, in which the thickness of the wall and the applied load changed. The current theoretical basis for the evaluation of fire behavior of masonry walls is also due to this work. In 1987, Lawrence and Gnanakrishnan [55] published the most extensive overview of experimental investigations, including the results of 146 walls under fire. In 1988, Cook [56] compared the deflections versus fire exposure time of steel, concrete and clay masonry structures. In this study, the non-linearity of the temperature distribution in the case of masonry structures was highlighted, recognizing the very low thermal conductivity as the main cause. Similarly, Shields et al [57] investigated the thermal and mechanical responses of masonry walls, made with calcium silicate walls. In 2001, Laverty et al. [58] analyzed the slenderness ratio of half-scale wall panels, with different height, subjected to different loads and fire. The research studies of Al Nahhas et al. [59] and Nguyen et al. [60,61] were devoted to the analyses of a more modern technology, focusing on masonry walls made of six-cell concrete blocks and of 6-hole burnt-clay bricks, respectively.

(a)   (b)
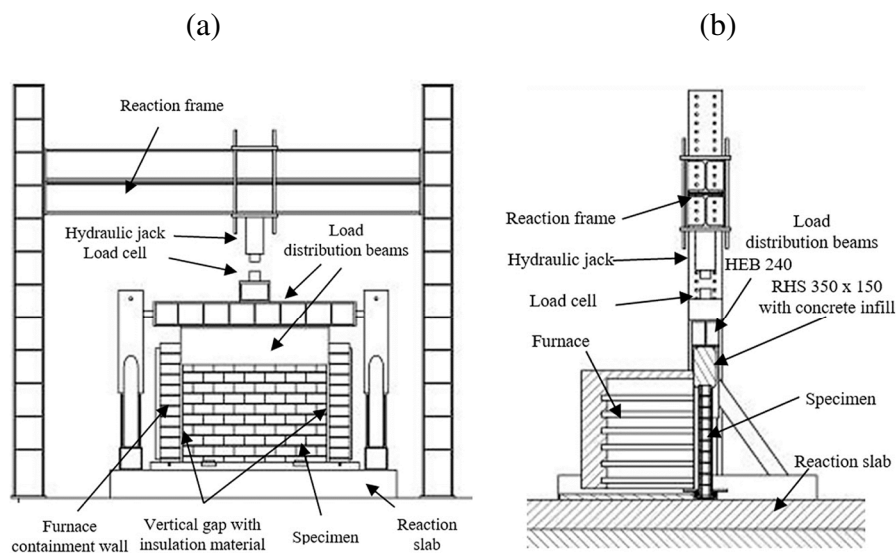
Figure 7 - Experimental setup from [65]: (a) Front view; (b) Longitudinal cut view

Also worth mentioning is the extensive experimental campaign conducted by Rene and Ayala [62], in which lightweight concrete blocks were used for a total of 21 walls. Further investigations were recently performed using several types of new hollow-clay blocks [63,64] and three-cell concrete blocks [65]. As a representative example of experimental fire test setup previously described, the scheme recently adopted by Lopes et al. [65] is reported in Fig.7. Instead, Fig.8 illustrates the sequence of the sudden collapse observed while testing one of the wall made with three-cell concrete blocks.
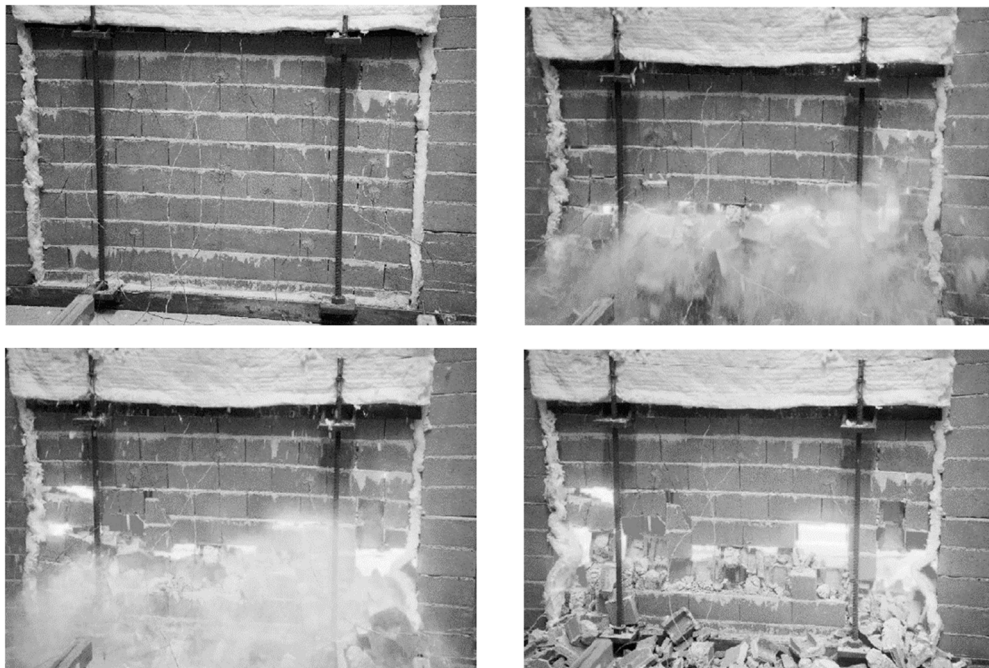
Figure 8 – Figures redrawn from [65, 72]: Sequence of pictures of the sudden collapse of a concrete wall exposed to fire on one side.

A growing body of knowledge is forming in the subject of under-fire masonry, year by year and "brick by brick" to such an extent that relevant studies [66] are also being undertaken for the evaluation of the thermal response of masonry walls coated with various types of fire protectives.

The failure mechanisms, temperature distributions, and displacements observed during the experimental tests have allowed the development and the validation of appropriate numerical models capable of predicting the thermal and mechanical response of such structures according to different loading conditions and constraints. Among these, it is worth mentioning the work carried out by Nadjai

et al. [67, 68], in which a novel calculation model called MasSET was validated both in the case of walls with a separating function (i.e., not axially loaded [56]) and in the case of load-bearing walls [55]. Fig.9a shows a typical fire test simulation of a masonry wall with one-side exposed, showing the direction of displacements and damaged areas. Andreini and Sassu [69] developed an analytical model based on the evaluation of a variable crushing domain depending on the period of exposure to fire, for masonry walls under combined compression and bending. As example, Fig.9b illustrates the failure domains for a 20 cm thick wall at various fire exposure periods. Many other works were based on the development of finite element models [70-73].
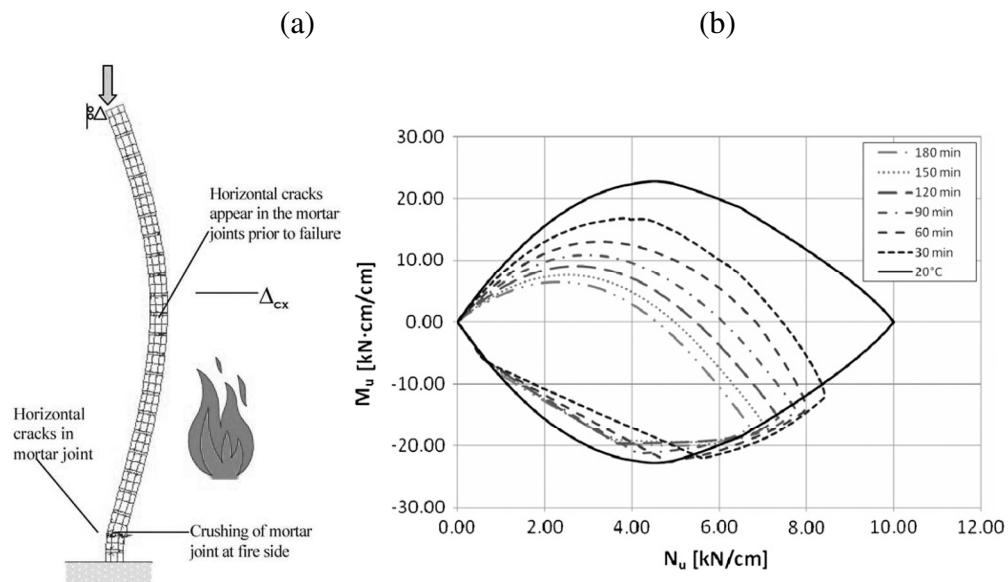
Figure 9 - Analysis of (a) clay masonry wall exposed to fire on one side through a dedicated numerical model (Figure modified from [67]); (b) interaction domains of a 20 cm thick wall for stated periods of exposure. [please note that ultimate normal stress and bending moment are expressed per unit of wall length] (Figure modified from [69]).

1.2.5 Research studies on masonry arches and vaults

Due to an increasing need to repair and consolidate existing structures, considerable efforts have also been made in recent decades in understanding the ancient ceiling construction technologies, such as that of masonry arched structures. From the point of view of computational models, considerable progress has been made, and nowadays there are several strategies available for the analysis of curvilinear

structures, also applicable the most complex geometries and materials. In fact, despite the term masonry is generally attributed to the composite material made by blocks (or units) and joints of various types, it tends to be characterized by negligible tensile strength, overall good compressive strength, and highly predictable failure planes (generally at the block-joint interface). These characteristics have enabled the development of several calculation strategies that are generally applicable to masonry construction. These strategies range from "old" simple graphical methods to complex systems of nonlinear equations, involving varying degrees of practicality and computational burden.

Regarding the arched structures, it all began back in the 17th century, when the compressed arch structure was associated with the hanging chain, whose shape can be likened to a catenary in tension under its own weight (Hooke, 1676).

As shown in Fig.10, this concept was used by Poleny to analyze the Dome's of St. Peter's in Rome in 1748. In the early 18th century, first approaches to evaluate the equilibrium by means of graphical schemes were introduced. These include those recognized to Coulomb and Mascheroni (see Fig. 11).
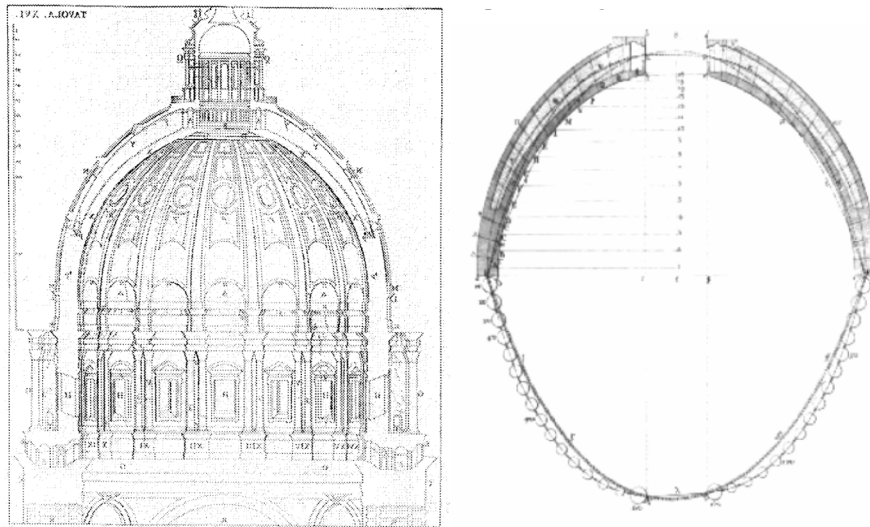
Figure 10 - Analysis of the Dome's of St. Peter's in Rome in 1748
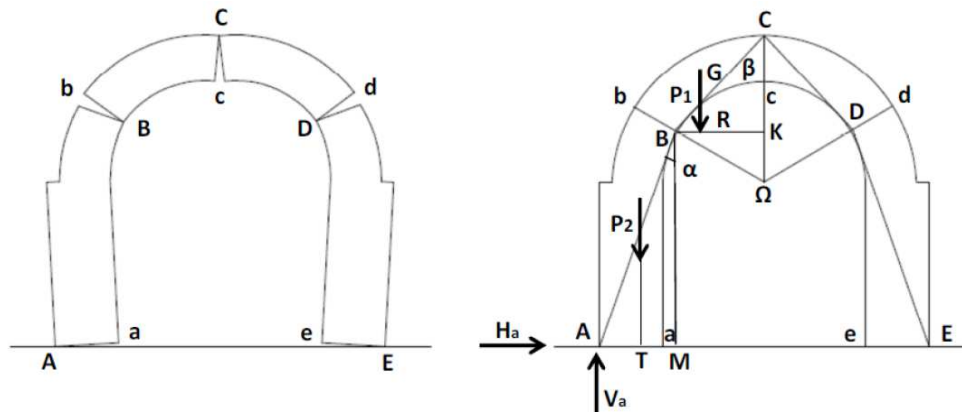
Figure 11 - Equilibrium by means of graphical scheme (Mascheroni, 1785).

With the development of the theory of elasticity, new approaches were developed and, between them, Mery provided the namesake method [74] for the construction and assessment of the line of thrust by means of a graphical procedure (see Fig.12), also called "middle third rule", which combined the traditional graphical approaches with the strength-elasticity concepts.

Later developments took place in the 20th century and, to this day, the new theory is ascribed to Heyman [75] through his renowned book "The Stone Skeleton", although mentions must at least be made of the previous excellent works of Kooharian [76] and Pippard [77-78]. Heyman himself recognized them as some of the *modern investigators of the voussoir arch*. The main finding [78] was the evaluation of the collapse, which may occur when a sufficient number of hinges are formed to give a mechanism, as shown in Fig.13.

On the other hand, Heyman [75] proposed to apply plasticity theorems to masonry structures, assuming an infinite compressive strength of masonry, while tensile strength is null, and considering sliding between blocks to be impossible. These conclusions were drawn following several observations. Namely, despite the stone itself may have some tensile strength, the joints will not and, as a consequence, tensile forces cannot be transmitted from block to block.

Furthermore, due to the general low stress levels in these structures, the compressive strength may be assumed infinite for the purposes of calculation.
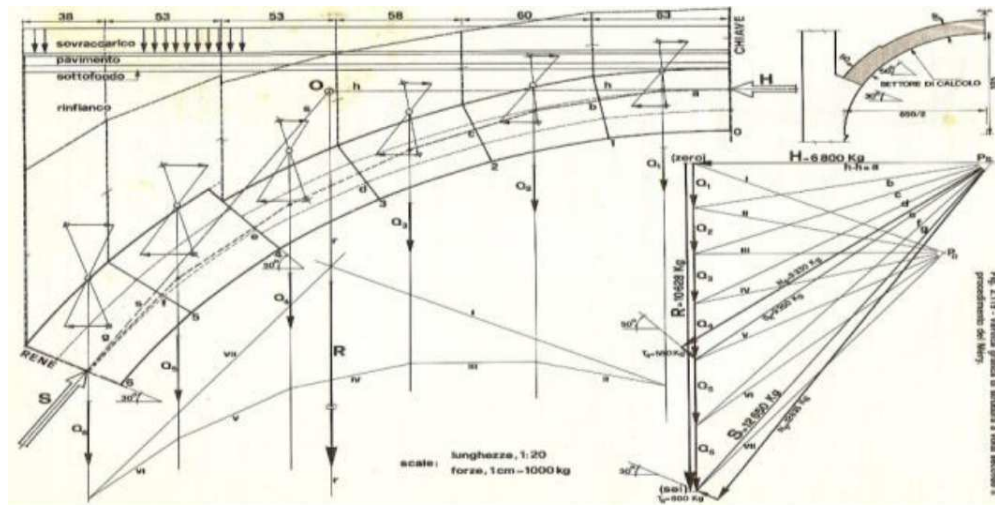
Figure 12 - Funicular polygon for the determination of internal forces. Application of the Mery's Method for the construction of the thrust line with the middle third rule.
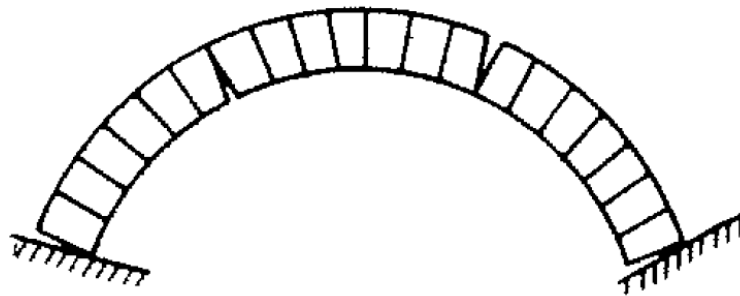
Figure 13 - Collapse mechanism of a voussoir arch [77]: four-hinges mechanism

Hence, due to the assumption of sliding between stones does not occur, the "hinging" at the free edge, previously proposed by Coulomb, is the only possible failure mechanism. Finally, the Heyman's Safe Theorem [75] states: "*If a line of thrust can be found which is in equilibrium with the external loads and which lies wholly within the masonry, then the structure is safe*".

In addition to the historical approaches mainly based on graphical solutions [79], the scientific community has put a lot of effort to the computational analysis of masonry structures in the past 50 years. Thus, based on Heyman's assumptions several limit-analysis methods were developed in the last decades, based on either

the kinematic or static theorem, and with application to both 2D [80-81] and 3D [82-83] structures. The latter are still used so far due to the reliability of the results obtained with the minimum computational burden and data requirement. Some studies [84] were also conducted to examine the limit of the scope of applicability of the Heyman's hypotheses.

As an alternative to limit analysis, as stated by Tralli et al. [85], the failure of masonry structures can also be investigated through an incremental-iterative analysis, generally performed through Finite Element Method. One of the main advantages is given by the additional information provided about displacements and post-peak response, whereas the only ultimate load for the predetermined failure mechanism is generally obtained if a thrust network method (TNM) is considered. In this approach, a series of load steps are applied to the structure and, for each of them, the structural response is evaluated [86,87] through an iterative calculation considering the geometric and mechanical non-linearities of masonry. These models can be applied to both nonlinear static analysis, namely the so-called pushover analysis generally used to evaluate the seismic response, and nonlinear dynamic analyses, in which the structure is subjected to time-dependent phenomena.

It must be highlighted the importance of taking into account a proper geometrical discretization of the structure [87-89], its actual imperfections and existing crack pattern, besides the effect of friction between blocks, and of the contribution of the infill [90] for a more refined analysis.

With the time, different approaches and scales of representation of the material properties have been proposed. As deeply reviewed by D'Altri et al. [91], four modelling strategies can generally be adopted for the analysis of masonry structures: geometry-based models, continuum models, block-based models, and microelement models.

Regardless of the type of modelling and type of analysis performed, the formulation of such a large number of computational methods and their validations has been enabled by a high number of experimental investigations conducted worldwide, in which full-scale or reduced-scale masonry curved shells were loaded until failure. Among them, masonry arches and barrel vaults [92-95], cross vaults [96-98], spherical [99] and pavilion domes [100] represent the most recurring structural schemes. Fig.14 illustrates an example of the typical prototypes used for the experimental investigations of full-scale curvilinear masonry structures.

(a)

(b)

(c)   (d)
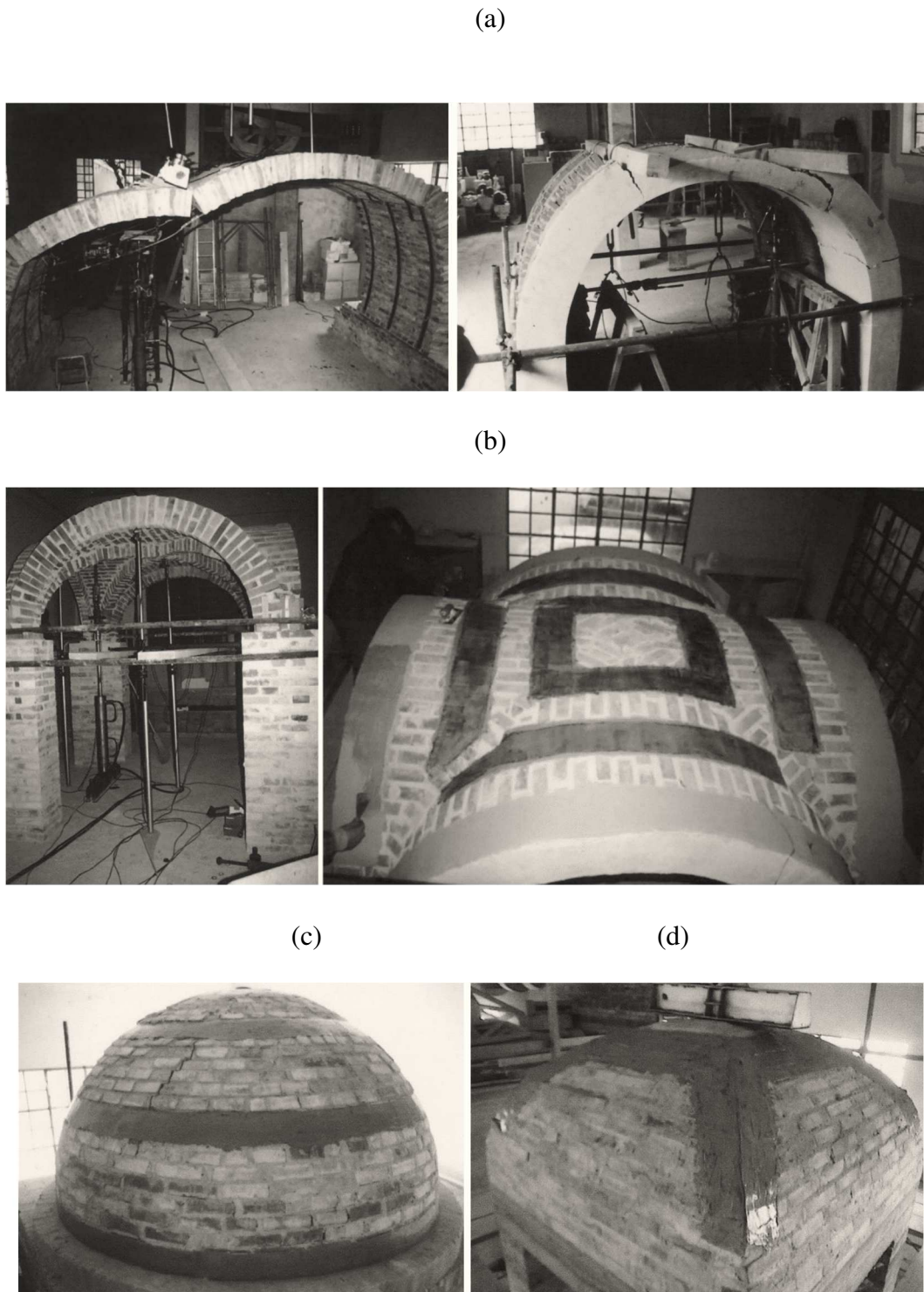
Figure 14 - Prototypes of different arched structures (a) barrel vaults, (b) cross-vault, (c) spherical vault and (d) pavilion vault. (Figures modified from [101])

These images are taken from the study of Foraboschi [101], who overviewed one of the most extensive experimental campaign, with more than 50 investigations on arches, vaults and domes [102-107].

Despite many other studies followed in the last two decades, almost all experimental investigations are nowadays devoted to the analysis of the actual structural responses with or without various strengthening composites made with fiber reinforced polymers - FRP [101, 108-112], carbon fiber-reinforced polymer - CFRP [113-116], glass fiber-reinforced cementitious matrix – GFRCM [117-118], Steel Fiber Reinforced Mortar - SFRM [119-121], Fabric-Reinforced Cementitious Matrix – FRCM [122-123]. Due the results of these studies, the use of non-corrosive composites is gradually replacing traditional techniques as those based on steel reinforced shotcrete for the strengthening of masonry structures. In fact, experimental evidences showed an increase of ultimate displacement (i.e., ductility) and of loadbearing capacity of the structure when these strengthening techniques are used. A failure load also 15 times higher than that achieved in case of unreinforced masonry can be observed [123].

It should be noted that some research studies were also carried out to understand the behavior of curved masonry structures undergoing differential settlements [124-126] or subjected to blast loads [127-129].

1.3 Objectives.

Although arches, vaults, and domes are considered outdated construction technologies in the field of masonry structures, they continue to play a significant role in our architectural heritage, particularly in European countries.

An interesting survey [130] carried out in the end of 20th century showed that 40% of existing bridges of the European railway network are made of masonry arched structures. Moreover, unreinforced masonry constructions account for 62.2% of the total inventory in Italy, as reported by Frankie e al. [131].

Engineers and architects are often called to assess these structures under various types of action. As in new construction, a certain level of safety and load-bearing capacity must be guaranteed also for curvilinear masonry structures under fire scenario [132-133]. As highlighted in the previous sections, the evaluation by direct testing is not feasible, extensive experimental campaigns have never been undertaken, and conventional methods are not applicable. Thus, the evaluation of

the fire resistance R must be ensured by design through calculation, even if no numerical model has been developed so far.

Based on the aforementioned drawbacks, two main objectives have been set on behalf of this thesis.

First of all, the thesis lays the foundations for the creation of databases relating to all the experimental tests conducted in Italy, including those in collaboration with or by third parties, in the last ten years. In these tests, concentrated and distributed loads, insulated and uninsulated masonry vaults were analyzed.

The second goal is to introduce new computational tools to analyze this specific scenario, which has remained unresolved for many years. Thus, the experimental results are used to validate two new numerical models herein proposed. In fact, a simplified calculation model, for practical use in the professional world, and an advanced calculation model, for more rigorous analyses, are introduced.

1.4 Research significance

Different empirical, graphical, and numerical models were developed in the last decades to analyze the behavior of masonry arches and vaults. Most of these models were carried out to predict the behavior of curvilinear structures under static and dynamic loads, especially in historical constructions. Studies on the performance under fire scenario of both masonry vaults and arches are very scarce in the technical literatures. The author believes that this detailed study, dealing with the introduction of simplified and rigorous numerical models, is carried out for the first time and will be very useful to predict the structural behavior under extreme loading of our architectural heritage.

1.5 Summary of the chapters

In the following chapters, the issue of "masonry vaults under fire" is analysed according to the following scheme.

In chapter 2, all experimental analyses are described in detail, starting from those conducted by the author and those carried out by third parties, to follow. All measured experimental data are illustrated and individually discussed.

In chapter 3, the simplified calculation model, based on the well-known Heyman's Safe Theorem combined with the reduced section method, is described. The outcomes of a masonry arch tested under monotonic load are used to validate prediction in absence of fire. And therefore, the results obtained from the experimental tests, reported in chapter 2, are used to validate the calculation model in the event of fire.

In chapter 4, the new advanced calculation model is introduced. Its capability of accounting the thermal response, the mechanical degradation, and the restrained thermal expansion of statically indeterminate arched structure, is described step by step. The model is finally used to evaluate the first tests conducted by the author.

In chapter 5 a real case study is assessed. They concern a church undergoing a change of use for which a certain fire resistance is required by law. The simplified calculation model is used to analyse the largest cross-vault present there. To achieve the aim, the scope of applicability of the model is extended to different geometric configuration of the vault.

In Chapter 6, main findings and recommendations for future work are outlined.

Chapter 2

Experimental analyses

All the experimental investigations conducted over the last decade on curvilinear masonry structures exposed to fire at the intrados are described in this chapter[1]. As ascertained in recent the publications [134-135], this subject has remained almost totally unaddressed by the research community so far.

In total, five experimental tests were performed on single ring barrel vaults, made with local raw materials namely clay bricks and cement-lime based mortar. In each of them, different loading schemes were adopted and, in two cases, the beneficial effect of fire protectives is also considered.

The first two vaults, hereafter referred to as *V.01.u* and *V.02.u* (where subscript "u" indicates "uncoated"), were tested by Fantilli and Burello [134]. These investigations were carried out in 2020 thanks to the collaboration between the Politecnico di Torino and the Italian fire brigade.

---

[1]*Part of this chapter has been previously published in:*

1. Fantilli, A.P. and Burello, N.S. (2022) 'Masonry arches and vaults under fire', Journal of Building Engineering, Vol. 56, 104740.
2. Fantilli, A.P. and Burello, N.S. (2023) 'Experimental and numerical analyses of curvilinear masonry structures exposed to high temperatures', January 2023International Journal of Masonry Research and Innovation 1(1):1 DOI: 10.1504/IJMRI.2023.10055405

The experimental campaign focused on evaluating the fire resistance R of two masonry barrel vaults subjected to distributed loads, in accordance with the most common serviceability load conditions. Following the application of the static load, the vaults were exposed to fire on one side, namely on the intrados.

These tests were inspired by the first investigation [136] conducted by the fire brigade in 2015, where a similar prototype vault was built (*V.03.u* in the present work), but with only two concentrated loads, in addition to self-weight. *V.01.u*, *V.02.u* and *V.03.u* were built and tested with the help and under the supervision of Italian fire brigade in the experimental laboratory located in Capannelle (Roma).

In addition, the experimental results obtained from two barrel vaults coated with protective materials [135], *V.04.c* and *V.05.c* (where subscript "c" indicates "coated"), are also discussed. These prototypes were respectively insulated with a traditional cement plaster combined with an intumescent paint (*V.04.c*) and with a gypsum mortar (*V.05.c*). Geometrical properties and load conditions were (more or less) those adopted for *V.03.u*. Unlike the first three investigations, these vaults were simultaneously tested in the laboratories of Istituto Giordano (Rimini, Italy).

2.1 Uncoated vaults with distributed loads

2.1.1 Geometry and materials

These tests were performed in the laboratory of the Italian fire brigade. As shown in Fig.15, the oven is characterized by an internal chamber approximately 3.2 x 3.2 x 4 m^3 in size. A series of gas burners is arranged along the walls of the chamber, while the original roof consists of a modular structure made of simple supported steel beams HE220B covered with highly insulating panels. Following the removal of the central modules of the roof, the masonry vaults were directly built as part of the roof of the oven chamber through the use of a polystyrene rib (see Fig.16a). The flanges of the roof beams were used as abutments of the masonry vaults. The remaining part of the roof and the end parts of the vaults were insulated with highly fire-resistant materials, as illustrated in Fig.16b and Fig.16c respectively.

As schematically reported in Fig.17a and Fig.17b, the prototypes *V.01.u* and *V.02.u* presented the same geometry. Each vault had a clean span length $L = 2200$ mm, a net height $f = 483$ mm, an intrados radius $r = 1490$ mm and abutment angles $\alpha_0 = 42.5\,°$ resulting in overall opening angle $\alpha = 95°$.

V.01.u and *V.02.u* were constructed with 38 rows of 4 bricks each, with a total width $w \sim 1000$ mm. Clay bricks, having sizes 55 x 120 x 250 mm^3, were arranged along the short side, giving the vault ring a thickness t_m =120 mm. They were stacked with a traditional cement-lime based mortar with a mean bed-joint thickness in the midsections of 10 mm. Readers can find additional details about the constituent materials in the section 2.4.
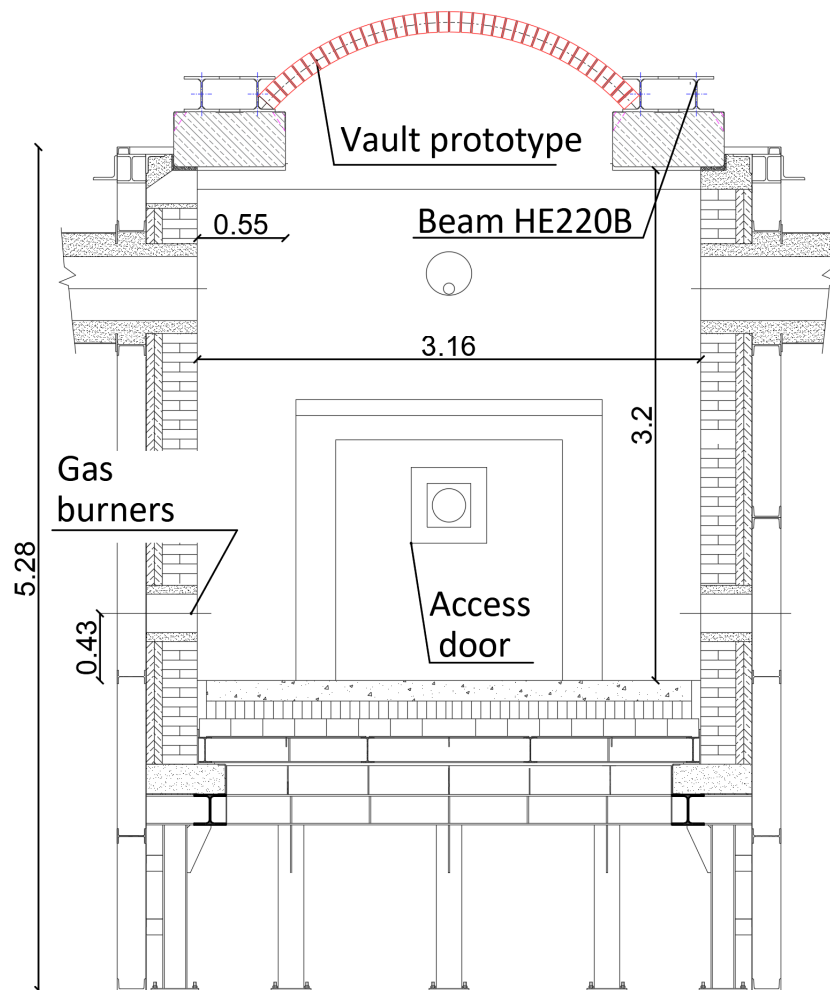
Figure 15 - Front cut-view of the experimental oven– Fire brigade - Rome (measures in m)

The differences between the tests were the load configuration. In addition to self-weight given by bricks and mortar, namely $\gamma_m = 17 \div 18$ kN/m³, *V.01.u* were subjected to a light infill given by loose sand confined by side panels. As depicted in Fig.17, it was intended to simulate a non-cohesive backfill having a density γ_{fill} = 13.75 kN/m³.

As shown in Fig.18, light-weight concrete (having density of $\gamma_{cls} = 20$ kN/m³) was instead poured on the extrados of *V.02.u* and, once hardened, sandbags were added in order to apply an equivalent variable load of $Q = 2.10$ kN/m² on the whole surface.

(a)

(b)   (c)
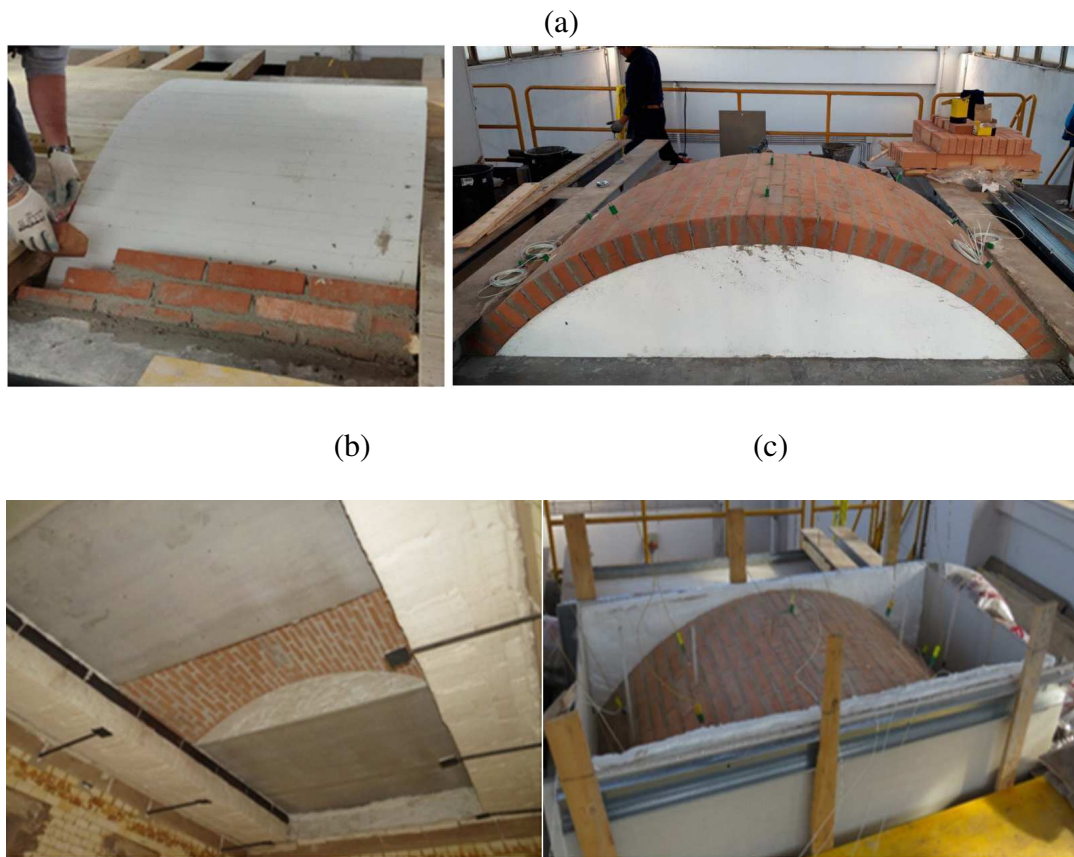
Figure 16 - (a) Construction of *V.01.u*; (b) Closure of the roof using high-insulation panels – intrados view; (c) Closure of the end parts of the vault – extrados view

(a)

(b)
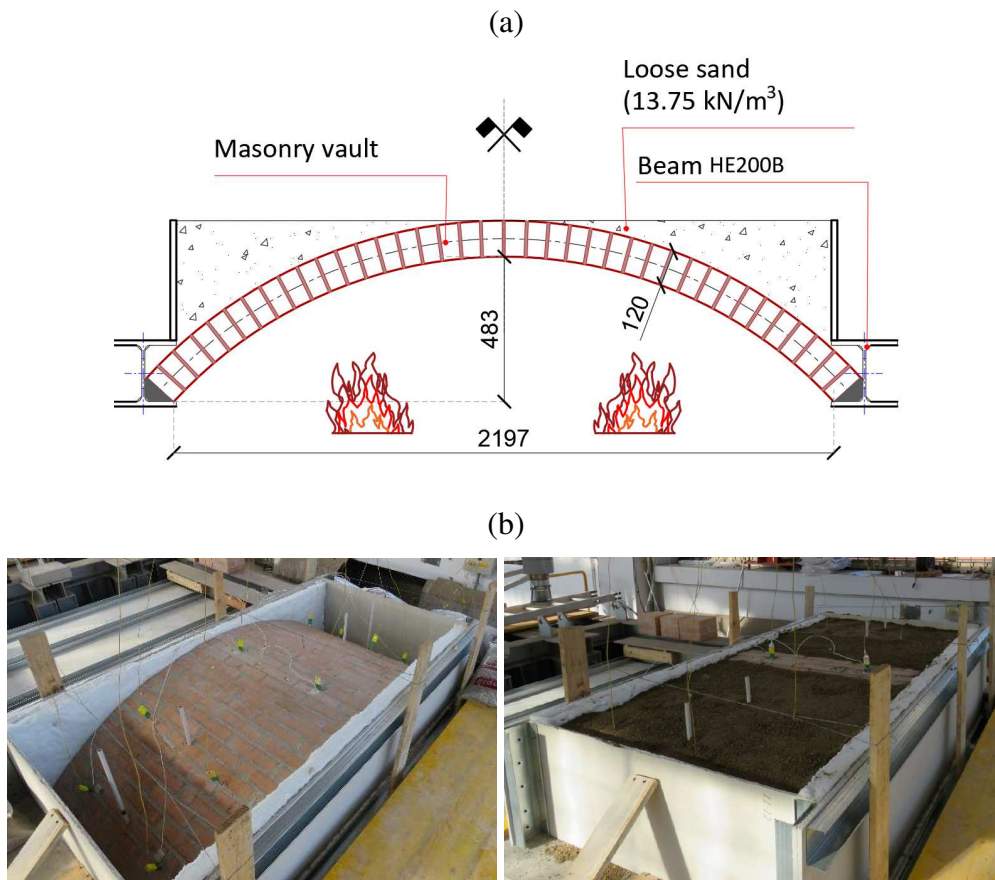
Figure 17 - Prototype V.01.u: (a) longitudinal cut view (measures in mm); (b) extrados cross-capture of V.01.u before and after the application of loose sand.

2.1.2 Monitoring system

Thermal and mechanical responses were analyzed by means of thermocouples and displacement transducers, respectively.

In addition to those used to regulate the heating of the chamber, several thermocouples were used to investigate the temperature distributions in the prototypes. High-temperature thermocouple (TC) type K, with an accuracy of ± 1.5 °C and probe temperature range - 40°C ÷ 1000°C, were placed on the intrados, inside the masonry, and on extrados of the vaults.

According to the scheme reported in Fig.19, 16 TCs were used in total and they were distributed along the whole vault profile. Temperature increments were

measured at the intrados and at the extrados of the vault in the center, at a nominal distance of 930 mm from the midspan (i.e., close to the abutments). Whereas they were placed at a depth of 60 mm, namely in the middle of the cross-section, within mortar and bricks at around 530 mm from the midpoint.

(a)

(b)
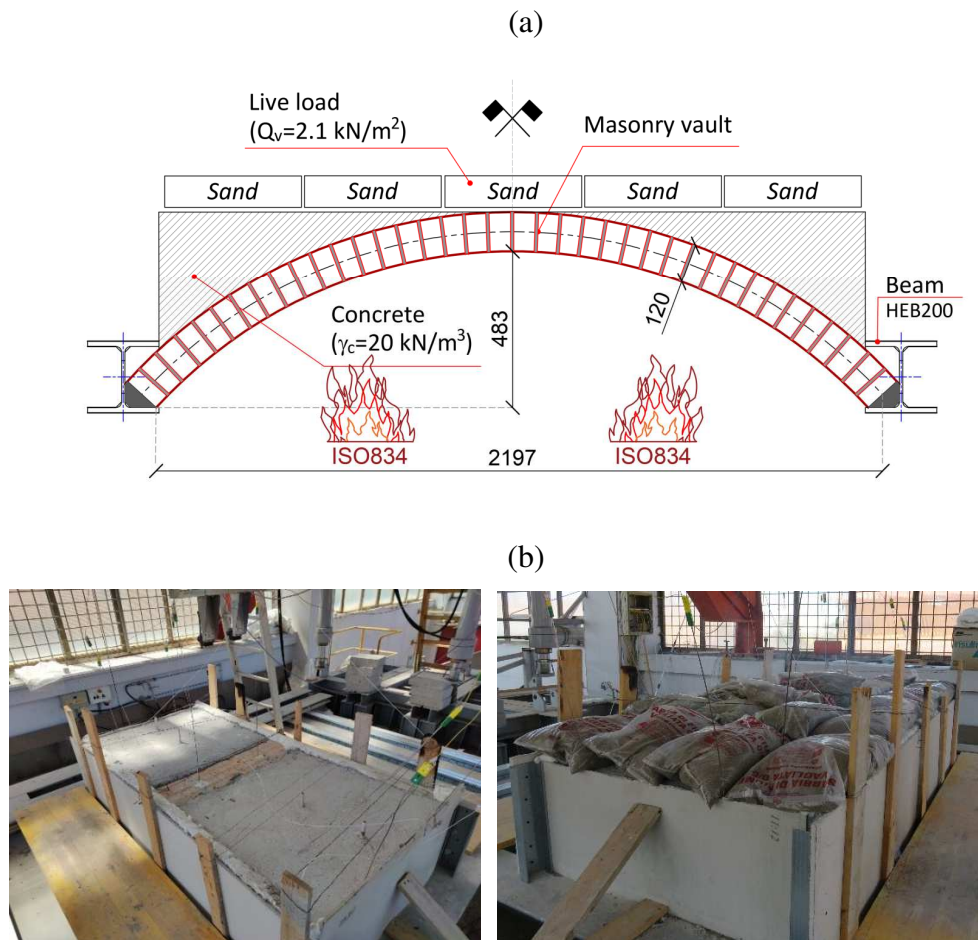
Figure 18 - Prototype V.02.u: (a) longitudinal cut view (measures in mm); (b) extrados cross-capture before and after the application of sand-bags on hardened light-weight concrete.

To evaluate the mechanical response of the structure, a total of six wire potentiometers (POTs) were located along the vaults. Two of them (POT_5 and POT_6) were used to measure the midspan deflection of the vault. As clarified in Fig.19, vertical displacements were also measured at 530 mm, POT_2 and POT_3, and at 930 mm, POT_1 and POT_4, from the center.

(a)

(b)
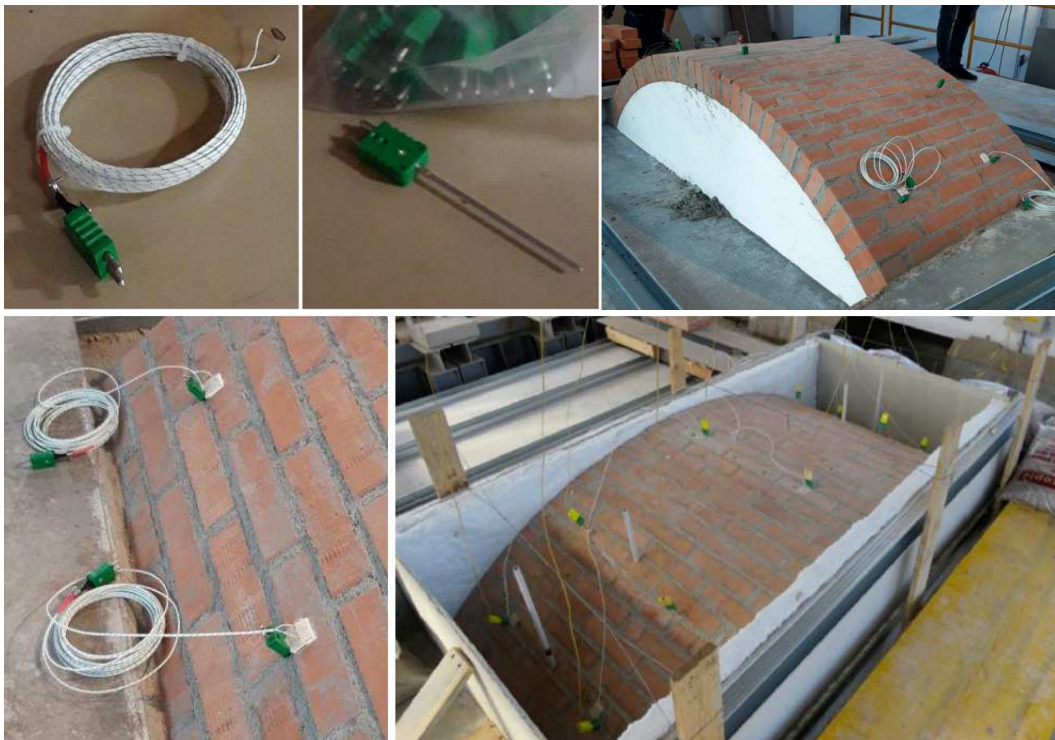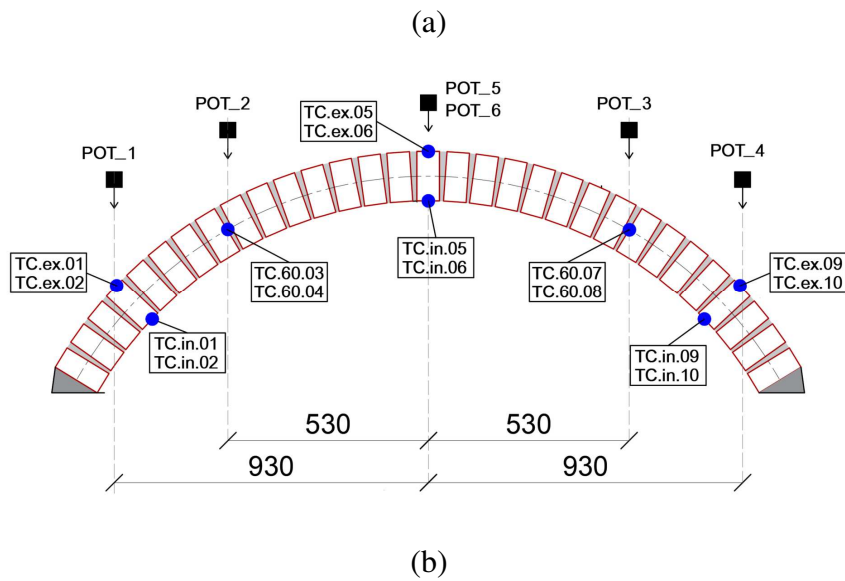
Figure 19 - (a) Thermocouples (TC) and potentiometers (POT) used to measure temperatures and displacements in *V.01.u* and *V.02.u*. (ex = extrados; in = intrados; 60 = distance from the boarder in mm; lengths in mm); (b) Installation of sensors on the vault.

2.1.3 Experimental results

The fire investigations were performed only when instrumentation and loads were properly applied to each prototype, after 28 days of curing at room temperature. The oven chamber was heated in accordance with the standard fire curve [137], the so-called ISO834 curve described by eq.5:

$$T = 20 + 345 \cdot log \left(8 \cdot t + 1 \right) \tag{5}$$

where t = time expressed in minutes and T = temperature expressed in degrees Celsius.

Eight thermocouples placed within the chamber were used to regulate the heating process. As shown in Fig.20a and Fig.21a, where the mean temperatures of the chamber are also reported (with a blue dashed line), the curve ISO834 is properly reproduced in both the tests of *V.01.u* and *V.02.u*. In fact, with the exception of the very early ages of heating, the two curves (theoretical and experimental) are almost perfectly overlapped.
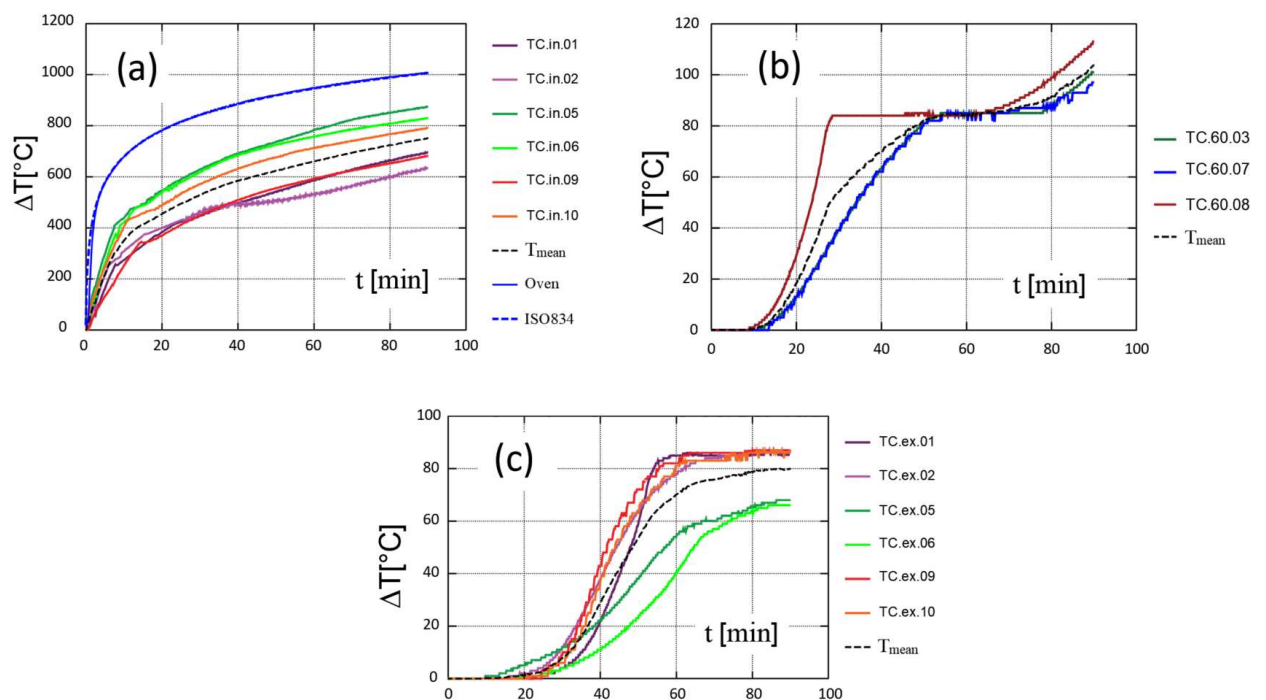
Figure 20 - Increments of temperature of V.01.u at: (a) intrados; (b) mid cross-section and (c) extrados. (Tenv = 12°C)
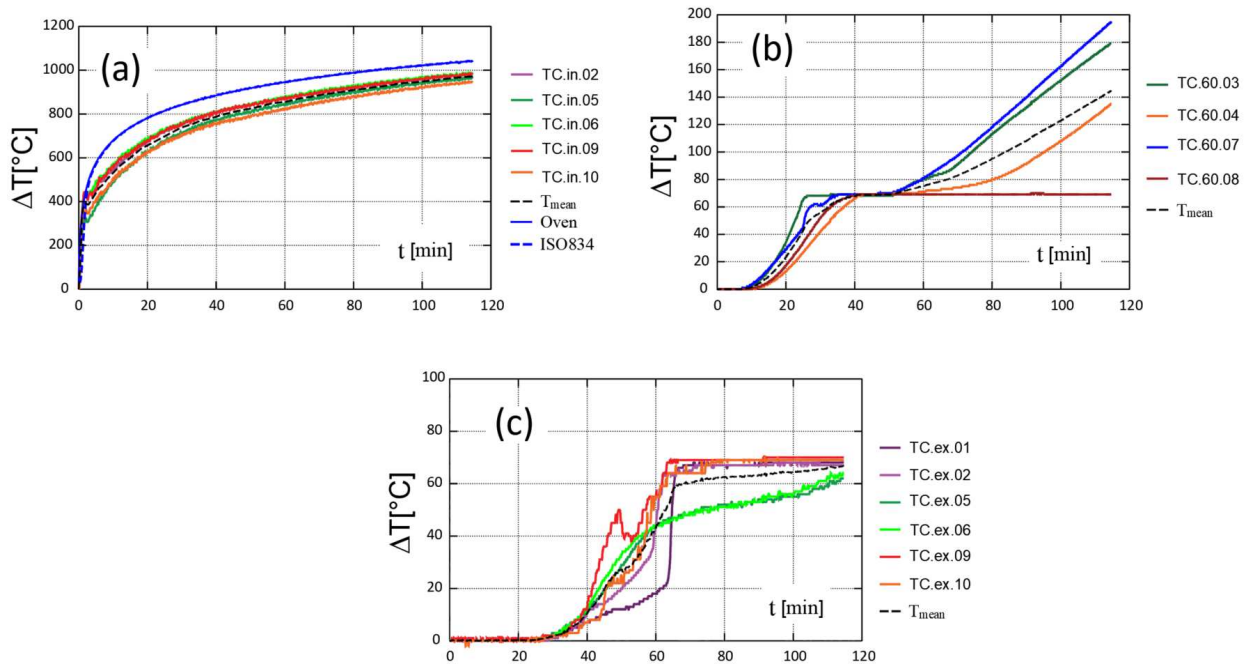
Figure 21 - Increments of temperature of *V.02.u* at: (a) intrados; (b) mid cross-section and (c) extrados. (T_{env} = 30°C)

In the same diagrams, also the increments of temperatures measured on the exposed surface are illustrated (identified with "*in*" namely "intrados"). As expected, temperatures measured at the intrados of the vaults were generally lower than those measured at the level of gas burners. In the case of the light loaded vault (i.e., *V.01.u* where only loose sand was applied) a significant scatter can also be observed if the curves are compared, whereas it is very low in the case of heavily loaded curves (*V.02.u*). Similarly, in the case of *V.01.u*, an higher dispersion was also registered if comparing the mean temperature profile at the intrados T_{mean} is compared with that of ISO834.

Within the masonry thickness, it is possible to observe that when the total temperature (i.e., $T_{tot} = T_{env} + \Delta T$) reached 100°C, it remained constant for the time necessary to the complete evaporation of the moisture content (see Fig.20b and Fig.21b). The thermocouple TC.60.04 malfunctioned during the testing of *V.01.u,* and it was therefore removed from the diagram. In both the tests, the temperature of 100 °C was reached also on the surfaces not exposed to fire, as depicted in Fig.20c and Fig.21c.

Simultaneously, the vertical displacements δ with time of exposure were measured, as schematically reported in Fig.22 and Fig.23 for *V.01.u* and *V.02.u*,

respectively (see also Fig.19a). Deflections are assumed conventionally negative when raising and positive in the case of settlement. As shown, the high thermal gradients led to a rise in the central zones (i.e. around the keystone) and a general lowering near the springers of the vaults.
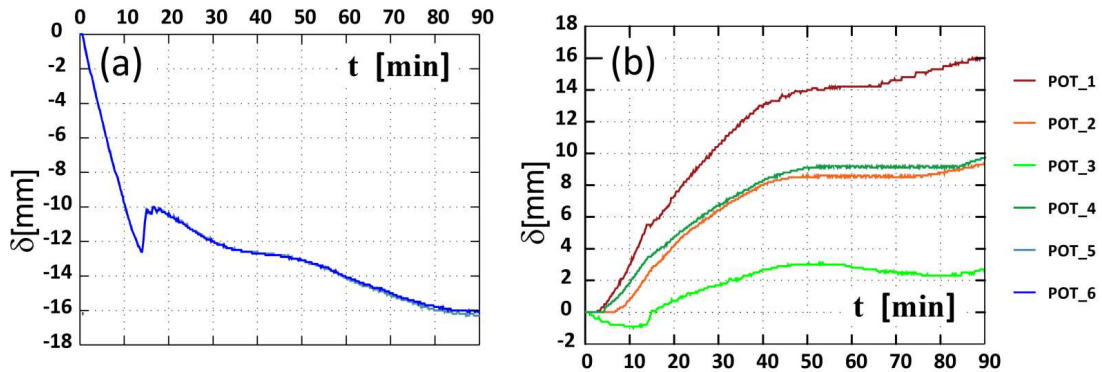
Figure 22 - Displacements measured in V.01.u by POTs in (a) midspan and (b) in other points of the vault.
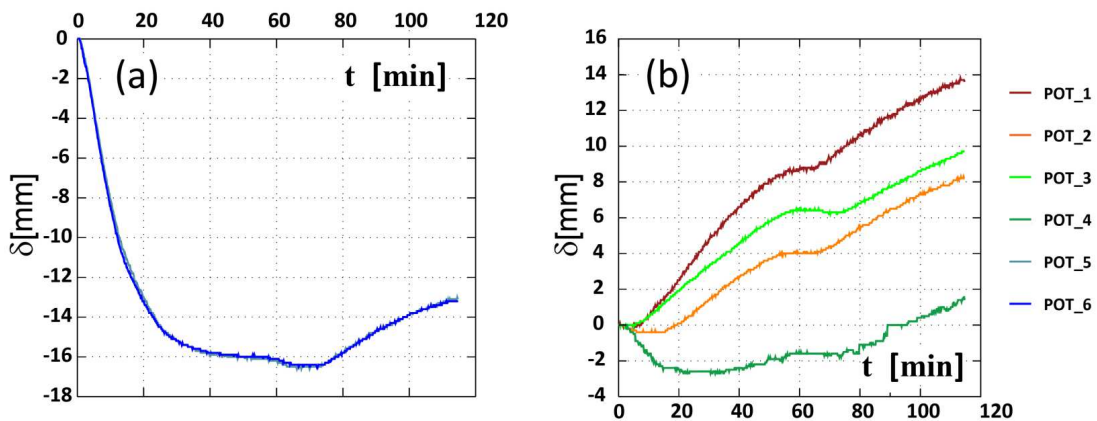
Figure 23 - Displacements measured in V.02.u in (a) the midspan and (b) in the other points of the vault.

In the case of *V.01.u*, for which the test lasted 90 minutes, the displacements in the middle showed an increasing monotonic behavior, with the exception of a drop around the 15th minute (se Fig.22a), reaching a displacement at the peak $\delta = 16$ mm.

Similarly, also for *V.02.u* a strong rise of the midspan was observed in the first few minutes of heating, until a sort of steady state condition was reached between 40 and 75 minutes, where the displacements fluctuated around 16 mm. Thereafter,

until the end of the test (115 minutes), a gradual decrease was recorded up to a final displacement slightly lower than 14 mm in the midspan.

Due to the high risk of damaging the instrumentation in the event of a sudden collapse of the masonry vaults, the interruption of the test was dictated to maintain safe conditions in the laboratory. During the tests, from the very first minutes, the vaults cracked in several places, as evidenced by the alternately opposing displacements.

As shown in Fig.24, where the crack pattern near the centerline of *V.01.u* is reported, the failure of the brick/mortar interface allowed the bricks to rotate to the point of glimpsing the kiln chamber below. However, due to the voluminous nature of the distributed loads, it was not possible to capture additional photos of the formation of other crack patterns during the test. Both the vaults gradually settled back to their initial geometry after the furnace was turned off.

Figure 24 - Failure of brick/mortar interface and raising at the arch-crown of vault #1 during the fire exposure.

It was therefore not possible to photograph the intrados of the vaults in a deformed configuration. Spalling phenomenon did not occur. The filling materials were removed and the masonry vaults were demolished.

2.2 Uncoated vault with concentrated loads

2.2.1 Geometry and materials

V.03.u was tested by means of the same oven chamber used for *V.01.u* and *V.02.u* (see Fig.15). According to the technical report [136] and the more recent investigations [134-135], the same materials were used to assemble the vault. However, the geometry of the vault and the loads applied were different. As shown in Fig.26, *V.03.u* had a shorter clean span length $L = 1611$ mm, a net heigh $f = 465$ mm, an intrados radius $r = 930$ mm, abutment angles of 30°, and an overall opening angle of $\alpha = 120°$.
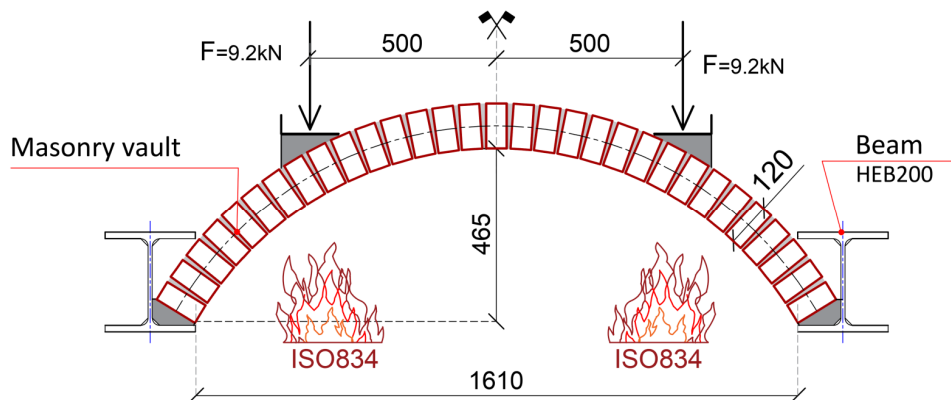
Figure 25 - Prototype *V.03.u*: longitudinal cut view (measures in mm)

In this case, a longer prototype was constructed with a total width of (approximately) 2000 mm, given by 8 bricks for each row (see Fig.26). Two concentrated loads were applied at a distance $d_F = 500$ mm from the center of the structure by means of two hydraulic jacks. Each load was distributed along the width of the vault through a system made of two concrete curbs anchored to the extrados of the vault and "L" shape steel profiles. The load was gradually applied up to F = 9.20 kN for each hydraulic jack. Once reached the steady state, the fire test was conducted maintaining the load under force control.

Figure 26 - Construction process of *V.03.u* (Figures from [136]).

2.2.2 Monitoring system

The instrumentation used for this investigation (namely thermocouples and wire potentiometers) was the same. Also for *V.03.u*, 8 thermocouples were used to piloting the heating of the oven, whereas 36 TCs were placed on the vault. As depicted in Fig.27, temperatures were measured in corresponding of the midspan, of the abutment and in between. In each section, the thermocouples were located at four different points: on the borders (i.e., on extrados "ex" and intrados "in"), at 50 mm and 75 mm from the inferior edge. For each blue point in Fig.27, three TCs were placed along the width of the vault at a distance of 500 mm from each other.
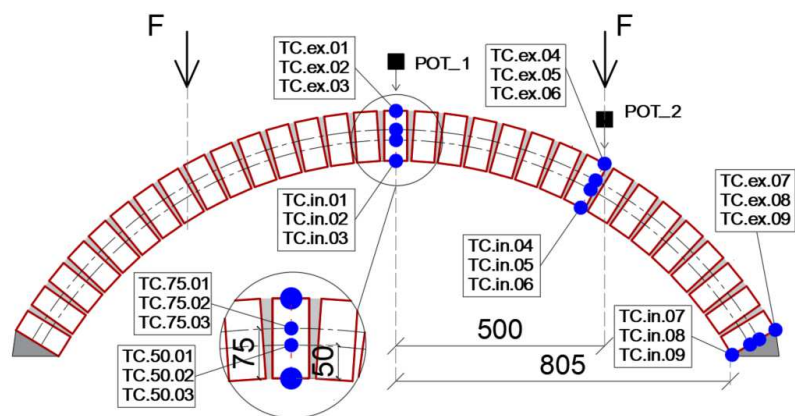
Figure 27 - Thermocouples (TC) and potentiometers (POT) used to measure temperatures and displacements in *V.03.u*

To evaluate the mechanical response of the structure, only two POTs were located along the vaults and, more precisely, one was placed under one hydraulic jack and one was placed in the middle.

2.2.3 Experimental results

Fig.28 summarizes the increments of temperature registered at the intrados (Fig.28a), at 50 mm and 75 mm from the intrados (respectively in Fig.28b and Fig.28c), and at the extrados (Fig.28d). Also for *V.03.u*, as for *V.01.u*, the temperature profiles at the intrados presented a great discrepancy with respect to those registered at the level of gas burners. The test ended after 54 minutes of exposure, reaching a mean temperature at the extrados of approximately 62°. The vertical displacements are instead reported in Fig.29. The structure raised in the center and settled around the borders. Also in this case, a wide crack pattern was observed around the keystone (see Fig.30a).
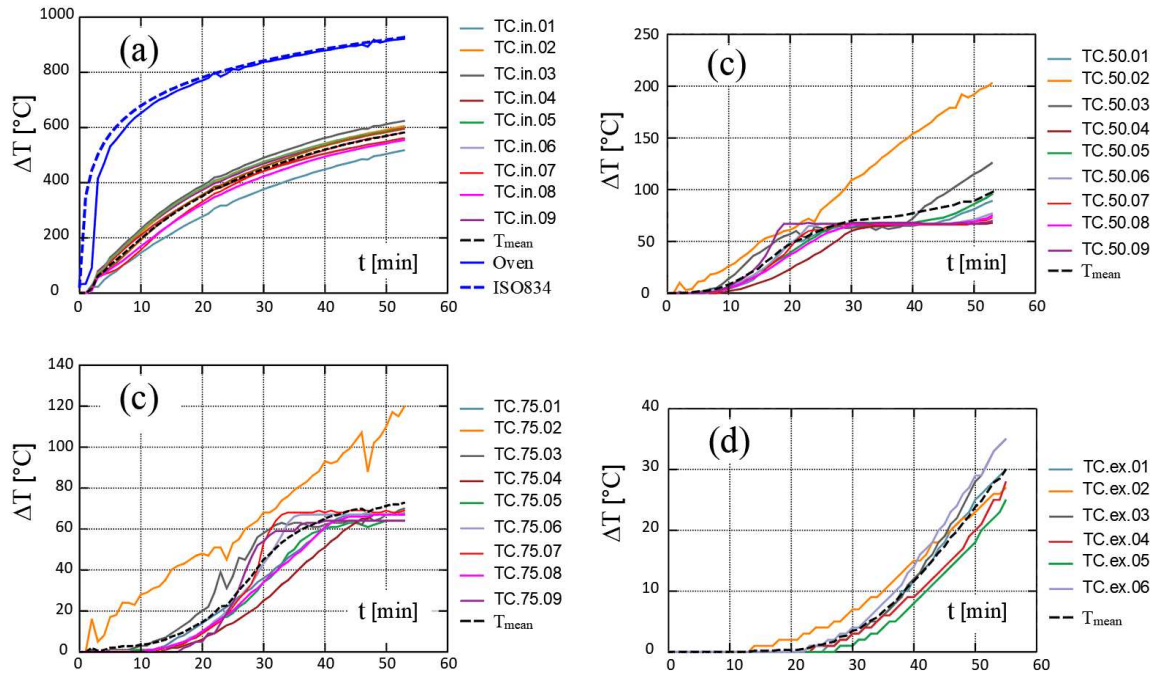
Figure 28 - Increments of temperature *V.03.u* at: (a) intrados; (b) 50 mm from intrados; (c) 75 mm from intrados; (d) extrados. (T_{env} = 32°C)
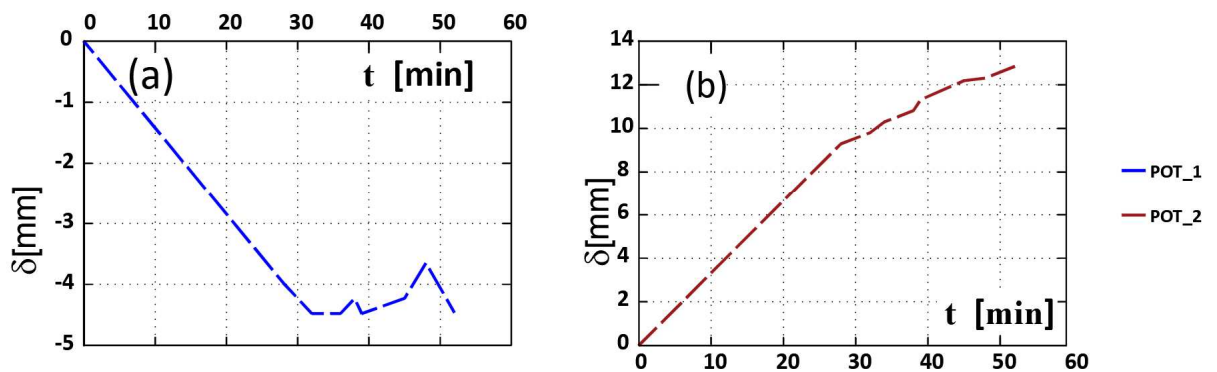
Figure 29 - Displacements measured in *V.03.u* in correspondence of (a) the midspan and (b) the hydraulic jack.

(a)

(b)

Figure 30 - *V.03.u*: (a) crack pattern in the midspan (extrados view); (b) internal view
of the vault after the fire test

2.3 Masonry barrel vaults coated with insulating materials

2.3.1 Geometry and materials

Two masonry vaults coated with fire protectives were also tested in 2016 at Istituto Giordano (Rimini, Italy). The tests were carried out in an experimental oven with an opening on the upper side (oven mouth), lined internally with refractory bricks and equipped with diesel-fueled double-flame burners on the long sides and two suction chimneys on the short sides. The kiln is equipped with a hydraulic jack with a maximum load of 295 kN.

The construction process of these vaults differs from that adopted in the test previously described. As illustrated in Fig.31, the entire roof of the furnace chamber was first constructed, leaving space for the subsequent construction of the arch prototypes. Each barrel vault was assembled on the same supporting construction, consisting substantially of a reinforced concrete slab with a nominal thickness of 200 mm, in which 2 rectangular openings were made (1600 mm × 1500 mm^2 each). Details of the reinforcement bars used to reinforce the ceiling were not provided.

Each opening was bordered on the short sides by 2 steel beams IPE 160 - S235 partially embedded in the concrete slab. Similarly to uncoated vaults, steel beams were used as abutments for the masonry vaults. In these cases, the ends of the vaults were closed by means of masonry walls with variable length according to the curvilinear profile. In order to limit the bending of the supporting structure during the exposure to fire, also the concrete slab was insulated with a pre-mixed insulating plaster "Promaspray P300" having a thickness of 45 mm.

The manufacturer's aim was precisely to investigate the differences when fire protectives were applied to the intrados of the vault. For this reason, V.03.u was adopted as reference and the geometry of V.04.c and V.05.c was exactly the same of the previous case (namely span length, height, internal radius, abutment angle, etc.), as shown in Fig.32a. From a geometrical point of view, the only difference was given by the width of the prototypes, which was reduced to 1500 mm (i.e., three quarters of that of V.03.u [136]) using 6 bricks per row instead of 8.

Figure 31 - Sequences of images taken during the construction of *V.04.c* and *V.05.c*

A traditional cement plaster (having thickness t_p = 10 mm and a density γ_{pl} = 14.50 kN/m^3) was applied on *V.04.c*. The intrados of the plaster was then treated with a layer of one-component fixative primer in water emulsion. Finally, the white intumescent paint was applied by spraying with a high-pressure pump in two successive coats (nominal quantity of 1.5 kg/m^2 with negligible thickness). The paint is made with synthetic resins and fireproof fillers, with an expansion temperatures range of 180÷200 °C and expansion ratio of 1:40.

A premixed gypsum plaster, with t_p = 15 mm and γ_{pl} = 3.60 kN/m^3, was instead applied directly on the intrados of *V.05*.c, as shown in Fig.32b. It is composed by hydraulic binders, vermiculite and special additives. It has been applied without a fixative primer by a standard plastering machine in a single pass.

(a)

F=6.9kN   F=6.9kN

500   500

Masonry vault

Fire protective

120

465

1611

(b)   (c)
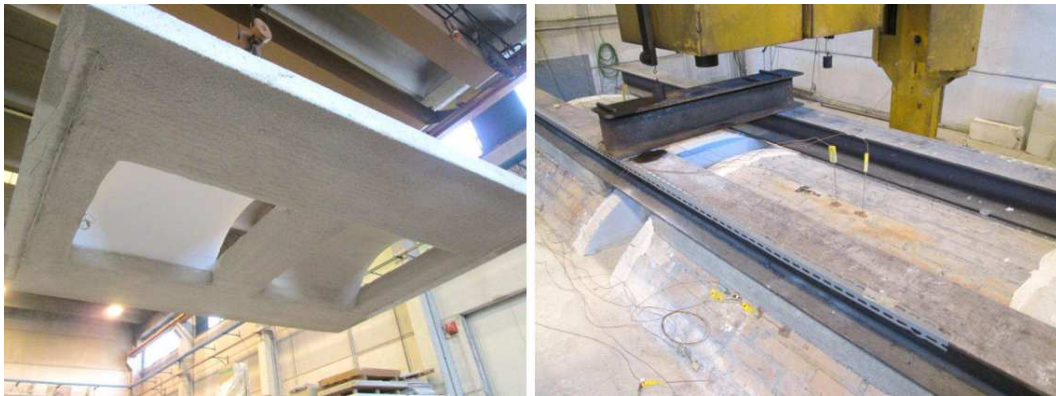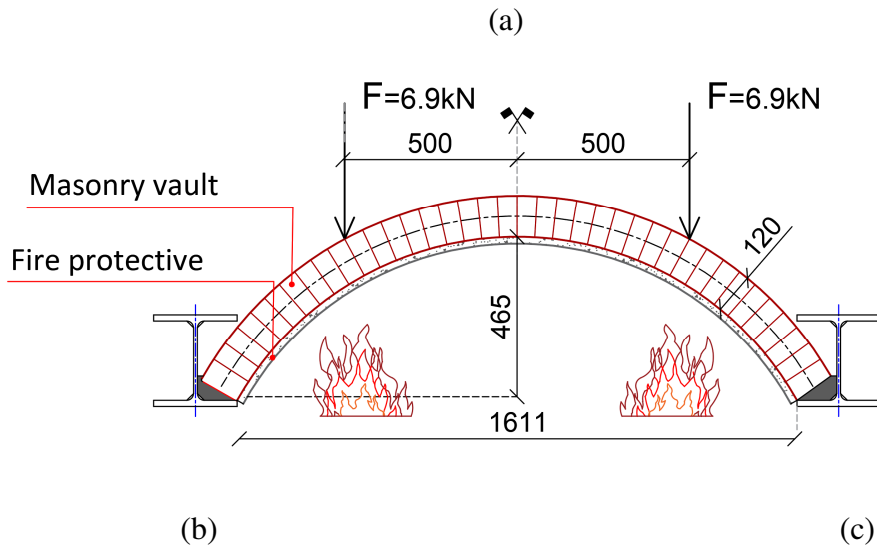
Figure 32 - Prototypes *V.04.c* and *V.05.c*: (a) longitudinal cut view (measures in mm); (b) white intumescent paint applied on the intrados of *V.04.c* and gypsum plaster applied on *V.05.c*; (c) Extrados view of the vaults.

Accordingly, due to the reduced width of the vaults, also the concentrated loads were proportionally reduced from 9.2 kN [136] to 6.9 kN for each side of the vaults. More precisely, a total load of 27.60 kN was transferred and distributed to the masonry vaults by means of two steel beams HE200 S235, supported by dedicated cast-in-situ concrete kerbs directly anchored on the extrados of the vaults.

2.3.2 Monitoring system

Also for these vaults, the acquisition system used for temperature measurement was based on the use of K-type thermocouples for both chamber and masonry vault

temperatures. As depicted in Fig.33, a total of 20 TCs (4 for each depth) were symmetrically placed along the whole profile on intrados, extrados and at 50 mm and 75 mm from the exposed surface. The TCs were placed in the middle zone of the vault with respect to the width.
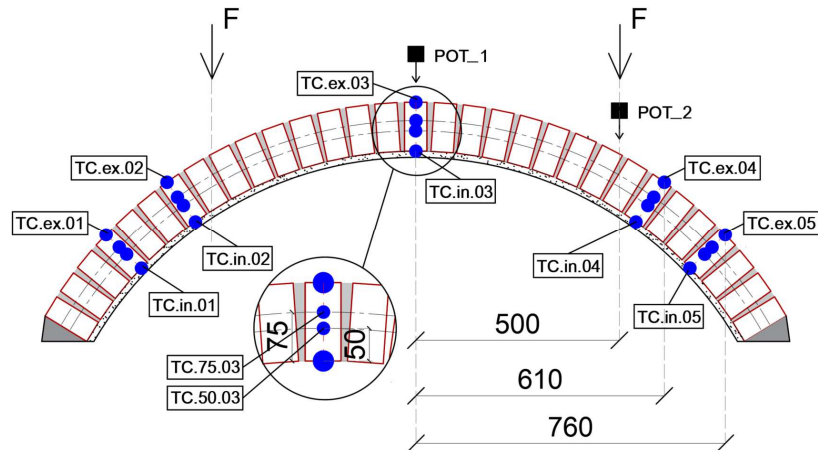
Figure 33 - Thermocouples (TC) and potentiometers (POT) used to measure temperatures and displacements in *V.03.u*

Also in this case, only vertical displacements were monitored. More precisely, the midspan deflection (POT_1) and the one in correspondence of one hydraulic jack (POT_2) were measured with the time of exposure to fire, as in the case of *V.03.u*.

2.3.3 Experimental results

Fig.34 and Fig.35 show the temperature increments measured in correspondence of four points: intrados (between coating and masonry), extrados and two points inside the masonry. The theoretical reference temperature [137] and the actual temperature reached are shown with the blue, dashed and continuous lines respectively, in Fig.34a and Fig.35a. As expected, a high deviation between the chamber temperature and the temperature actually reached at the soffit was observed, especially in the case of a vault lined with gypsum mortar (*V.05.c*).

Similar to previous experiments, following the initial sharp rise in temperatures, a state of momentary equilibrium was reached when temperatures reached 100°C. This phenomenon is particularly evident within the masonry.

Also deformations were similar (see Fig.36 an Fig.37). In fact, steep rises in the center of the vaults and sagging at the loads were observed. The phenomenon of lowering of the vault centerline after reaching the peak value previously observed in *V.02.u*, was also observed in *V.04.c* and *V.05.c*.

Due to the considerable duration of the tests namely 180 minutes (3 hours), a steep lowering of the center line was observed, moving from $\delta = -11$mm (at $t = 100$ min) to $\delta = 6$mm (at $t = 180$ mi)n in the case of *V.04.c* (see Fig.36a). Although smaller in magnitude, there was also a deviation from $\delta = -4$ mm to $\delta = +4$ mm in a similar time variation in *V.05.c*.
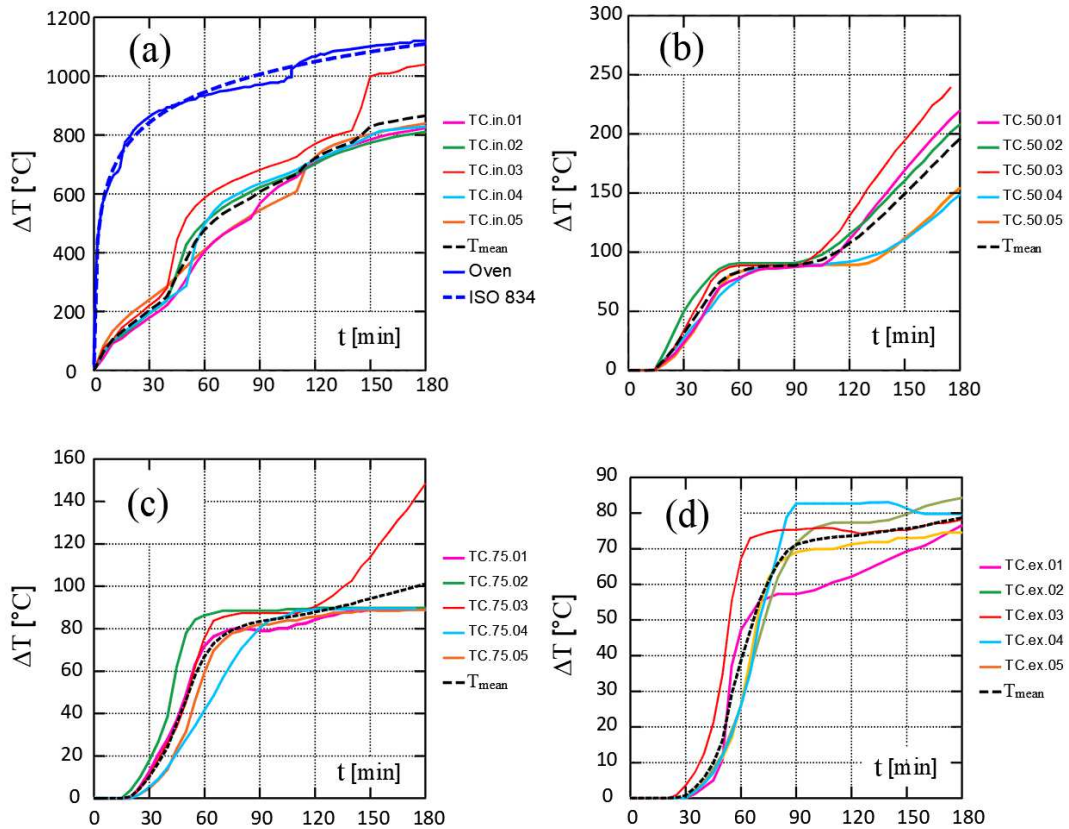
Figure 34 - Increments of temperature of *V.04.c* at: (a) intrados; (b) 50 mm from intrados; (c) 75 mm from intrados and (d) extrados. (Tenv = 10 °C)
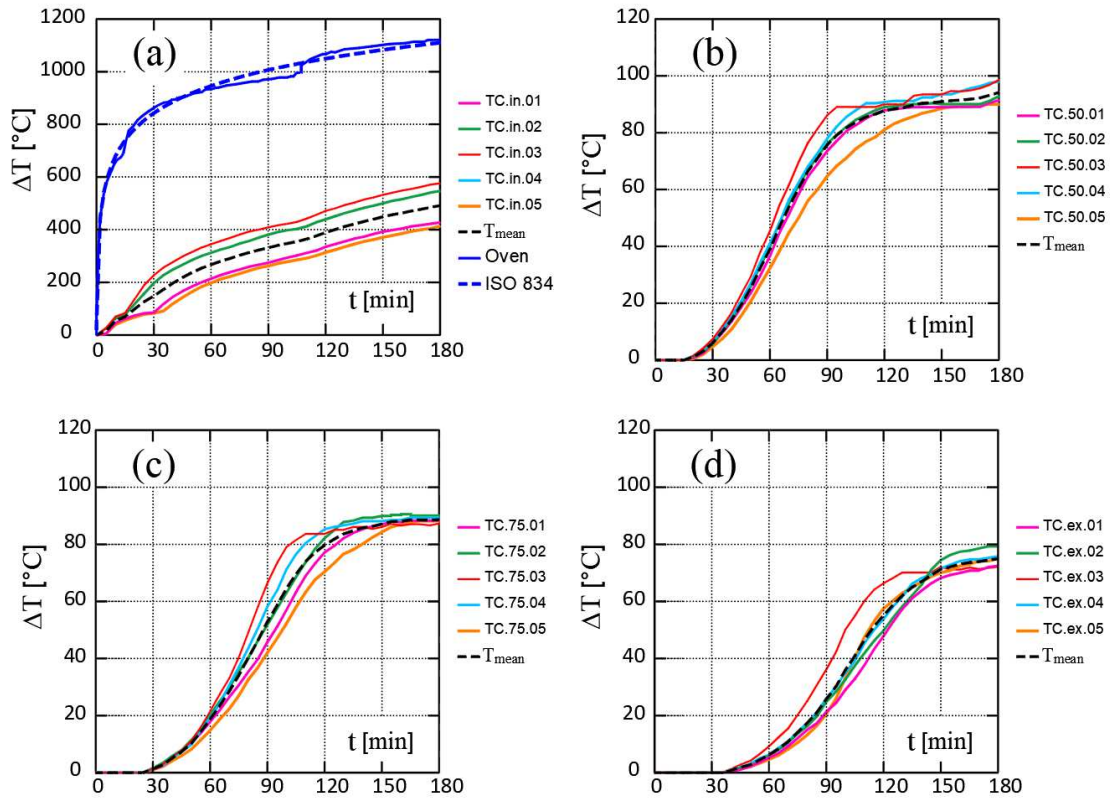
Figure 35 - Increments of temperature of *V.05.c* at: (a) intrados; (b) 50 mm from intrados; (c) 75 mm from intrados and (d) extrados. (Tenv = 10 °C)
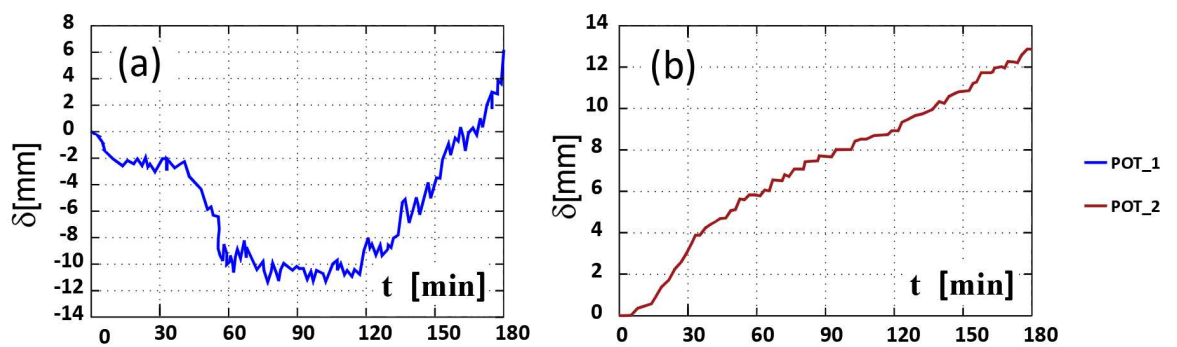
Figure 36 - Displacements measured in *V.04.c* in correspondence of (a) the midspan and (b) the hydraulic jack.
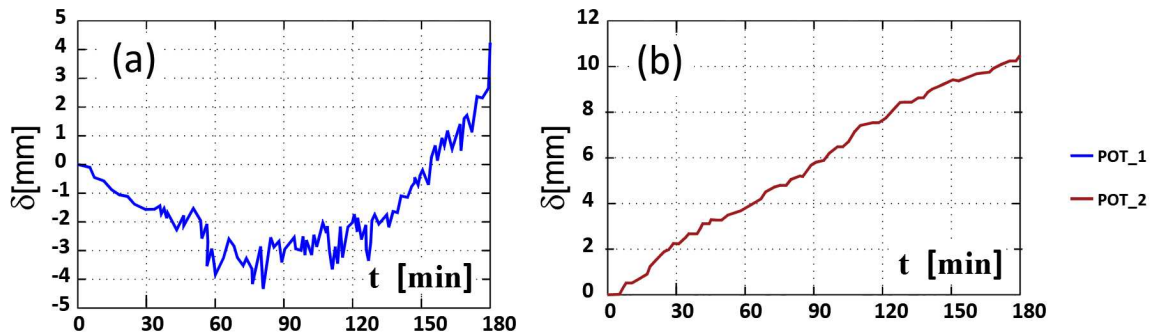
Figure 37 - Displacements measured in *V.05.c* in correspondence of (a) the midspan and (b) the hydraulic jack.

As shown in Fig.38a, due to the high deformation of the vault as a result of fire exposure, a detachment between the confinement partition and the *V.04.c*. soffit occurred. In addition, looking at the view from the inside (Fig.38b), evident signs of degradation of the intumescent paint and extensive cracks on the gypsum plaster can be found in *V.04.c* and *V.05.c*, respectively. Spalling of the masonry was not observed at the end of the experiment. After the heating of the kiln was interrupted, the floor was raised, placed on the floor and the structure was then demolished.

2.4 Cold mechanical characterization

In addition to the tests conducted on the vault prototypes, a barely cold mechanical characterization of the masonry was also carried out. Although similar materials were used in all 5 tests, it is worth noting that laboratory tests were performed to determine the cold mechanical characterization on masonry prisms only in the case of *V.01.u, V.02.u* [134,135] and *V.03.u* [136], whereas no mechanical tests were performed on individual materials.

According to the technical declaration of the manufacturers, the units were solid burnt-clay bricks (55 x 120 x 250 mm^3) characterized by a mean compressive strength $f_b \geq 40$ MPa [3], a density of 1697 kg/m^3 and 0 % of void area.

(a)

(b)

Figure 38 - (a) Failure between the intrados of *V.04.c* and the top of the confinement wall; (b) Intrados view of *V.04.c* and *V.05.c* after the fire test.

The premixed cement-lime based mortar can be instead classified as a mortar M5 [9] at 28 days of curing, with a Young's Modulus of around 8000 MPa, and with a density of about 1850 kg/m^3 in hardened state, according to EN1015-10 [138]. The water was added in accordance with the manufacturer's recommendations (i.e., 17.5-19.5% in weight).

To determine the cold compressive strength of the vaults, different types of masonry prisms were used. As depicted by Fig.39, the masonry prisms were made by three layers jointed with the mortar (mean bed-joint thickness 10 mm) and were characterized by different shapes:

- Type A: $250 \times 250 \times 185$ mm^3, with 2 bricks per layer alternately crossed at 90° [134, 135];
- Type B: $250 \times 120 \times 185$ mm^3, with 1 brick per layer – without head-joints [134, 135];
- Type C: $250 \times 120 \times 185$ mm^3, with 1 brick in the first and last layers, and two half bricks in the second one [136].
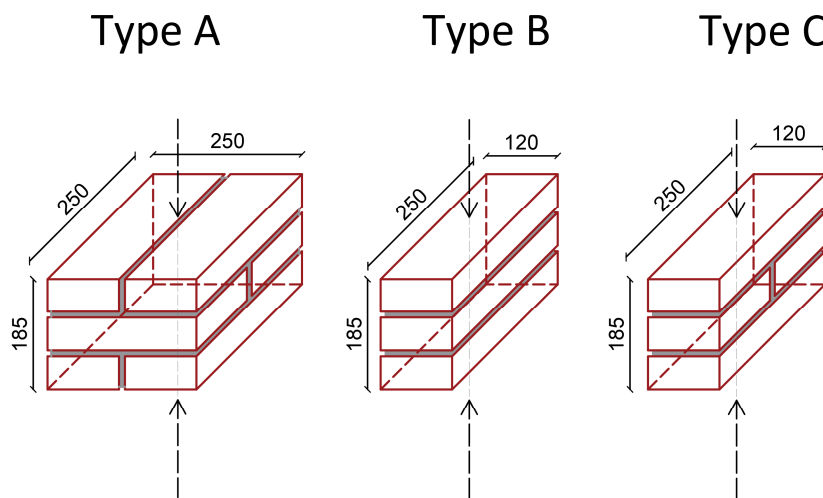
Figure 39 - Uniaxial compression tests on masonry prisms during the investigations of V.01.u and V.02.u (masonry prisms of type A and B) [134-135] and of V.03.u (type C) [136].

For each type, three samples were subjected under uniaxial compressive test at room temperature (i.e., approximately $T_{env} = 20$°C). As reported in Table 3, a mean compressive strength $f_m = 19.10$ MPa were measured with the Type A specimens, whereas $f_m = 14.50$ MPa and $f_m = 11.80$ MPa were obtained in the case of bricks

stacked without and with head joint namely in the cases of Type B and Type C, respectively. The standard deviation and the coefficient of variation are also reported.

Table 3: Results of the uniaxial compression tests on masonry prisms. (the standard deviation and the coefficient of variation are reported in parentheses).

Type of sample	Sizes	Compressive strength (MPa)
Small prisms (Fantilli and Burello, 2022) [135]	250×250×185 mm³	19.10 (1.06 ; 0.055)
Stacked without head joint (Fantilli and Burello, 2022) [135]	250×120×185 mm³	14.50 (1.47 ; 0.101)
Stacked with head joint (Vigili del Fuoco, 2015) [136]	250×120×185 mm³	11.80 (1.40 ; 0.119)

2.5 Summary of the experimental investigations

In this chapter, a detailed report of all the tests performed in the las decade has been depicted. Five masonry barrel vaults made with conventional clay bricks and a lime-cement based mortar (class M5) were used. From a geometrical point of view, the vaults presented similar properties, as summarized in Table 4.

V.01.u and *V.02.u* were tested with the aim of analyze the fire behavior of the masonry vaults under the effect of the most common and realistic loads (i.e., uniformly distributed loads). Conversely, V0.4.c and V.05.c were tested with the purpose of investigating the effect of different fire protectives. Thus, the same load configuration of V.03.u was used, even if a reductive scaling factor of ¾ was adopted (see Table 5). For those vaults, two concentrated loads were applied in the proximity of the midspan.

In all the cases, temperatures at different depths within the cross-section and displacements at certain points of the structures were measured. The acquiring system are compared in Table 6. These tests provide important information for the development and validation of thermal and mechanical response models.

Finally, as shown in later chapters, although all tests were stopped before reaching the actual collapse of the structures, these durations can be used as a lower limit of the fire resistance of the vaults.
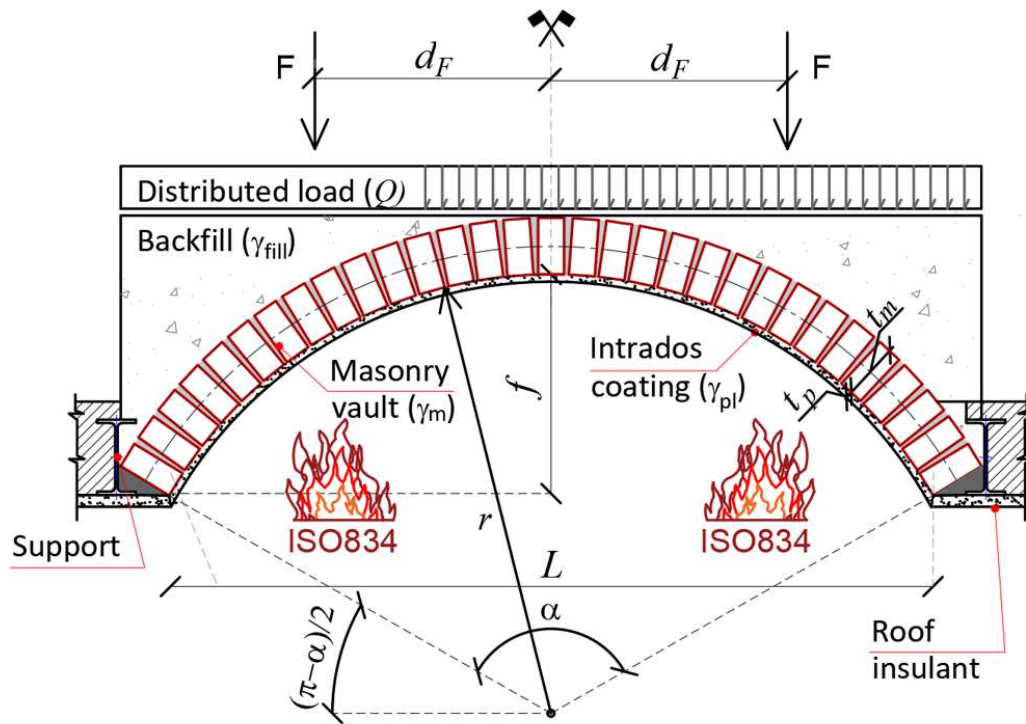
Figure 40 - The generic cross-section of a curvilinear masonry vault specimen [135].

Table 4: Geometrical properties of masonry curvilinear prototypes [135].

Parameters	*V.01.u*	*V.02.u*	*V.03.u*	*V.04.c*	*V.05.c*
L (mm)	2200	2200	1611	1610	1610
f (mm)	483	483	465	465	465
t_m (mm)	120	120	120	115	115
t_p (mm)	0	0	0	10	15
w (mm)	1000	1000	2000	1500	1500
r (mm)	1490	1490	930	930	930
α (°)	95	95	120	120	120

Table 5: Material properties and load configuration of masonry curvilinear prototypes [135].

Parameters	V.01.u	V.02.u	V.03.u	V.04.c	V.05.c
γ_m (kN/m^3)	17.00	17.00	17.00	17.00	17.00
γ_{pl} (kN/m^3)	0	0	0	14.50	3.60
γ_{fill} (kN/m^3)	13.75	20.00	0	0	0
Q (kN/m^2)	0	2.10	0	0	0
F (kN)	0	0	2×9.20	2×6.90	2×6.90
d_F (mm)	0	0	500	500	500

Table 6: Position and number of thermocouples used during the experimental investigations. (Distances are referred to the intrados)

Parameters	V.01.u	V.02.u	V.03.u	V.04.c	V.05.c
Intrados	6	6	9	5	5
50 mm	0	0	9	5	5
60 mm	4	4	0	0	0
75 mm	0	0	9	5	5
Extrados	6	6	9	5	5

Chapter 3

Simplified calculation method

In this chapter, a simplified calculation model for the evaluation of the fire resistance R of masonry barrel vaults or arches is proposed[1]. The simplified model is based on the limit analysis approach briefly introduced in §1.5. The goal is to compute the number of acceptable thrust lines taking into account the reduction of cross-sectional thickness and the change in compressive strength in the inner zones due to fire exposure.

Firstly, the basic assumptions on which it is based are discussed. Next, the calculation algorithm for the thermal and mechanical responses are examined.

---

[1]*Part of this chapter has been previously published in:*

3. Fantilli, A.P. and Burello, N.S. (2022) 'Masonry arches and vaults under fire', Journal of Building Engineering, Vol. 56, 104740.
4. Fantilli, A.P. and Burello, N.S. (2023) 'Experimental and numerical analyses of curvilinear masonry structures exposed to high temperatures', January 2023International Journal of Masonry Research and Innovation 1(1):1 DOI: 10.1504/IJMRI.2023.10055405

As described in the following sections, the model consists of three stages: structural discretization, calculation of thrust lines, and fire assessment.

Finally, the numerical model is used to evaluate the fire resistance R of the masonry barrel vaults previously described in Chapter 2.

3.1 Assumptions

As stated by the well-known Heyman's Safe Theorem [75], the curvilinear masonry structure can be considered "safe" if it is possible to define, by calculation or graphical method, at least one Line Of Thrust (hereinafter *LOT*) which entirely lies within the masonry arched profile. More precisely, the original assumptions of this theorem are:

i) the structure is made of compressive-only material (no tensile strength);

ii) the material constituting the masonry has infinite compressive strength;

iii) the shear failure mechanism cannot occur (sliding between the blocks is negligible).

According to these criteria, the arch system can fail only in the case of the formation of the so-called four-hinge mechanism. To extend this method to curvilinear masonry structures exposed to fire action, it is necessary to verify if the basic assumptions and the adopted failure mechanism are still valid.

3.1.1 No-tension material

Starting with the first assumption (i), it is generally known that units and mortar present a low tensile strength which becomes negligible when they are assembled to construct masonry structure.

In fact, bricks and mortar present generally modest tensile strengths. In [31], a average tensile strength of 0.64 MPa with standard deviation of 0.15 MPa for the clay bricks (see Fig.41a), whilst the average tensile strength of mortar was 0.25 MPa (s.d. = 0.04 MPa, see Fig.41b). Furthermore, brick/mortar interface has a very low tensile strength already at room temperature. As an example, Fig.41c-d shows the results of an experimental campaign carried out to evaluate some of the bond strengths of the brick / mortar interface. The units stacked with lime or cement mortars were tested under uniaxial tensile test at room temperature, as depicted in

Fig.41c. Very low strengths with not negligible scatter were measured for all the binder to sand ratios, as shown in Fig.41d.

In addition, even if for refractory purposes, recent study [139] investigated the tensile and shear strengths of the brick/mortar interface when subjected to high temperatures. For one type of the investigated masonry, the bond was so weak at room temperature (roughly 0.2 MPa) that uniaxial tensile tests at elevated temperatures were not carried out at all.

The authors stated that "*The tensile strength can be considered as zero whatever the temperature*". Thus, especially under fire conditions this contribution shall be disregarded from a structural point of view.

(a)   (b)   (c)

(d)
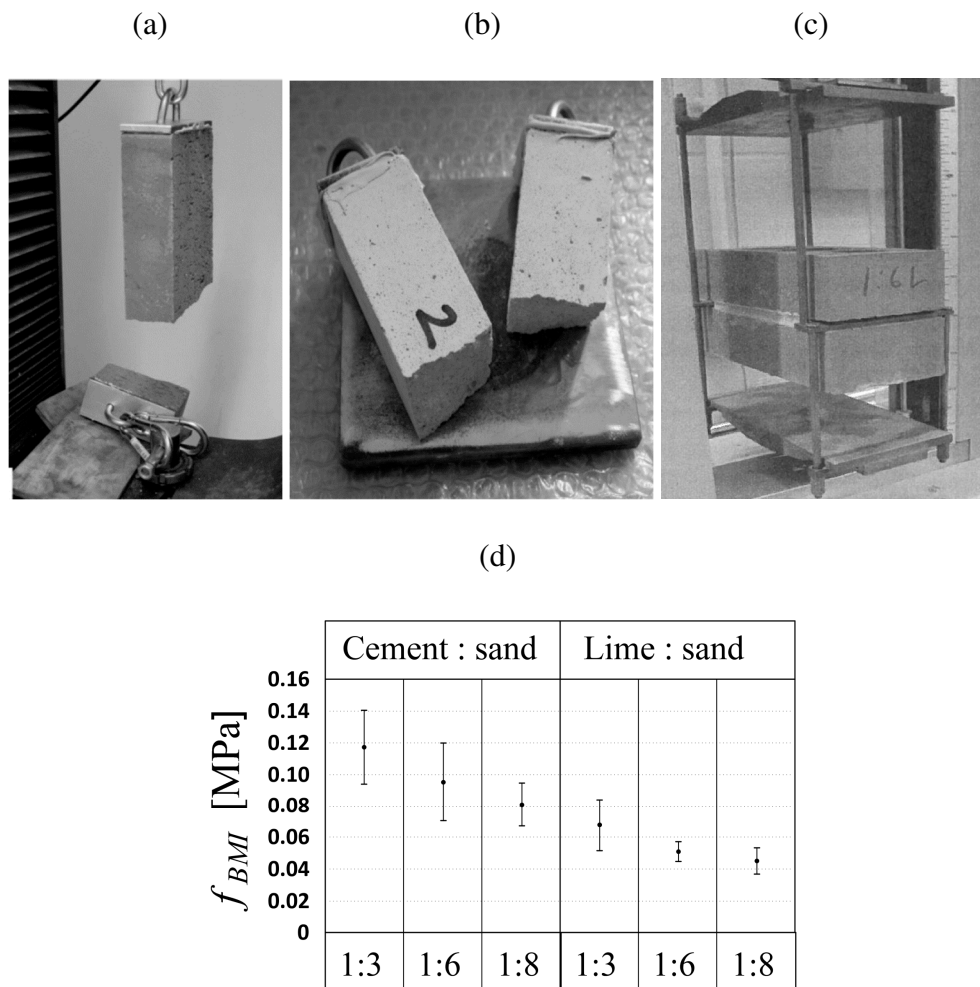
Figure 41 - Direct tensile test carried out on (a) clay bricks 290×140×65 mm^3 having f_b > 20 MPa [30]; (b) mortar prism 40×40×160 mm^3 [30]. (c) Direct tensile test on bond

strength between brick and mortar interface [29]; (d) Means and standard deviations of the tensile bond strength results (Figure redrawn from [29]).

3.1.2 Infinite compressive strength

Considering the infinite compressive strength (ii), the assumption may appear unsafe. It was introduced because the compressive stresses generated within the masonry are often so low compared to the compressive strength of the materials.

This assumption allowed the LOTs to pass exactly over the lower or upper edges of the resistant sections, effectively creating infinite stresses (see Fig.42.(i)). While some authors recommended taking this effect into account by reducing the resistant section a priori, Harvey [140-141] and other authors [142-143] proposed adopting the actual strength of the material. In this way, assuming a perfectly plastic constitutive law in compression (see Fig.1c), the acting normal stress is balanced by an equivalent stress block in the vicinity of the plastic hinges. This solution, with its pros. [144] and cons. [145], seems to fit very well the development of a simplified calculation model for masonry under fire conditions. In fact, in the event of fire exposure, building materials are subjected to progressive degradation of the compressive strength (see Fig.3c and Fig.6) to such an extent that current standards [1] requires to disregard the compressive strength above a prescribed temperature (see Table 2). For this reason, assuming the actual compressive strength of the masonry (i.e., cold compressive strength) in order to assess ineffective and residual zones, it is of a paramount importance in the event of fire, as shown in Fig.1.
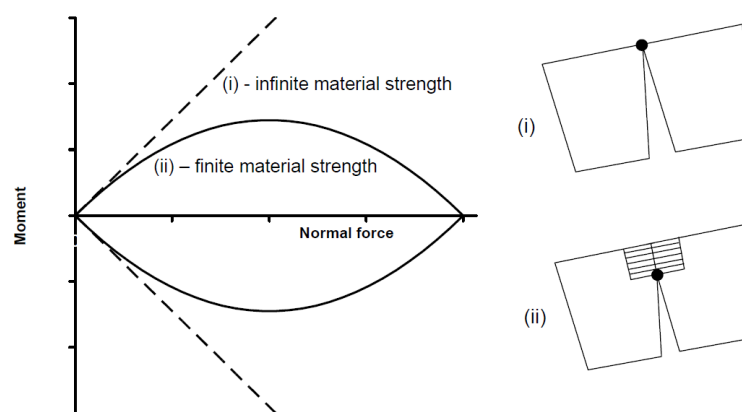
Figure 42 - Contact surface moment vs. normal force failure envelopes for (i) infinite or (ii) finite masonry. (Source: [143])

3.1.3 Shear failure

Many numerical models still used nowadays are based on the assumption of infinite friction (iii), namely mutual sliding between blocks cannot occur. As witnessed by several experimental campaigns [101-123], this assumption seems to be valid at least for unstrengthened masonry arches, while shear failure (as well as crushing of masonry) also occurred in the case of arches consolidated with high-performance materials, as shown in Fig.43. Considering the fire tests described in chapter 2, these phenomena were not observed in any investigation. Moreover, the vaults settled back into their original position once they returned to ambient conditions (i.e. after the cooling phase). Thus, also according to the simplified approach proposed by the current standard [1], this assumption is maintained in the proposed simplified numerical model.

(a)   (b)

(c)
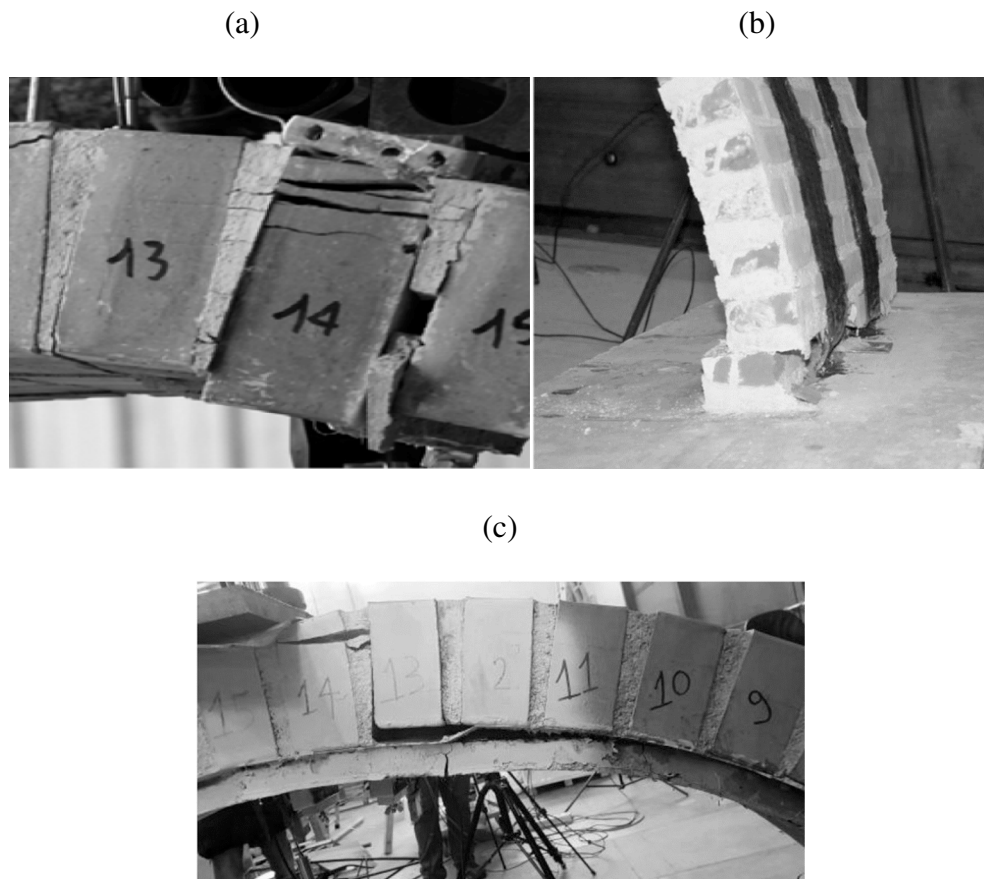
Figure 43 - Sliding between blocks and mortar joint in case of strengthened masonry arches (Sources: (a) Sacco et al. [111]; (b) Oliveira et al. [112]; (c) Zampieri et al. [119]).

3.1.4 Four-hinges mechanism

Masonry vaults exhibited extensive cracking phenomena in the vicinity of the midspan without any sliding being recorded, to which the formation of so-called plastic hinges can be attributed [134].

In order to understand the behavior of masonry arched structures exposed to fire, the tests conducted on *V.01.u* and *V.02.u* are taken as a reference. In fact, the sensors based on 6 points arranged along the whole span length, make it possible to predict the global kinematic of the structure.

Figures 44a and 45a show the vault displacements recorded during the fire exposure in accordance with Fig.22 e Fig.23, respectively. By arranging the displacements along the profile of the vaults, the presence of further hinges can be assumed in addition to that observed in the centerline. As the sign of the deflection changes (from raising to settlement) moving from the crown to the springers, further hinges must be localized in between. As hypothesized qualitatively in Fig.44b and Fig.45b, the presence of at least three hinges is necessary for the vault to be subject to displacements compatible with those measured.

From the standpoint of conventional structural analysis, considering the arched structure with three redundancies when unloaded, three plastic hinges turn the vault into a statically determinate structure.
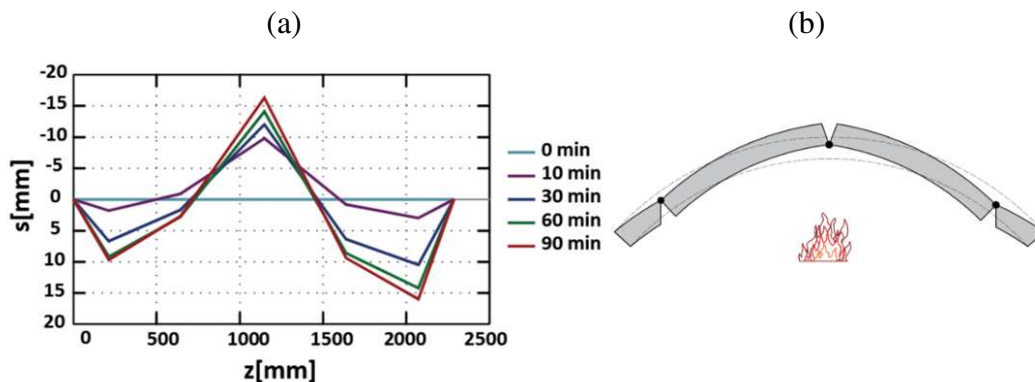
Figure 44 - (a) Displacements measured during the fire exposure in vault *V.01.u*; (b) Qualitative distribution of hinges in *V.01.u.*

(a)   (b)
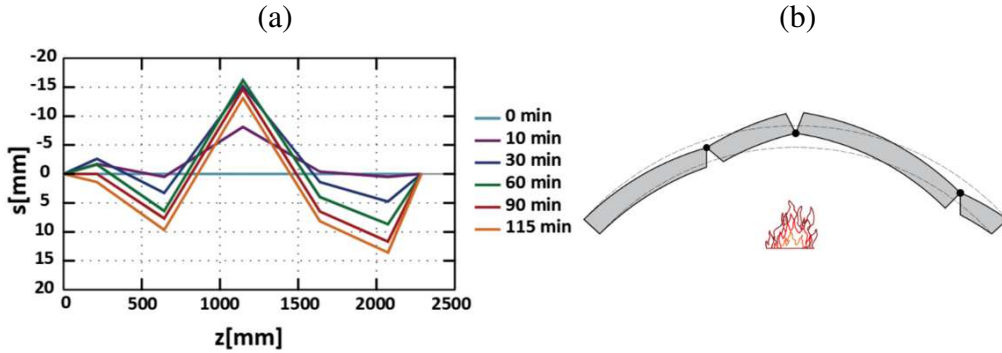
Figure 45 - (a) Displacements measured during the fire exposure in vault *V.02.u*; (b) Qualitative distribution of hinges in *V.02.u.*

Similar to unreinforced arches subjected to direct loads [101-123] , it appears reasonable to assume that the failure of curvilinear structures is produced by the four-hinge mechanism also under the fire action.

3.2 The algorithm

In the following sections, several equations are introduced to calculate the main parameters. For a better understanding of them, readers should refer to the International System of Measurement. Displacements are expressed in mm, concentrated forces in N, stresses in MPa (1 MPa = 1 N/mm^2), distributed loads in N/mm^2, density in N/mm^3, time in seconds and temperature in °C.

3.2.1 Structural discretization

In the case of curvilinear structures with an axis of symmetry, only one of the halves can be analyzed (Fig.46). It is divided into N blocks, starting from the support ($i = 1$) up to the keystone ($i = N$). The forces (i.e., $P_{G1,i}$ = self-weight, $P_{G2,i}$ = permanent load due to the backfill material, $P_{Qv,i}$ = live loads, P_I = concentrated load applied to the Ith cross-section) acting on the ith block ($1 \leq i \leq N$) are calculated with the following equations:

$$P_{G1,i} = \frac{\gamma_{G1} \cdot \Delta z \cdot \frac{H_{b,I}+H_{b,I-1}}{2} \cdot b_1}{\cos(\alpha_i)} \tag{6}$$

$$P_{G2,i} = \gamma_{G2} \cdot b_2 \cdot \Delta z \cdot \frac{\left[\left(y_{sup,I-1}-y_{I-1}-\frac{H_{b,I-1}}{2 \cdot \cos(\alpha_{i-1})}\right)+\left(y_{sup,I}-y_I-\frac{H_{b,I}}{2 \cdot \cos(\alpha_i)}\right)\right]}{2} \tag{7}$$

$$P_{Qv,i} = Q_v \cdot b_3 \cdot \Delta z \qquad (8)$$

where γ_{G1} = density of the structural material; γ_{G2} = density of the backfill material; Q_v = live load; b_1 = width of the masonry cross section; b_2 = width of the backfill material; b_3 = width used to compute the live load; $H_{b,I}$ = height of the Ith cross-section (I and I-1 refers to the limits of the ith block); $\Delta z_i = z_I - z_{I-1}$ = length of the ith block; α_i = angle of inclination of the ith block; $y_{sup,I}$ = ordinate of the upper edge of the backfill material in correspondence of the Ith cross-section.

The resultant of the vertical loads R_{TOT} and its distance z_{Rtot} from the origin (of [ZY] axes) are calculated as:

$$R_{tot} = \sum_{i=1}^{N} R(i) = \sum_{i=1}^{N} P_{G1,i} + P_{G2,i} + P_{Qv,i} + P_I \qquad (9)$$

$$z_{Rtot} = \frac{\sum_{i=1}^{N} R(i) \cdot z_R(i)}{R_{tot}} = \frac{\sum_{i=1}^{N} R(i) \cdot \left[z_{i-1} + \frac{P_{G1,i} \cdot d_{PG1,i} + P_{G2,i} \cdot d_{PG2,i} + P_{Qv} \cdot d_{PQv,i} + P_I \cdot \Delta z_i}{R(i)} \right]}{R_{tot}} \qquad (10)$$

where $R(i)$ = resultant of the ith block; $z_{R(i)}$ = distance of $R(i)$ from the origin of [YZ] axes; $d_{PG1,i}$, $d_{PG2,i}$ and $d_{PQv,i}$ are, respectively, the distances of the forces $P_{G1,i}$, $P_{G2,i}$ and $P_{Qv,i}$ from the Ith-1 cross-section (see Fig.46).
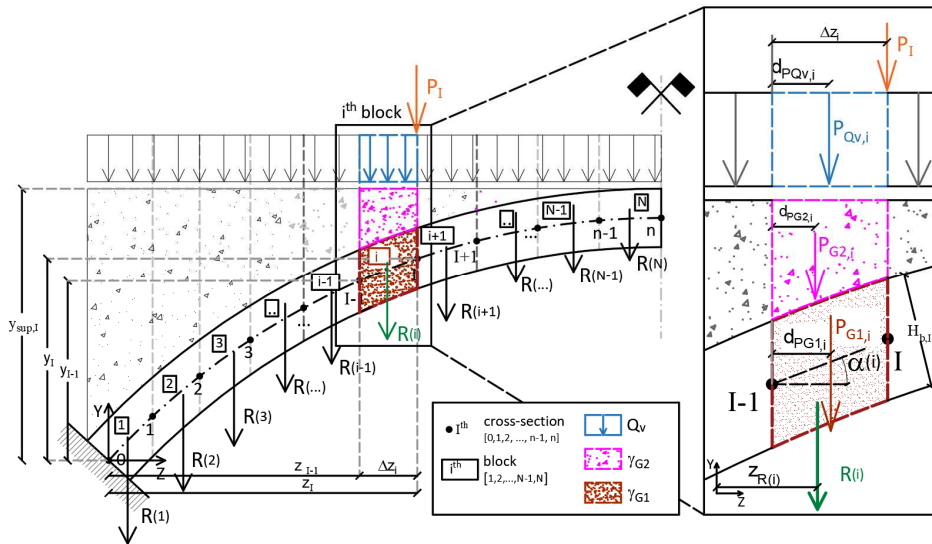
Figure 46 - Discretization of a generic curvilinear structure with an axis of symmetry.

3.2.2 Calculation of the lines of thrust

The development and application of the following calculation is based on one of the experimental findings previously discussed in Chapter 2, namely the masonry vaults were not affected by the detachment and fall of material from the exposed side for the whole duration of the fire. Thus, under the hypothesis that spalling does not occur, the forces previously defined remain constant during the exposure to elevated temperatures. As illustrated in Fig.47, the geometry of each LOT is a function of the points of passage "A"- in correspondence of the support ($I = 0$), and "B" – on the axis of symmetry ($I = n$).

A and B can assume any position within the height of the two cross sections, moving from the intrados ($j = 0$) to the extrados ($j = m$, where m = number of points used to divide the height $H_{b,I}$). In particular, the coordinates of these points are:

$$point\ A \begin{cases} z_k(A) = z_0 + \frac{H_{b,0}}{2} \cdot \sin \alpha_0 - \frac{H_{b,0}}{m} \cdot \sin \alpha_0 \cdot j \\ y_k(A) = y_0 - \frac{H_{b,n}}{2} \cdot \cos \alpha_0 + \frac{H_{b,n}}{m} \cdot \cos \alpha_0 \cdot j \end{cases} \quad j = 0,1,\dots,m \quad (11)$$

$$point\ B \begin{cases} z_k(B) = z_N \\ y_k(B) = y_N - \frac{H_{b,n}}{2} + \frac{H_{b,n}}{m} \cdot j \end{cases} \quad j = 0,1,\dots,m \quad (12)$$

where $1 \le k \le m \times m$ refers to the kth LOT calculated after fixing the points A and B (see Fig.2). For each couple of these points, the intensity of the horizontal force H_k, the angle of inclination β_k, and the reaction S_k of the support can be calculated as follows:

$$\tan(\beta_k) = \frac{z_{Rtot} - z_{k(A)}}{y_{k(B)} - y_{k(A)}} \tag{13}$$

$$H_k = R_{tot} \cdot \tan(\beta_k) \tag{14}$$

$$S_k = \sqrt{R_{tot}^2 + H_k^2} \tag{15}$$

Accordingly, each LOT is a polygonal line with *N+2* points, including A, B, and the points that lie on the lines of action of the resultants $R(i)$. For the kth line of thrust, the intensity of the force $S_{k,w}$, the inclination $\beta_{k,w}$ (with respect to the horizontal direction), and the coordinates of wth node are:

$$S_{k,w} = \sqrt{\sum_{i=w+1}^{N} R(i)^2 + H_k{}^2} \tag{16}$$

$$\tan(\beta_{k,w}) = \frac{\sum_{i=w+1}^{N} R(i)}{H_k} \tag{17}$$

$$w = \begin{cases} z_k(w) = z_R(w) \\ y_k(w) = y_{w+1} - \tan(\beta_{k,i}) \cdot \left(z_k(w+1) - z_k(w)\right) \end{cases} \quad if \ w = 1, \dots, N \tag{18}$$

The calculation is repeated for each combination of A and B, obtaining $m \times m$ lines of thrust.
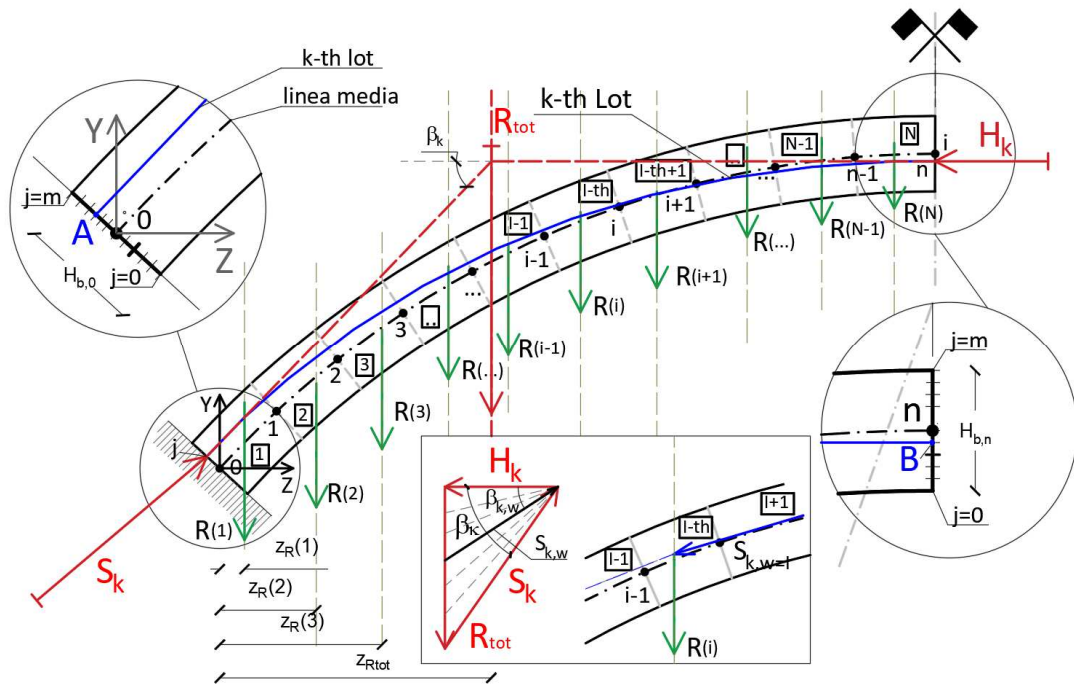
Figure 47 - Computation of the kth line of thrust (A and B are arbitrarily assumed).

3.2.3 Fire assessment

Although the points A and B are always within the cross sections (imposed condition, see Fig.47) at $I = 0$ and $I = N+1$, respectively, not all the $m \times m$ lines of thrust are acceptable. In fact, for a given fire duration, some parts of LOT may fall outside the resisting longitudinal section. In addition, the applied actions $S_{k,w}$ can generate compressive stresses higher than the material strength [140].

To take into account both these situations, the thickness of the ineffective cross section can be calculated by following the reduced cross section approach, currently adopted for vertical members (see Eurocode 6 Part 1-2 [1]).

Referring to Fig.1, the part of the cross section having a temperature $T > \theta_2$ (A_{ineff} in Fig.2b) is ineffective, therefore the design value of the compressive strength is $f_d = 0$. In the coldest zone (A_{res} in Fig.2b), $T < \theta_1$ and $f_d = f_{d\theta1} = f_m(20°C)$ (namely the compressive strength measured at 20°C). When $\theta_1 \leq T \leq \theta_2$, the masonry is partially damaged, and an intermediate strength $f_d = f_{d\theta2} < f_{d\theta1} = f_m(20°C)$ shall be assumed. In the case of "Clay units with general purpose mortar", $\theta_2 = 600°C$, $\theta_1 = 100°C$, and $f_{d\theta2} = f_{d\theta1} \times c_{cl}$ (see Table 2), where the value of the reductive factor c_{cl} shall be assumed according to National Annexes of Eurocode 6 1-2 [1].

Thus, knowing the temperature profiles $\theta_1(t)$ and $\theta_2(t)$, and assuming uniform radial heat diffusion over the soffit of the vaulted element, it is possible to know the thicknesses of the ineffective, damaged and residual zones in each exposure period.

As the temperature gradient increases within the masonry arch profile, the ineffective thickness t_{ineff} increases in turn. As a consequence, the number of LOTs which fall within the resisting zone tends to reduce. For instance, in Fig.48a the LOTs colored in blue are acceptable, whereas those in red fall outside the resisting thickness and cannot be accepted.

The selection of the LOT has to be based also on the general properties of masonry materials. Assuming no tensile strength and the absence of shear failure, the acceptability criterium of the blue curves must furtherly include the assessment of compressive stress $\sigma_{Ed,w}$, which should be lower than f_d in each node. Fig.48b illustrates the resisting section in the wth node of the kth thrust line, for which the following condition has to be satisfied:

$$\sigma_{Ed,w} = \frac{S_{k,w}}{b \cdot 2 \cdot \bar{e}_{k,w}} < f_d \tag{19}$$

where $\bar{e}_{k,w} = (H_{b,I} - t_{ineff})/2 - e_{k,x}$ and $e_{k,w}$ = eccentricity of the force $S_{k,w}$.

The way to use $f_{d\theta2}$ and $f_{d\theta1}$ (see Fig.1c) for the verification of Eq.19 is postponed in the following sections, where the values of θ_l, θ_2 and c_{cl} for the validation of the numerical model are discussed.

(a)   (b)
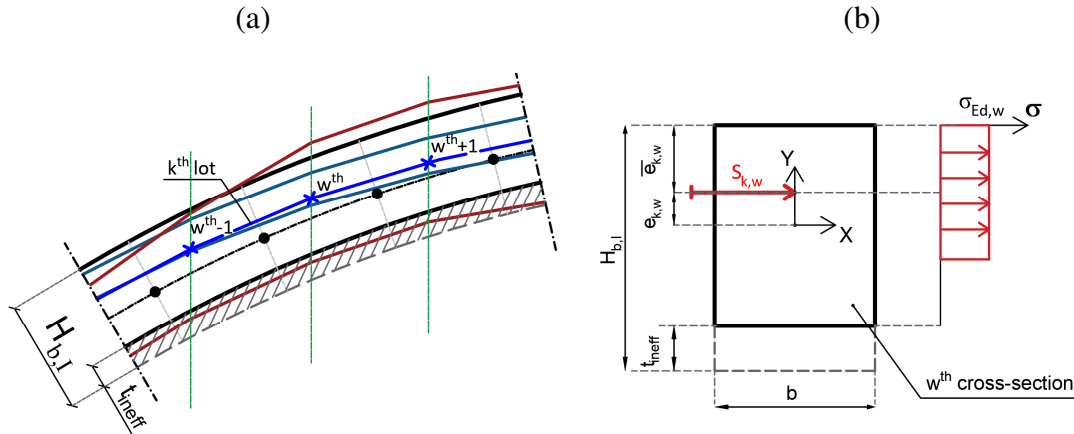
Figure 48 - Acceptable lines of thrust with respect to (a) longitudinal section of the vault and (b) with respect to the wth cross-section.

As the resisting cross-section thickness of the curvilinear structure reduces with the exposure to elevated temperatures, the fire resistance R can be evaluate as the period of time (expressed in minutes) at which at least one LOT satisfies the assessment criteria previously described.

3.2.4 Thermal response models

To apply the LOT approach in combination with the residual cross-section method, it is necessary to model the thermal response of the structure. In this section, the simplified tabulated method [1] currently used for masonry wall is firstly extended to curvilinear masonry structure [134]. Following, a more rigorous thermal model, based on a finite difference method (FDM) [146], has been developed and implemented [136].

3.2.4.1 Simplified thermal analysis

As described in Chapter 1, current standard [1] provides simplified diagrams which illustrate the temperature profiles at stated period of exposure, as a function

of the type of material used to assemble the wall. The use of these data is allowed in the absence more refined information provided by test results. Therefore, no computation is required for the definition of isotherms in masonry.

As an example, Fig.2 illustrates the temperature distributions for masonry made with clay units and general purpose mortar. Thus, considering $\xi = 0$ mm as corresponding to the inferior surface of the vault exposed to fire, it is possible to define t_{ineff}, t_{red} and t_{res} at stated periods of exposure, when θ_2, θ_l and c_{cl} are assumed.

In the present work, those parameters are assumed according to the Italian Annex [147] which states (the following the text has been translated by the author from the Italian language):

"*while pending for new experimental evidences, the application of the simplified method set out in Annex C of Eurocode 6 1-2 [1], for the fire resistance classification of structural elements subject to fire brigade inspections, can be applied independently of the structural element considered, cautiously setting the parameter "$f_{d\theta2}$" equal to zero in the intermediate temperature zone*".

In other words, the National Annex [147] permits the use of the simplified method (including simplified heat mapping) for the evaluation of any kind of masonry structure (including curvilinear-axis structures) provided that any masonry contribution is supposed to be zero where a temperature $T > \theta_l$ is reached (i.e., $c = 0$ for any kind of masonry, see Table 2).

Thus, the thickness of the cross section at temperatures higher than θ_l (e.g., $\theta_l = 100°C$ in the case of clay masonry structures) is ineffective.

3.2.4.2 Advanced thermal analysis

During a fire, heat transmission occurs by means of various physical phenomena [60] depending on the medium through which it passes, as described below:

- convection and radiation in the environments in contact with the structural element;

- conduction, through the solid part of the structure;

- radiation, within the voids if present (i.e., no convection motion occurs).
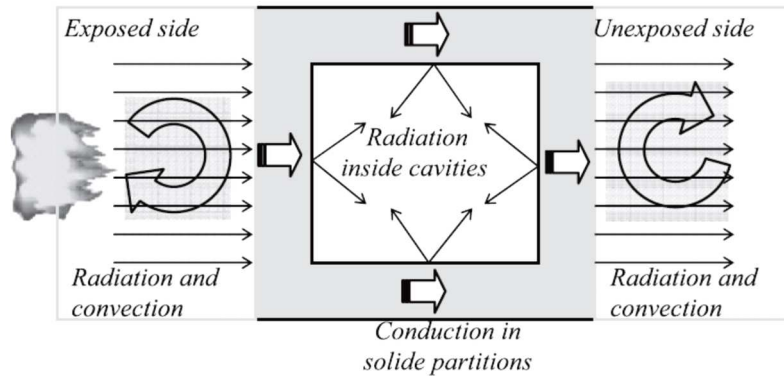
Figure 49 - Heat transfer process from the fire environment to the unexposed side of the structural element (Source [60]).

In vaults and arches made with solid units, the thermal analysis can be performed assuming a radial heat conduction through the thickness of the masonry, uniformly distributed along the curvilinear profile. According to the first law of heat conduction, known as Fourier's law [148], the flux of heat in a homogeneous body is in the direction of, and proportional to, the temperature gradient:

$$\frac{\partial T}{\partial t} = \beta \frac{\partial^2 T}{\partial \xi^2} \tag{20}$$

where t = time; T = temperature; ξ = distance from the intrados (see Fig.1a); β = $\lambda/(\rho\,c_a)$ = thermal diffusivity; λ = thermal conductivity; c_a = specific heat capacity; and ρ = gross dry density.

As the thermal properties of masonry (i.e., λ, ρ and c_a) are temperature-dependent parameters, their curves are assumed in accordance with Annex D of Eurocode 6 Part 1-2 [1]. More precisely, all these parameters are normalized with respect to the values at 20°C (see Fig.3a), which are herein assumed as $\lambda_{20°C} = 0.42$ W/m K, $c_{a,20°C} = 564$ J/kg K, and $\rho_{20°C} = 1700$ kg /m^3.

Eq.(20) may be solved using the forward finite difference method. As shown in Fig.50, after discretizing the time t and the distances along the coordinate ξ (n = maximum number of $\Delta\xi$, m = maximum number of Δt), the temperature of the ith point at the $j+1^{th}$ time can be calculated as follows:

$$T_{i,j+1} = \beta\varphi \cdot T_{i-1,j} + (1 - 2\beta\varphi) \cdot T_{i,j} + \beta\varphi \cdot T_{i+1,j} \tag{21}$$

where $\varphi = \Delta t \, / \, \Delta \xi^2$ (see Fig.51); $0 \leq i \leq n$ and $0 \leq j \leq m$.

It is worth noting that, in order to guarantee the stability of the numerical calculation, the following inequality must be fulfilled:

$$\Delta t \leq \frac{1}{2} \Delta \xi^2 \qquad\qquad\qquad (22)$$
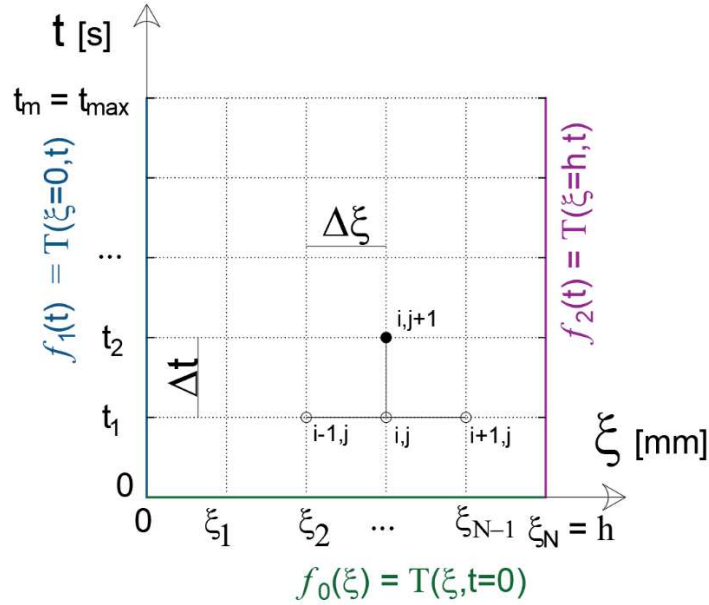
Figure 50 - Finite difference method for the calculation of temperature distributions

In other words, for each instant j and point i within the cross-section, it is possible to calculate the temperature at the next time step $T_{i,j+1}$, starting from three adjacent values of temperatures: $T_{i-1,j}$, $T_{i,j}$ and $T_{i+1,j}$. The whole temperature distribution is obtained by means of an iterative procedure moving from $j = 0$ to $j = m$-1, and from $i = 1$ to $i = n$-1 (see Randall [149] for further details).

However, the following boundary conditions are required:

- temperature profile at the intrados $f_1(t)$ during the fire exposure;
- temperature profile at the extrados $f_2(t)$ during the fire exposure;
- temperature profile along the cross-section $f_0(\xi)$ in absence of fire (i.e., the environmental temperature).

In the following sections, these functions are respectively imposed in compliance with the average values experimentally measured (T_{mean}) for each vault when the fire resistance R is calculated adopting the advanced thermal model.

3.3 Numerical predictions and experimental outcomes

To validate the simplified model proposed in this section, the predicted loadbearing capacities are compared with those experimentally measured in several tests. Firstly, an experimental test carried out by other authors [119-120] is used as reference. It consisted of an unreinforced masonry arch subjected to only concentrated load monotonically increased up to failure. In this case, the model is used to predict the ultimate and thus, to preliminarily validate the numerical model in the case of ordinary actions. A parametric analysis on the two main geometrical input for discretization of the structure (namely the number of the blocks and the points of passage of the LOTs) is also carried out.

Thereby, the model is used to evaluate the fire resistance (expressed in minute) of the masonry vaults previously described in Chapter 2, which were tested under various static loads and exposed to fire at the intrados. Both simplified and advanced thermal models are used and the different numerical predictions of R are compared.

3.3.1 Masonry arch without fire action

Zampieri et al. [120] measured the ultimate load of the unstrengthened masonry arch depicted in Fig. 51a. According to the scheme reported in Fig.40, the masonry arch had $L = 1430$ mm, $f = 610$ mm, $t_m = 110$ mm, $w = 245$ mm, r = 720 mm, $\alpha = 164°$, a density $\gamma_m = 16.00$ kN/m^3. The cold mechanical characterization measured a mean compressive strength of 19.5 MPa, whereas the load P, applied in the arch crown, was monotonically increased up to the failure (ultimate load $_{Pu} = 0.44$ kN).

As the test was carried out at environmental temperature (20°C), the proposed model is only used to estimate Pu (i.e., $t_{ineff} = 0$ mm for each step of load), in correspondence of which none of the computed LOT is acceptable. However, to perform a correct limit analysis, suitable values of N (i.e., number of blocks - Fig.46) and m (i.e., points of passage of LOTs - Fig.47) must be used, because numerical outcomes may be affected by these parameters.

(a)

(b)   (c)
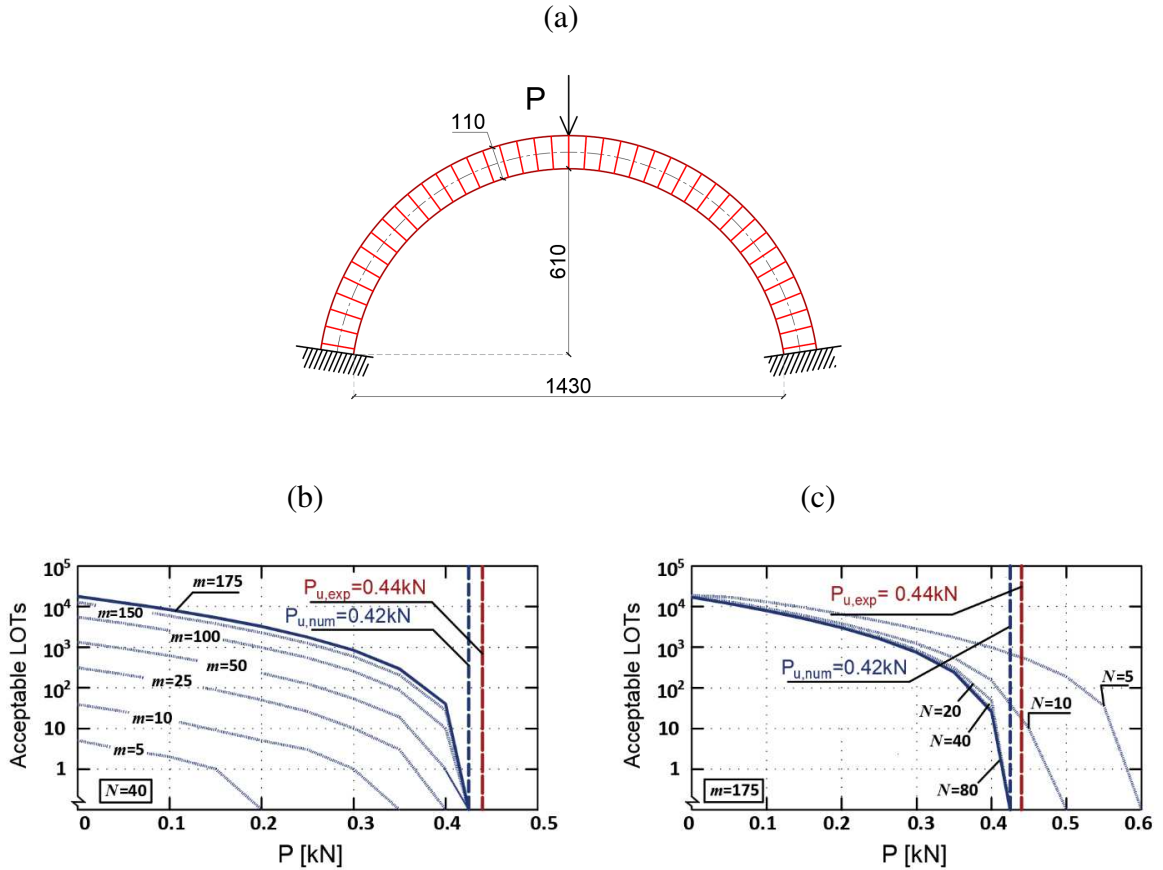
Figure 51 - Masonry arch subjected to monotonically increased load applied in the midspan: (a) Geometry of the arch [120]; (b) Numerical results as a function of the number of LOTs - $m \times m$. (c) Numerical results as a function of the number of blocks – N.

Fig.51b, where the number of favorable LOTs is plotted as a function of the applied load P, shows the variation of the predicted loadbearing capacity when m varies (in this case $N = 40$). Similarly, when m is fixed, P_u depends on the number of blocks in which the semi-arch is divided (see Fig. 51c, with $m = 175$). Nevertheless, when $m \geq 50$ and $N \geq 20$, the mesh dependence vanishes, and the proposed model estimates an ultimate load $P_{u,num} = 0.42$ kN close to that experimentally measured (i.e., $P_{u,exp} = 0.44$ kN). Obviously, the values of m and n are not the same for all the geometries (especially referring to span length and thickness) of arches and vaults, thus new analyses must be iteratively performed by increasing m and N until the numerical results do not change.

3.3.2 Masonry vaults with fire

In this section, the simplified model is used to evaluate the fire resistance of the masonry vaults reported in Chapter 2. Since the tests did not lead to the actual collapse of the prototypes, it was only possible to define the minimum R provided by these structures as summarised in Table 7.

The fire assessment of the vaults herein investigated is performed by assuming m = 200 points of passage of LOTs (see Fig.47), in correspondence of the midspan and springer cross-sections (i.e., computing a total of 40000 LOTs), and discretizing the structures in N = 80 blocks [134]. For the size of the vaults herein investigated, such values are sufficient to obtain reliable results and a reasonable computational burden. For the geometrical properties describing the vault profiles, material properties and load arrangement, readers may refer to the summary tables reported in §2.5. For each vault, R is evaluated assuming three different hypotheses:

- Simplified thermal analysis namely according to the temperature profiles proposed by current standard [1] and reported in Fig.2. According to §3.2.4.1, the ineffective thickness of the vaults are determined assuming c_{cl} = 0 [147] and therefore $\theta_2 = \theta_l = 100°C$. The numerical prediction is labelled as "Smp_100°C" which stands for "simplified analysis with a limit temperature of 100°C";
- Advanced thermal analysis in accordance with §3.2.4.2, assuming c_{cl} = 0 [147] and $\theta_2 = \theta_l = 100°C$ (hereinafter "Adv_100°C");
- Advanced thermal analysis (§3.2.4.2), assuming $\theta_2 = 600°C$, $\theta_l = 100°C$ (see Table 2 [1]), and a reduction[2] factor $c_{cl} = 0.4$ ("Adv_600°C").

---

[2] A reduction factor c_{cl} = 0.4 is also taken into account. It has been chosen on the base of several experimental results available in the current literature. Compressive tests on cement-lime based mortar, clay units, and masonry prisms were carried out by means of HMC (i.e., under fire conditions – see Fig.6a) and RMC (i.e., residual conditions – see Fig.6b). By superimposing the mechanical properties of clay-masonry prisms and individual components, it is possible to observe that the highest damage is in cement-based mortars, in the proximity of 600°C. Thus, if mortar is the weakest part of the structure, masonry system should guarantee at least a residual compressive strength of 40% at 600°C (i.e., c_{cl} = 0.4 at θ_2 = 600°C) if high-strength cement-based mortars are not used [41, 49].

Table 7: Minimum fire resistance R of masonry vaults subjected to fire at the intrados (R is expressed in minutes)

	V.01.u	*V.02.u*	*V.03.u*	*V.04.c*	*V.05.c*
Fire resistance (R)	52	90	115	180	180

Accordingly, Fig.52a-Fig.56a illustrate some of the temperature profiles calculated by means of the advanced thermal analysis. It has to be reminded that the temperatures plotted in correspondence of $\xi = 0$ mm (i.e., the intrados) and of $\xi = 120$ mm (i.e., the extrados), are the actual temperatures registered during the fire tests, previously reported in Chapter 2. For each vault, the thermal analyses were performed assuming steps of 2 minutes-increment from, $t = 0$ min (i.e., absence of fire) to the whole duration of the fires simulated in the corresponding experimental tests (see Table7).

For each vault, the duration of the fire is considered as a lower-bound limit of the fire resistance. The experimental results (reported as red dashed lines and labelled with "End of test") are directly compared with the numerical predictions in Fig.52b-Fig.56b. The numerical curves are calculated with the aforementioned assumptions and are plotted with grey dashed curves (Smp_100°), light blue curves (Adv_100°), and the dark blue curves (Adv_600°).

It is worth mentioning that, in some cases, the experimental investigations were interrupted "too early", despite neither partial nor global collapse of the vaults occurred. For instance, in the case of *V.01.u*, it can be observed that fire exposure did not last enough to assess whether the model provides conservative estimations of fire resistance for any assumption made (see Fig.52b).

Referring to grey dashed curves (see Fig.52b-56b), the simplified thermal approach proposed by Eurocode 6 Part 1-2 [1] leads to more conservative results, even when compared to the advanced thermal mapping Adv_100°C where the reduction coefficient is still set $c_{cl} = 0$. In particular, the fire resistance of *V.04.c* (Fig.55b) and *V.05.c* (Fig.56b) is close to that obtained for *V.03.u* (see Fig.54b) and, therefore, fire protectives seem useless.
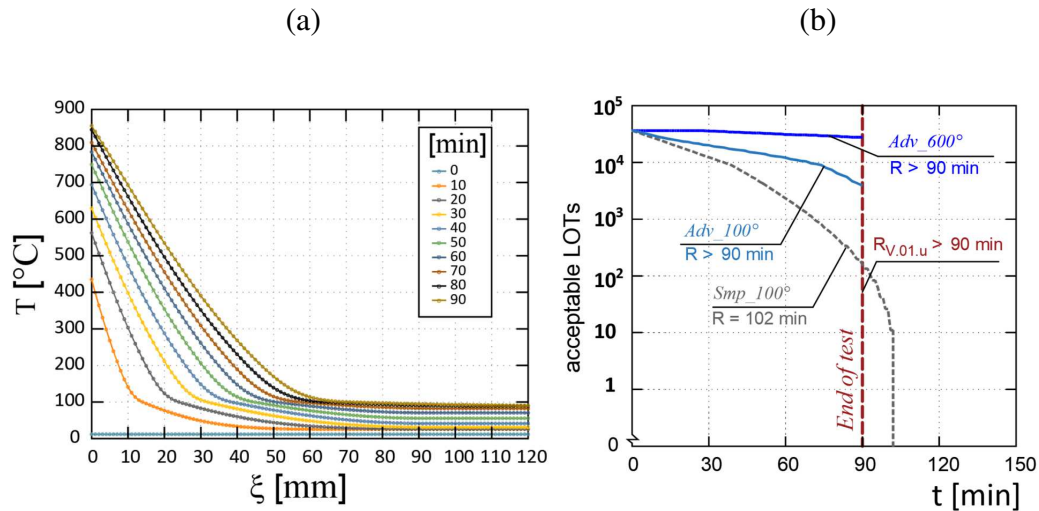
Figure 52 - Analysis of *V.01.u*: (a) Distribution of temperatures within the masonry thickness as a function of the time of exposure, calculated by means of advanced thermal analysis; (b) Comparison between experimental and numerical results. (Number of acceptable LOTs are plotted in a logarithmic scale).
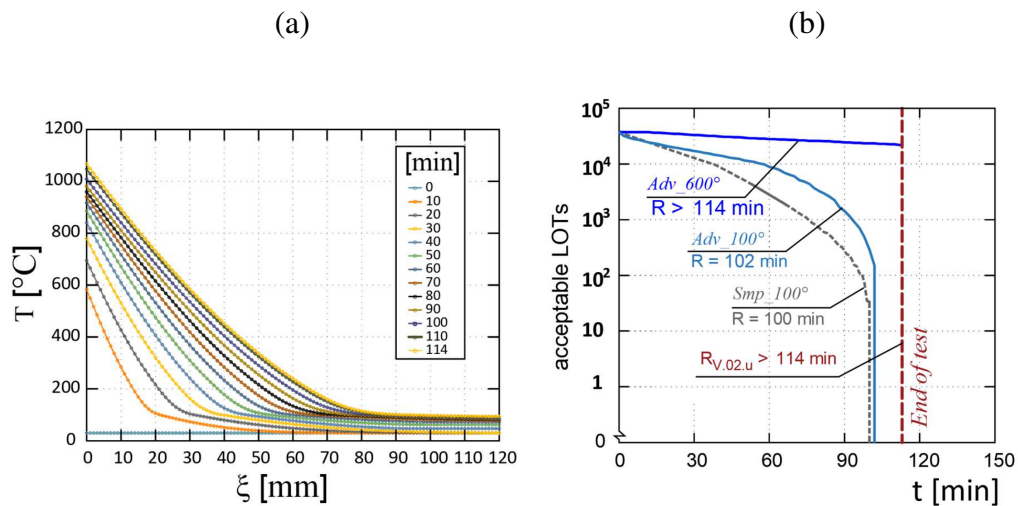
Figure 53 - Analysis of *V.02.u*: (a) Distribution of temperatures within the masonry thickness as a function of the time of exposure, calculated by means of advanced thermal analysis; (b) Comparison between experimental and numerical results. (Number of acceptable LOTs are plotted in a logarithmic scale).

(a)   (b)
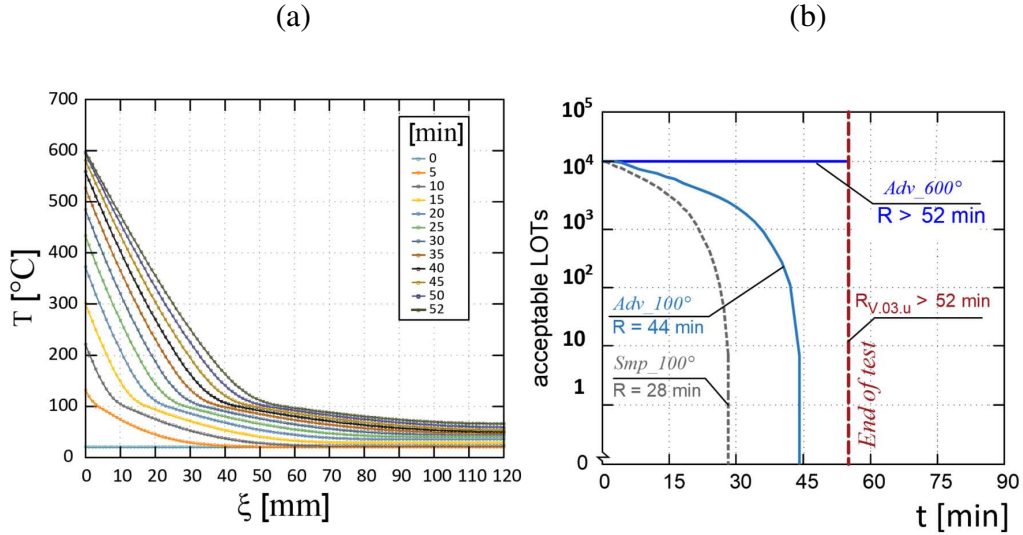
Figure 54 - Analysis of *V.03.u*: (a) Distribution of temperatures within the masonry thickness as a function of the time of exposure, calculated by means of advanced thermal analysis; (b) Comparison between experimental and numerical results. (Number of acceptable LOTs are plotted in a logarithmic scale).

(a)   (b)
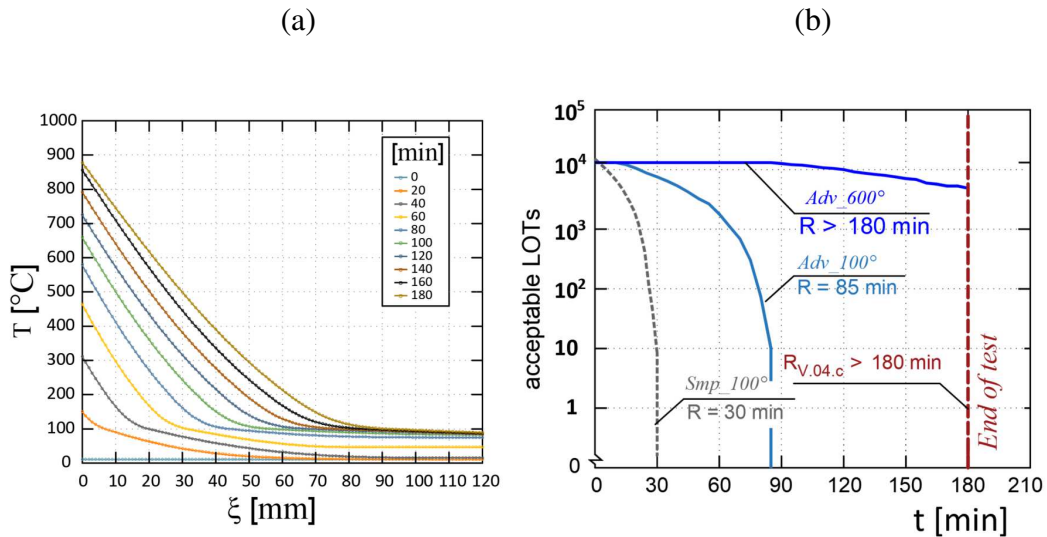
Figure 55 - Analysis of *V.04.c*: (a) Distribution of temperatures within the masonry thickness as a function of the time of exposure, calculated by means of advanced thermal analysis; (b) Comparison between experimental and numerical results. (Number of acceptable LOTs are plotted in a logarithmic scale).
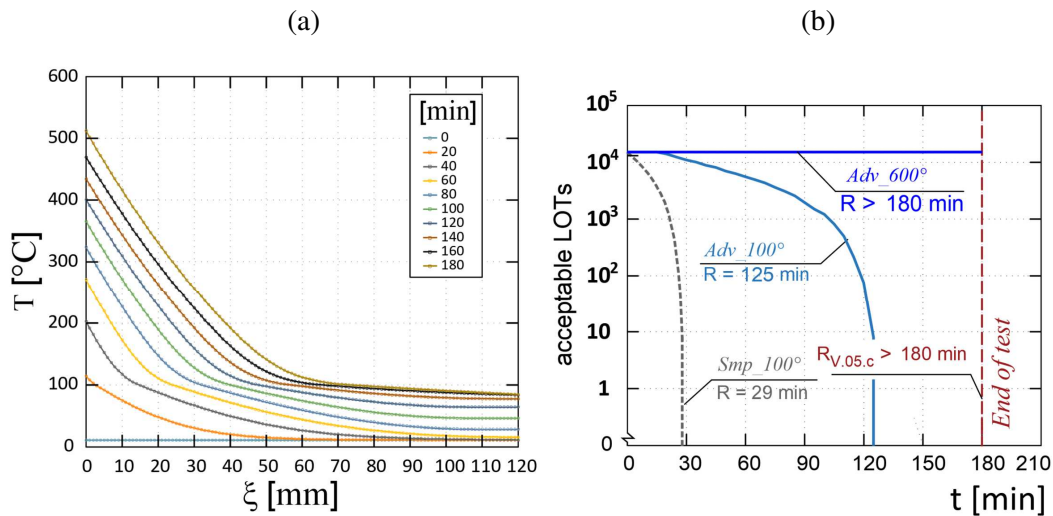
Figure 56 - Analysis of *V.05.c*: (a) Distribution of temperatures within the masonry thickness as a function of the time of exposure, calculated by means of advanced thermal analysis; (b) Comparison between experimental and numerical results. (Number of acceptable LOTs are

As expected, by assuming "tout court" the simplified mapping (Smp_100°C) does not allow for the consideration of any beneficial effects of layers of material interposed between the fire and the structural element.

On the contrary, maintaining the assumption $\theta_2 = 100°C$, but adopting a more refined thermal analysis (Adv_100°C), a better (even if conservative) estimation of the fire capacity R is provided (see light blue curves in Fig.52b-56b). Finally, as fire investigations did not last enough to achieve the maximum theoretical fire resistance, it is not possible to assess the effectiveness of numerical estimations when a reduction factor $c_{cl} = 0.4$ is assumed (dark blue curves). In some cases, only small decreases in the number of accepted pressure curves can be deduced by observing Fig.52b-53b, while in other cases the structure is apparently unaffected (see Fig.54b and Fig.56b).

3.4 Main findings

The results of the experimental and numerical analyses on masonry vaults, previously described, lead to the following conclusions:

- The absence of shear failures and the experimental evidences of the formation of the well-known plastic hinges at the brick-mortar interface lead to extend the approach currently used for the evaluation of masonry vault also in the event of fire.
- Reliable, but very conservative, predictions of the fire resistance are obtained when the analyses are performed assuming a reduction factor c_{cl} = 0 and the simplified thermal approach proposed in Eurocode 6 Part 1-2[1].
- A better evaluation of the fire resistance R, but still conservative, is achievable if a more refined thermal analysis is adopted.

As all the existing tests did not last enough to assess whether the proposed assumption (c_{cl} = 0.4) is conservative or not, it is desirable that future tests will finish with the collapse of the vaults.

Chapter 4

Advanced calculation model

This section describes the main aspects of an advanced calculation model dedicated to the evaluation of thermal and mechanical responses of masonry arches and vaults under static loads, and fire as well. The structure is modelled as a 2D curvilinear beam subject to fire on the intrados. To calculate the temperature profiles within the masonry thickness as a function of the time of exposure, the thermal response model previously described in §3.2.4.2 is also implemented in the new advanced model herein proposed. According to current European standard [1], the thermal expansion of the material is taken into account by means of the Colonnetti's theory of elastic coaction [150] and the vertical displacements of the structure are estimated by applying the Virtual Work Principle [151]. Following the description of the model, numerical results are compared with those experimentally measured in the case of uncoated masonry vaults reported in Chapter 2.

4.1 A numerical model

As stated by Cancelliere et al. [152], Timoshenko's beam model can describe better the kinematics of the beams having cross-sections with elevated thickness (t_m) to length (L) ratio. However, the model herein proposed is based on Euler-Bernoulli beam theory, thus shear effects are disregarded and only in plane effects are considered (i.e., normal actions and bending moments).

The arched structure is modelled as a 2D single curved beam double fixed at the extremities, as depicted in Fig.57a. It is geometrically determined by means of a global reference system located at the first node, with the X-axis in the direction

of the cross-section width. The beam is discretized in an arbitrary number N of blocks for which $N+1$ nodes are identified by the coordinates (z_i, y_i). For each node a local system is introduced in the centroid of the corresponding cross-section, which is discretized in an elevated number of fibers N_s (see Fig.57b). Each cross-section is considered orthogonal to the tangent of the curvilinear axis.

The stresses in corresponding of nodes $i = 0$ and $i = N$ are calculated according to the traditional matrix frame analysis [153]:

$$\{S\} = [K]\{\eta\} + \{S_0\} \tag{23}$$

where $\{S\}$ = matrix of nodal stresses; $[K]$ = stiffness matrix of the curved beam; $\{\eta\}$ = vector of nodal displacements; $\{S_0\}$ = vector of nodal stresses due to loads applied on the entire arch profile.

The vector $\{S_0\}$ takes into account explicit and implicit loads. With the conventional linear frame analysis only explicit loads are considered (namely self-weight, permanent and variable loads), whereas thermal gradient and material non-linearities are herein taken into account, as imposed deformations of the structure, by means of the Colonnetti's theory of elastic coaction [151]. Thus, an iterative routine is introduced in order to determine the state of equilibrium at a given period of fire exposure, since the acting stress state $\{S\}$ is function of the imposed deformations (which cause $\{S_0\}$ to vary), and vice versa. The routine is executed with small steps of time-increment in which temperatures increase within the cross-sections.

The calculation generally performed in the linear elastic field is adapted to non-linear analysis according to the following procedure:

i.   For a given period of fire exposure, the state of stress $\{S\}$ of the structure are calculated according to eq.23 and thus, the distributions of bending moment M_i and normal stress N_i acting on each cross-section (identified by the subscript "i", $0 \le i \le N$) are known;

ii. Calculate the curvature μ_i and the axial deformation λ_i for each section of the structure:

$$\mu_i = \frac{M_i}{E \cdot J_i} + \bar{\mu}_i \tag{24}$$

$$\lambda_i = \frac{N_i}{E \cdot A_i} + \bar{\lambda}_i \qquad (25)$$

where E = Young's Modulus of the masonry in the linear elastic stage at room temperature; J_i = moment of inertia of the uncracked cross-section; $\bar{\mu}_i$ = imposed curvature; A_i = uncracked cross-section area; $\bar{\lambda}_i$ = imposed axial deformation.

iii.   Calculate the deformation in each fiber of each section by means of:

$$\varepsilon_j = \lambda_i + \mu_i \cdot y_j - \varepsilon_{th,j} \qquad (26)$$
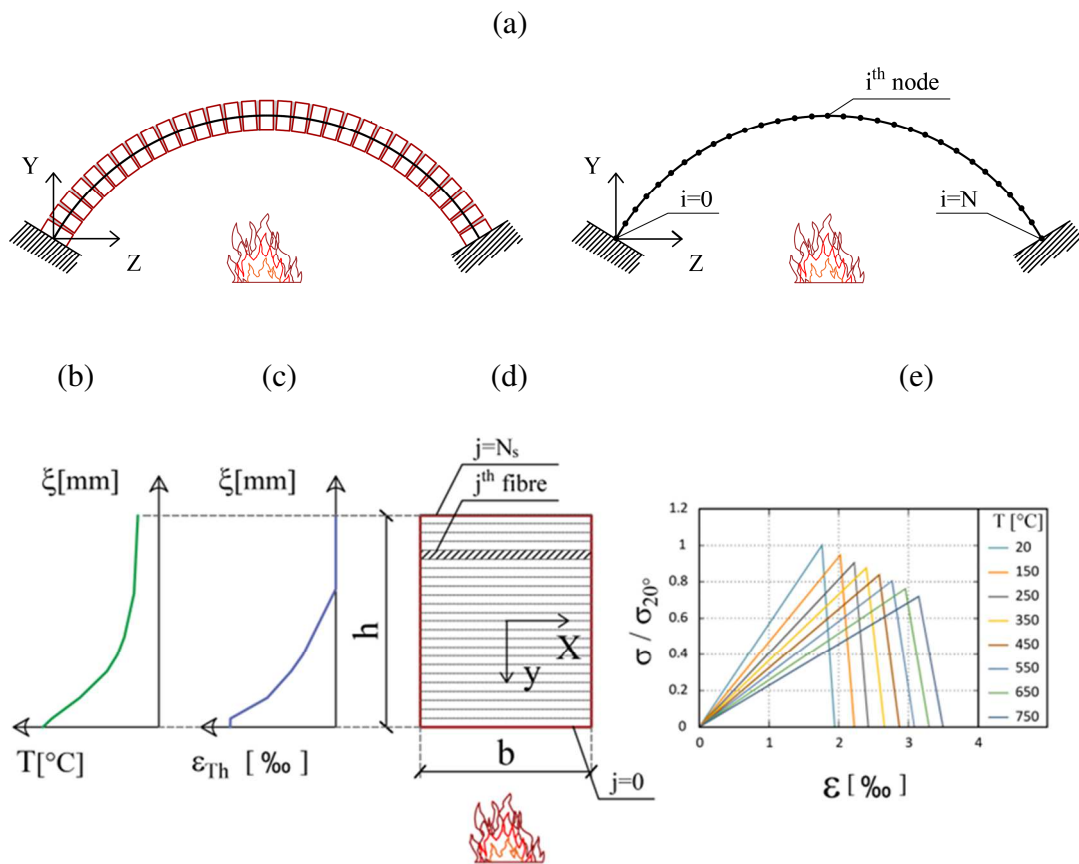
Figure 57 - (a) Masonry arch static configuration; (b) Temperature profile at time t; (c) Thermal strain distribution at time t; (d) Generic scheme of the jth cross-section; (e) Variable constitutive law as a function of the temperature (Figure redrawn from [1]).

where the subscript "j" indicates the jth fiber of the ith cross-section ($0 \le j \le N_s$, (see Fig.58b); ε_i = total strain; y = ordinate of the strip; ε_{th} = restrained thermal expansion according to Annex D of Eurocode 6 1-2 [1] (see Fig.4b and Fig.58c-d).

iv.   Calculation of the actual stress distribution within the sections:

$$\sigma_j = \sigma(\varepsilon_j, T_j) \tag{27}$$

where σ_j = stress magnitude at the jth fiber; $\sigma(\varepsilon_j, T_j)$ = constitutive law of the material which takes into account the temperature reached at the jth fiber and the corresponding degradation of the material compressive strength (see Fig.58e).

v.   Calculation of the resisting normal stress $N_{Rd,i}$ by means integrating of σ_j in each cross-section:

$$N_{Rd,i} = \int_{A_i} \sigma_j \, dA \tag{28}$$

For each section, if $|N_i - N_{Rd,i}| > tollerance$ the axial deformation of that section is corrected by an increment of $\bar{\lambda}_i$:

$$\bar{\lambda}_i = \bar{\lambda}_i + \Delta\bar{\lambda}_i = \bar{\lambda}_i + \frac{N_i - N_{risp}}{EA_i} \tag{29}$$

If the tolerance is checked in all the sections, the routine proceeds with the next step (vi), otherwise it comes back to the second step (ii).

vi.   Calculation of the resisting bending moment $M_{Rd,i}$:

$$M_{Rd,i} = \int_{A_i} \sigma_j \cdot y_j \, dA \tag{30}$$

For each section, if $|M_i - M_{Rd,i}| > tollerance$ the curvature of that section is corrected by an increment of $\bar{\mu}_i$:

$$\bar{\mu}_i = \bar{\mu}_i + \Delta\bar{\mu}_i = \bar{\mu}_i + \frac{M_i - M_{Rd,i}}{EA_i} \tag{31}$$

and calculations are repeated from step (ii).

vii.   If $\left|M_i - M_{Rd,i}\right| < tollerance,$ the equilibrium is achieved in all the sections namely and it is possible to proceed with the next period of exposure (i).

The routine previously described is repeated for each step of time, up to the maximum required period of exposure, or up to the step of increment at which it is not possible to reach convergence of external load and internal stresses. As highlighted in the routine, the actual thermal expansion law (see Fig.4b) and a variable constitutive law are assumed and used to determine respectively $\varepsilon_{th,j}$ and σ_j in each fiber of the cross-sections. Hence, a homogenous material is assumed, regardless of the effective position of the mortar joints and brick units, and by using the average values of the compressive strength (see eq. 3 [3] and Table 2). For each period of exposure, the model evaluates the stresses in each fiber of the section varying the Young's Modulus and the compressive strength according to the temperature (see Fig.58e). Accordingly, a no tension material is assumed also for the advanced numerical model, as discussed in §3.1.1. The procedure is illustrated in the iterative flowchart reported in Fig.59.

4.2 Numerical predictions and experimental outcomes

The experimental investigations carried out by Fantilli and Burello [134 -135] are predicted by means of the advanced numerical model previously described. The input data (namely, geometrical and material properties) are assumed according to Tables 3-4. The structures are modelled setting the nodes (i.e., the cross-sections) in correspondence of the mortar bed-joints ($N = 40$).

The thermal response model has been applied on the thickness t_m of the masonry. The mean temperatures at intrados and at extrados measured during the experimental investigations (i.e., temperatures depicted in Fig. 20 for *V.01.u* and Fig.21 for *V.02.u*, respectively) are imposed as boundary conditions for the evaluation of the thermal map of the cross-sections.

The temperature-dependent properties of the clay masonry are assumed according to current standard [1] namely $\lambda_{20°C} = 0.42$ W/m K, $c_{a,20°C} = 564$ J/kg K, and $\rho_{20°C} = 1700$ kg /m^3. The temperature profiles at the main periods of exposure are previously illustrated in Fig.52a (V.01.u) and Fig.53a (V.02.u).

The degradation of the material is taken into account by means of the variable constitutive law suggested for clay masonry [1], depicted in Fig.57e. A nominal compressive strength at room temperature $f_{m,20°C} = 12$ MPa is assumed to be equal

Input data:

-       Coordinates of the curvilinear centroid
        (y_i; z_i for $0 \leq i \leq N$)
-       Geometrical properties (t_m , w)
-       Material properties (γ_m, γ_{fill}, γ_{pl})
-       External loads (F_i , Q)
-       Temperature-dependant material properties
        ($\lambda_{20°C}$, $c_{a,\ 20°C}$, ε_{Th}, $\rho_{20°C} = \gamma_m$)
-       Mechanical properties ($f_{20°C}$; $E_{20°C}$)

| Calculation of the stiffness matrix [K] | Calculation of {T} by means of the Thermal response model (§3.2.4.2) | Calculation of the vector of nodal stresses due to external loads {S_0} |

Set time of exposure t ($t_0 = 0$ min)

Calculation of stresses[3]
{S}=[K]{η}+{S_0}

Calculation of stress distribution from {S}:
{M_i} and {N_i}

A   B   C

---

[3] At the first iteration, the vector {S_0} is only function of the explicit loads.
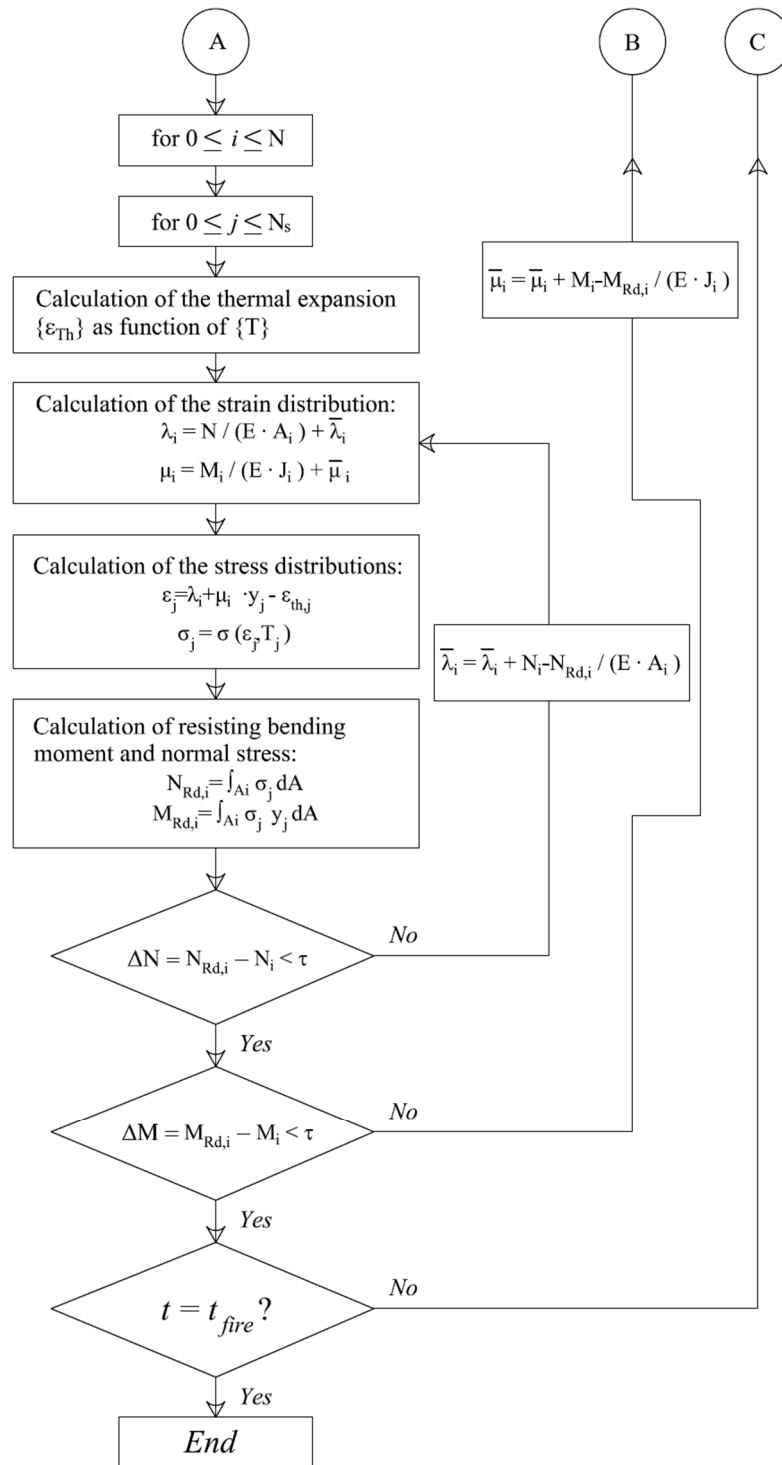
Figure 58 - Flowchart of the advanced numerical model

to the minimum average value obtained in the case of masonry prisms made with three layers of bricks and head-joints (see Table 3).

For the Young's Modulus $E_{20°C}$, some aspects must be considered. As observed by Cancelliere et al. [152], the mortar joints in an arch is generally characterized by more voids and imperfections (e.g., see Fig.31) due to the bricklayer process and the curved shape of the structure. This phenomenon inevitably affects both the actual compressive strength and deformability of the material. Therefore, the calculation model was used assuming $E_{20°C} = 1200$ MPa. It corresponds to $E_{20°C} = 100 \cdot f_{20°C} = 1200$ MPa and, despite this assumption is about 1/10 of the suggested value of eq.4 [1], it results very close to some experimental outcomes obtained by other authors [24].

The fire resistance R is evaluated by increasing the time of exposure of 2 minutes and by detecting the last period for which it is possible to reach the convergence. For each time of exposure, the displacements at the midspan, calculated by means of the advanced numerical model, are compared with those experimentally measured. Fig.59a and Fig.59b illustrate the displacement *vs* time curves of *V.01.u* and *V.02.u*, respectively.

As shown, the numerical curves (depicted in blue) correctly predict the general behavior of the structures as it reaches the same order of magnitude and direction of the displacements. Indeed, an initial steep rise, followed by a progressive dampening before reaching a stationary condition can be observed. It is worth noting that, in *V.02.u*, the progressive decrease of the displacements recorded from the 75th minute is not well predicted by the numerical model, which estimates a small increment of displacements. In both the numerical calculations, the convergence has been reached up to the end of the tests and therefore, the fire resistance R coincides with the duration of both the tests.

4.3 Main findings

A possible procedure for an advanced numerical model has been introduced. As recommended by current standard [1], a rigorous thermal response model according to temperature-dependent properties of the materials was developed with a the finite difference method. The distributions of temperature along the arched structures have been calculated according to those measured during the tests.

(a)

(b)
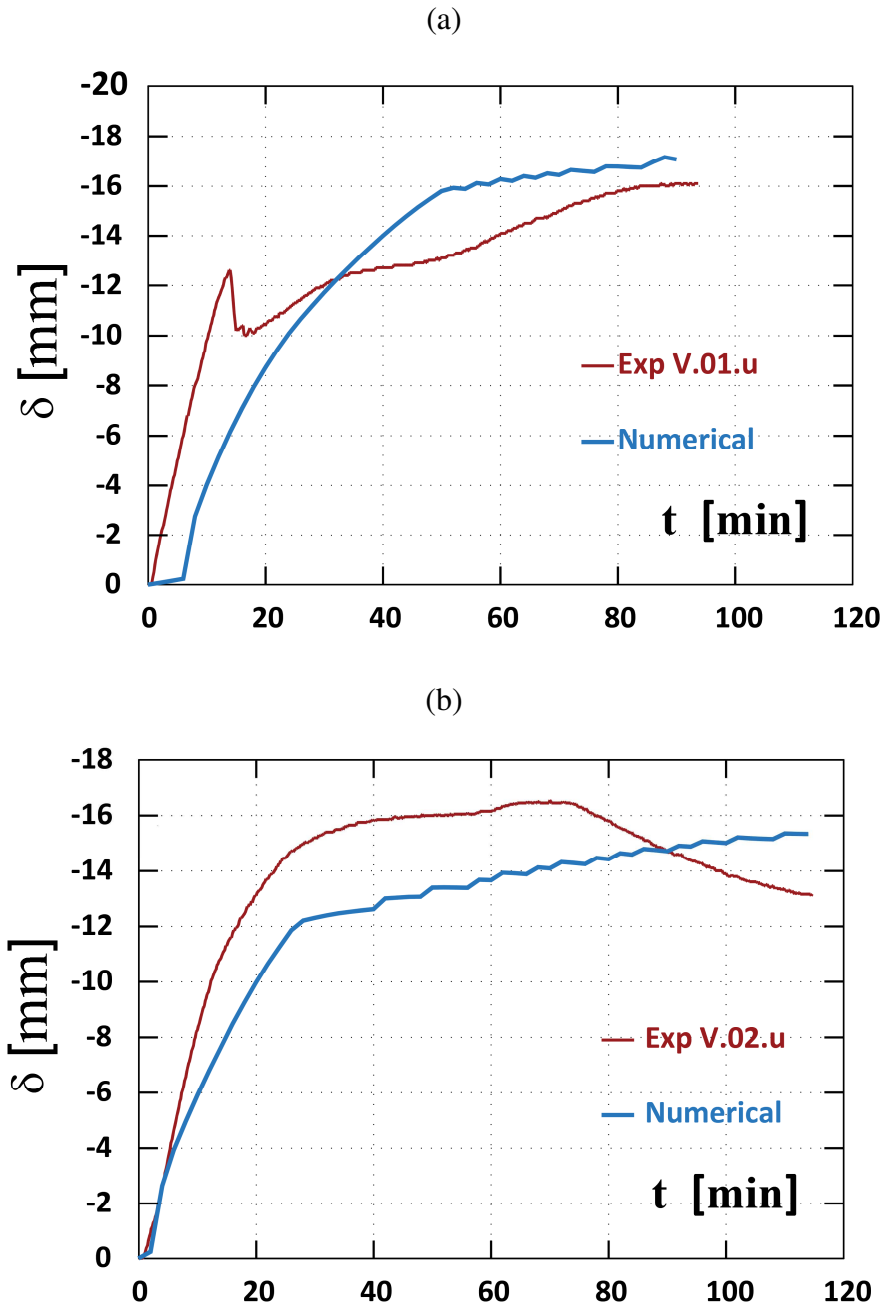
Figure 59   - Displacement δ *vs* time of exposure of (a) *V.01.u* and (b) *V.02.u*.

A mechanical response model capable of taking into account the thermal expansion of the materials has been developed according to the theory of the elastic coactions [150]. In this way, the rigid rotations given by the plasticization of some cross-sections is accounted by means of imposed strains. Subsequently, internal and external stresses are iteratively calculated up to reaching either the convergence, or the divergence (i.e., the failure) at each period of exposure.

This procedure, if set up with the parameters previously described, requires a high computational burden, as well as a precise management of the input parameters. However, even if many uncertainties have been encountered for the development of a more rigorous method, the advanced model is able to estimate the kinematic behavior of an arched masonry structure subjected to external loads and exposed at the intrados to fire action.

Chapter 5

Application to an existing masonry cross vault

The results of the fire resistance assessment of the masonry vaults in the former Church "Santa Maria del Salice" in Piazza Luigi Bima in Fossano (CN) are reported in this chapter. The analyses were required by the Italian association for the enhancement of artistic and cultural assets, in order to comply with the new use of the building. More precisely, a fire resistance greater than, or equal to, 30 minutes [154] is required for the structural elements of the central core room of the church. As illustrated in the following paragraphs, the analysis aimed at evaluating the fire resistance of the larger cross vault located in the central nave.

The safety measurement is carried out in accordance with the semi-probabilistic limit state method of the current Italian codes [155], as reported in chapter 8 and chapter 4 of this standard, concerning the measurement of the safety of existing structures and the fire resistance of masonry structures, respectively.

Furthermore, for the structures subjected to the control of the fire brigade, the Letter - Circular of the DCPREV Prot. N.4638 of 04/05/2013 [147], previously introduced in §3.2.4.2, is also taken into consideration.

To analyze the cross-vault, several aspects need to be considered. Usually, these structures were built many (if not centuries) decades ago and therefore it is difficult to know the geometry, as well as the mechanical and temperature-dependent properties of the materials. In addition to the lack of information, the difficulty in

carrying out truly representative experimental analyses for measuring these parameters must be underlined. For this reason, the simplified calculation model [134-135], described in chapter 3, which requires few input parameters, is herein used for the assessment.

5.1 Structural context

As shown in Fig.60, the vault is located in the central nave of the former church. It covers the largest surface area in plan, if compared with the other surrounding vaults. The geometry is that of a common cross vault, composed by four arches on the perimeter and two diagonal arches, crossing the center. The structure is supported by four piers (pillars/ load-bearing partitions) placed at the four vertexes. The four curvilinear surfaces of the vault are devoid of ribs in correspondence with the fusion points, namely with the diagonals. The current state of the vault is depicted in Fig.61, where a sequence of photos from the intrados and the extrados are shown.
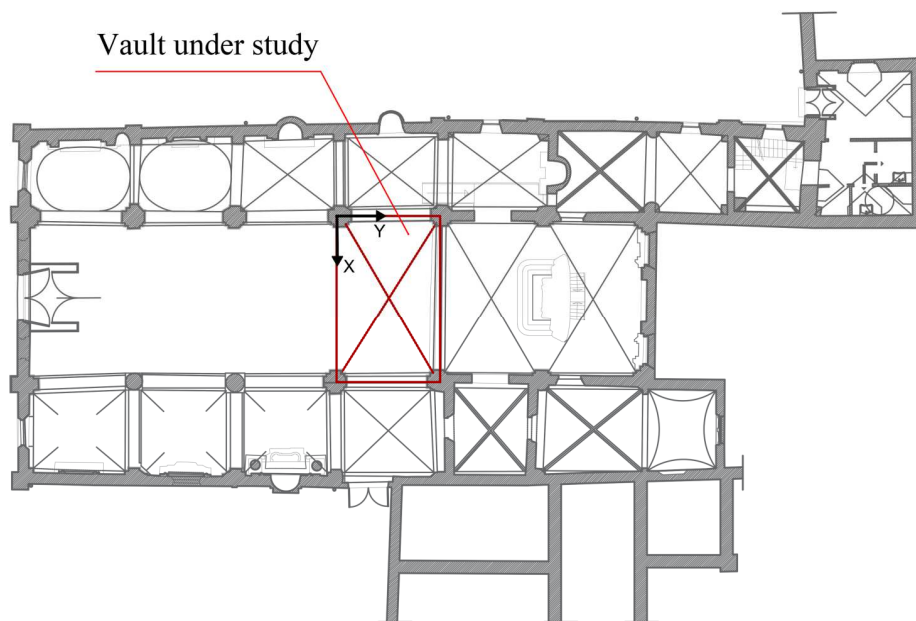
Figure 60 - Plan of the former church "S. Maria del Salice" in Fossano (CN) with the identification of the vault under study

The vault was retrofitted through a structural reinforcements in the early 2000s. A concrete cap was built on the entire extrados of the vault. It has, approximately, a thickness of 60 mm, and a steel mesh $\phi 6 - 200 \times 200 \text{ mm}^2$ located in the middle.

At the abutments of the vaults, the concrete shell was anchored to the extrados of the masonry nails.

Referring to the extrados surface at the vertices of the diagonals, the load-bearing structure have a net height of 1÷1.2 m, with respect to the extrados of the key ashlar.

5.2 Modelling the masonry cross-vault

The cross vault can be described by two circumferential arches having spans L_x = 8.00 m and L_y = 4.90 m (hereafter called "long side" and "short side", respectively), with a height f = 2.80 m in the respective keystones. The central core of the vault is made of masonry with t_m = 120 mm (bricks arranged along the short side) and of reinforced concrete on the extrados having $t_{concrete}$ = 60 mm, having the densities γ_m = 1700 kg/m^3 and γ_{cls} = 1400 kg/m^3, respectively. Therefore, the vault is characterized by a composite cross-section having an overall depth of 180 mm. As can be observed in Fig. 61, the soffit of the vault is unevenly coated with a layer of plaster with a nominal thickness t_p = 15 mm. The vault is not subjected to any permanent non-structural load (γ_{fill}) and/or variable loads (Q) on the extrados. Therefore, considering the accidental design combination of the loads [156], for the purposes of the fire resistance assessment, the vault is only subject to the self-weight of the structural materials, in addition to the action due to high temperatures of the fire.

Due to the geometrical symmetry, the analysis of only a quarter of the vault is performed. Specifically, reference is made to the semi-length of the two nails of the vault, highlighted in Fig.62 (in red on the long side and in blue on the short side). If a net height between the edge zones and the keystone h_0 = 1200 mm is conservatively assumed, the plan projection results in a surface of the abutments of 621 x 1013 mm^2 as illustrated in Fig.62b.

Figure 61 - Sequences of images of the central nave of the church showing the texture of the cross-vault and a view from the extrados.
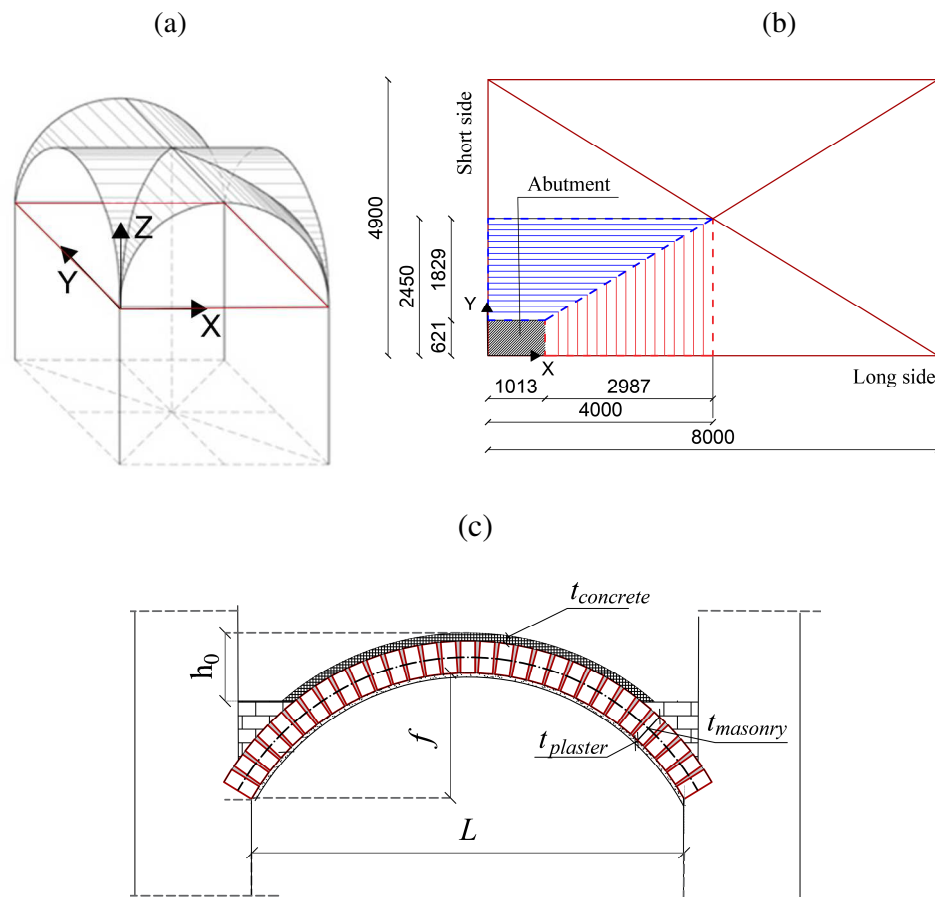
Figure 62 - The geometry of the cross vault: (a) 3D scheme; (b) plan view; (c) geometrical parameters of the arch element (i.e., nail of the vault along the perimeter). (measurements in mm)

5.3 Application of the simplified calculation model

The simplified calculation model, previously introduced for the analyses of masonry barrel vaults subject to fire, is herein modified to assess also the cross-vault. Therefore, the general rule, for which a structure is considered safe if at least one line of thrust lies entirely within the arch profile, is extended to a "thrust surface" that must lies within the vault boundaries [157-158].

The overall geometry of the cross-vault, considering the structural symmetry, is composed by two halved nails which are divided into 120 elements. The curvilinear axes of these nails are represented in Fig.63.
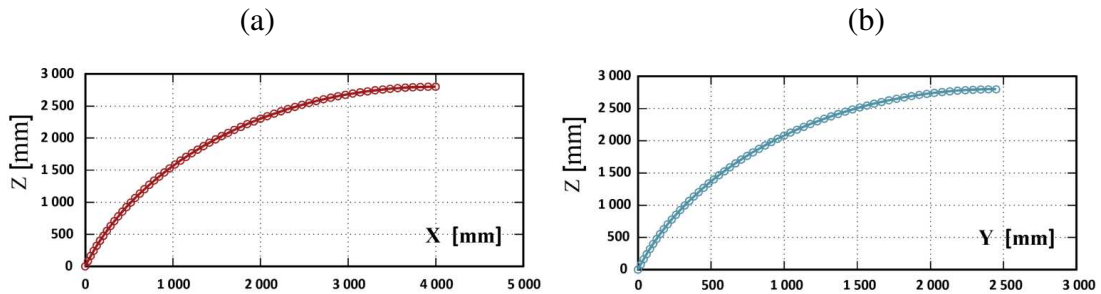
Figure 63 - Midlines of vault nails: (a) long side (X direction); (b) short side (Y direction).

The cross-section analysis is performed according to Fig.1, but considering the total depth h as the sum of t_m and $t_{concrete}$ (i.e., the two materials composing the structure). Thus, for the calculation of the temperature profiles at different time of exposure, a rigorous analysis should take into account also the temperature-dependent properties of the concrete [160]. Similarly to clay masonry, the properties of concrete can be modelled according to the curves depicted in Fig.65a-b, where the values are normalized with respect to those measured at room temperature.

A specific heat $c_{c,20°C}$ = 900 J/kg°C and a thermal conductivity $\lambda_{c,20°C}$ = 1.33÷1.95 W/m°C can be assumed for normal strength concrete. As shown in Fig.64a, if the moisture content u is explicitly considered, different curves can be adopted, reaching an higher spike around 100°C, when higher content of moisture are considered. The analytical formulations of those parameters for both concrete and steel reinforcements are reported in the current standard [160]. In this case, the advanced thermal analysis (see §3.2.4.2) is performed assuming the temperature-dependent properties of clay masonry and plain concrete, and the standard temperature-time fire curve [137] at the intrados.

Concerning to the mechanical properties, a rigorous approach should consider the degradation of the material by reducing progressively the compressive strength as function of the temperature (see Fig.64c), and subdividing the cross-sections into several zones at different mean temperatures (i.e., the so-called "zone method" in [160]). Nevertheless, as the concrete is not in direct contact with the environment under fire, a lower degree of accuracy is considered sufficient and hence, the so-called "500°C isotherm method" is adopted.

(a)   (b)

(c)
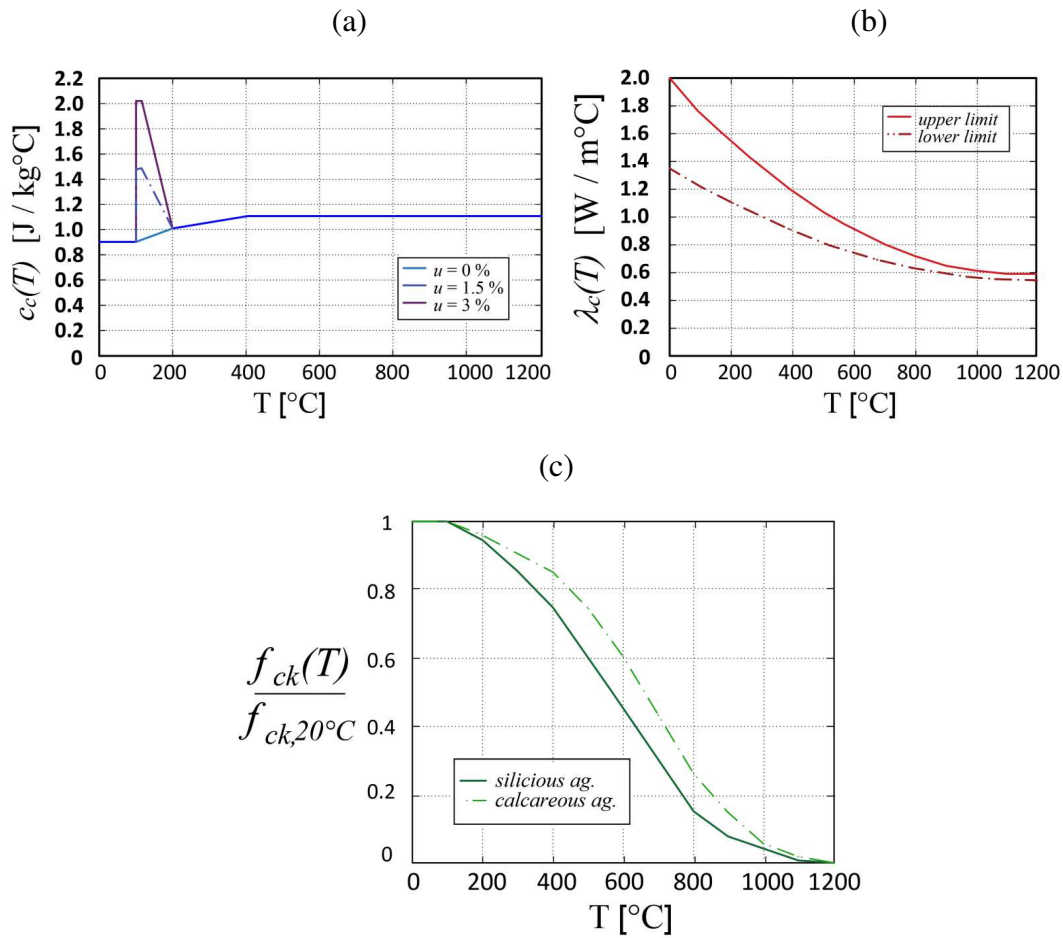
Figure 64 - Temperature-dependent properties of concrete[160]: (a) specific heat; (b) thermal conductivity; (c) characteristic curve of compressive strength.

Accordingly, the thickness of the ineffective zone (of the concrete part) is given by the depth of the cross-section, measured from the interface between concrete cap and the masonry arch to the fiber in correspondence of which $T = 500°C$. Thus, the heat damaged zone (namely the area of the cross-section above 500°C) is ineffective, whilst the initial compressive strength $f_{cls,20°C}$ may be assumed for the remaining zone (i.e., where $T < 500°C$).[4]

---

[4] In other words, the concrete cap can be damaged by exposure to fire only if it is possible to reach $T = 500°C$ throughout the depth of the masonry profile. From a practical point of view, in this circumstance the model is generally no longer able to detect acceptable LOTs, as it means that the entire underlying masonry cannot resist.

The fire assessment, previously described in §3.2.3 for the analysis of unreinforced masonry arched structures, is therefore modified considering also the composite cross-section and the variable width of the semi-structure. The geometry of the all possible LOTs (acting on the two semi-barrels vaults) is firstly verified, as in the traditional barrel vaults. In fact, if the contribution of the tensile strength is still neglected also for the concrete cap, a LOT can be accepted only when it entirely lies within the geometrical boundaries of cross-vault, which is given by the sum of the depths of the structural materials minus the ineffective thickness.

The values of the stresses must be calculated in each node. The two substructures are analyzed firstly along their axis, where the design values of the resisting normal stresses $N_{Rd,x}$ and $N_{Rd,y}$ are calculated by means of a stress block analysis:

$$\begin{cases} N_{Rd,X} = 2 \ b_Y(x) \ \bar{e}_{k,w,X} \ f_{d,m} \\ N_{Rd,Y} = 2 \ b_X(y) \ \bar{e}_{k,w,Y} \ f_{d,m} \end{cases} \tag{32}$$

where the subscripts X and Y indicate the two substructures; $b_Y(x)$ = width of the cross-section in direction of the axis Y and function of the coordinate x; $b_X(y)$ = width of the cross-section in direction of the axis X and function of the coordinate y; $\bar{e}_{k,w}$ = distance of the acting force from the border (see Fig.49b); $f_{d,m}$ is the design value of the compressive strength of the weakest material within the depth $\bar{e}_{k,w}$ (different values are assumed in the case of partially damaged and fully reactive masonry).

Finally, a generic LOT is considered verified and therefore the cross-vault is safe, if the following inequality is satisfied:

$$\left(\frac{N_{ed,x}}{N_{Rd,x}}\right)^{\alpha} + \left(\frac{N_{ed,y}}{N_{Rd,y}}\right)^{\alpha} < 1 \qquad\qquad \textit{for each node} \tag{33}$$

where, N_{ed} = design acting normal stress in the x- or y-direction of the ith section (namely the normal component of the acting thrust); N_{Rd} = design resisting normal stress in the x- or y-direction of the ith section; α = exponent of the interaction curve (cautiously set equal to 1 in the present case).

5.4 Evaluation of the fire resistance

To evaluate the fire resistance R of the cross-vault previously illustrated, the simplified thermal analysis (§3.2.4.1) and the advanced thermal model (§5.3), extended to the composite cross-sections, are used to evaluate the temperature profiles during the fire exposure. The temperature distribution is calculated neglecting any favorable effects of the plaster, i.e. cautiously assuming $t_{plaster} = 0$ mm. In other words, the standard fire curve [137] is applied directly to the masonry at the intrados and the thermal conduction is calculated through the two materials[5]. Fig. 66 shows the results of the two thermal response models where different temperature profiles for time of exposure are depicted. For the advanced thermal analysis, a fire duration of 180 minutes was considered, and the temperature profiles every 30 minutes are reported. Whether the temperature profiles of the simplified thermal analysis (see Fig.65a), or those calculated by means of the more rigorous calculation model (Fig.65b) are adopted, the T=500°C isotherm never reaches the height of the interface[6] (which coincides with the thickness of the masonry). Thus, the whole thickness of the concrete cap is considered as fully resistant.

The zones within the sections are defined in accordance with the recommendation of the Italian fire brigades [147], whereby the masonry is characterized by $\theta_2 = \theta_1 = 100°C$ (i.e., $c_{cl} = 0$). Hence, the ineffective thickness of the masonry (starting from the intrados) is calculated up to the isotherm T=100°C, for which the two curves reported in Fig.66 can be drawn. As shown, the ineffective thickness is more conservative when the simplified approach is adopted [1], especially in the range between 30 and 100 minutes of exposure. This outcome inevitably affect the final number of acceptable LOTs, because the depth of the damaged heated zone increases faster.

---

[5] In the absence of experimental data, for the rigorous calculation, $c_{c,20°C} = 900$ J/kg°C, $\lambda_{c,20°C} = 1.5$ W/m°C, and $\gamma_{cls} = 1400$ kg/m^3 are assumed for the concrete cap (see Fig.65), whilst $\lambda_{20°C} = 0.42$ W/m K, $c_{a,20°C} = 564$ J/kg K, and $\rho_{20°C} = 1700$ kg /m^3 are adopted for the masonry nails (see Fig.4).

[6] A markedly different condition would occur in the case of reinforced vaults where the bricks are arranged in "folio" [161]. In this case the thickness of the arched structure is given by the shortest side of the brick.

Obviously, as the fire progresses, both the resistant thickness of the arch and the mechanical resistance of the material tend to decrease and, consequently, the number of admittable pressure curves decreases. Hence, the thrust curves which do not simultaneously satisfy the two conditions, as described in the previous paragraph, are discarded from the number of admissible pressure curves. Therefore, the fire resistance R is still assumed to be equal to the period of fire exposure for which at least one LOT satisfies eq.33 in each node.

(a)   (b)
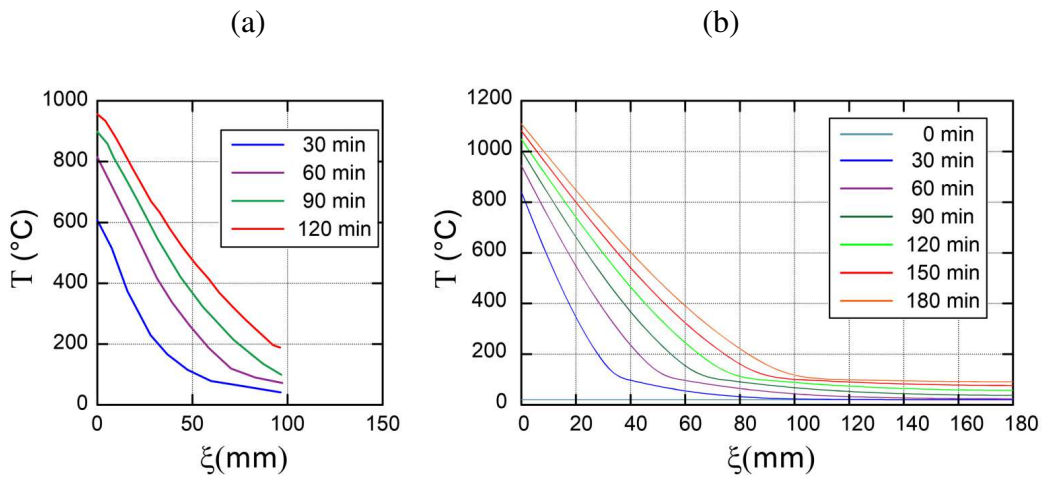
Figure 65 - Temperature distribution in composite sections: (a) STA: simplified approach of Annex C of EN 1996 1-2 [1] (valid solid for walls); (b) ATA: temperature distribution according to Annex D of EN 1996 1-2 [1].
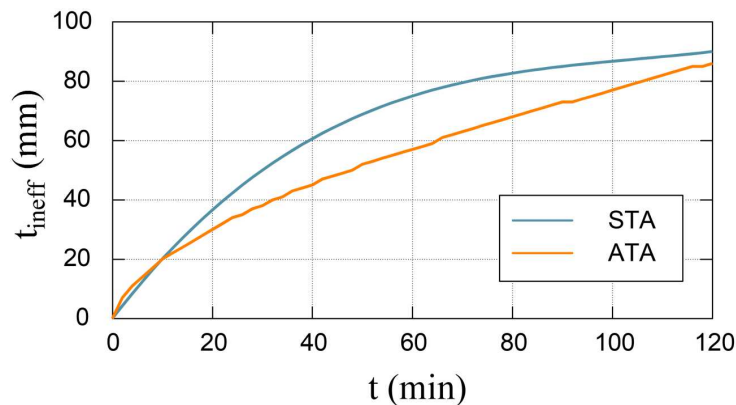
Figure 66 - Ineffective thickness measured from the hot surface as a function of fire exposure time, calculated by means of the simplified thermal analysis (STA) and the advanced thermal analysis (ATA).

The results of the analysis depend on the compressive strengths of the materials which, for the vault of Fossano, were not experimentally measured. For this reason, a parametric study is carried out by varying the compressive strength of the masonry $f_{m,20°C}$, while the compressive strength of the stiffening concrete shell $f_{cls,20°C}$ is constant. Vice-versa, the calculation is repeated by varying the $f_{cls,20°C}$, while $f_{m,20°C}$ is constant.

Fig.67 shows the number of thrust curves (LOTs) which simultaneously satisfy the verification criteria as a function of the time of exposure to fire. The temperature distributions are adopted according to the simplified thermal analysis (STA). In Fig.67a, the acceptable LOTs are drawn when $f_{m,20°C}$ varies between 0.35 MPa and 2 MPa, while $f_{cls,20°C}$ = 10 MPa (i.e., it is constant). Conversely, in Fig.67b, the changes in the number of LOTs over time are considered when $f_{m,20°C}$ = 0.5 MPa and $f_{cls,20°C}$ varies between 0.5 MPa and 10 MPa. The value of R corresponds to the last instant of fire exposure for which at least one pressure curve is acceptable.

As shown in Fig.68, the analyses conducted with the STA were repeated assuming the temperature distributions calculated with the advanced thermal analysis (ATA). Similarly, in Fig.68a, $f_{cls,20°C}$ is considered constant as $f_{m,20°C}$ varies. Conversely, in Fig.68b $f_{m,20°C}$ is constant and $f_{cls,20°C}$ varies.

The results show that a small variations in material resistance (namely f_m and f_{cls}) significantly affect the final value of fire resistance R. However, the curved depicted in Fig.67 and Fig.68 can be useful tools to assess existing vaults with a low level of knowledge. In fact, referring to the Table C8.5.I of the current Italian code [162], the mean values of the compressive strengths for masonry made with solid clay bricks and lime-based mortar may vary within the range 2.6 ÷ 4.3 MPa. In addition, in case of historical masonry with a mortar bed-joints thickness t_{bj} larger than 13 mm, the mean compressive strength must be safely reduced of 30% [162]. In the case of arched structure, due to the construction process, the thicknesses of the bed-joints is often larger than 13 mm.

Thus, having the minimum level of knowledge (LC1 in [162]), the mean compressive strength at room temperature of the masonry may be assumed according to the following equation:

$$f_{m,20°C} = \frac{0.7 \cdot fmin[2.6;4.3]}{1.35} = 1.34 \text{ MPa} \qquad (34)$$

where 1.35 is the confidence recommended for the minimum level of knowledge (i.e., LC1).

Instead, the compressive strength of the concrete shell does not play a significant role in the R-resistance of the vault. In fact, as shown in Fig.67b and Fig.68b, R changes slightly with $f_{cls,20°C}$.

(a)   (b)
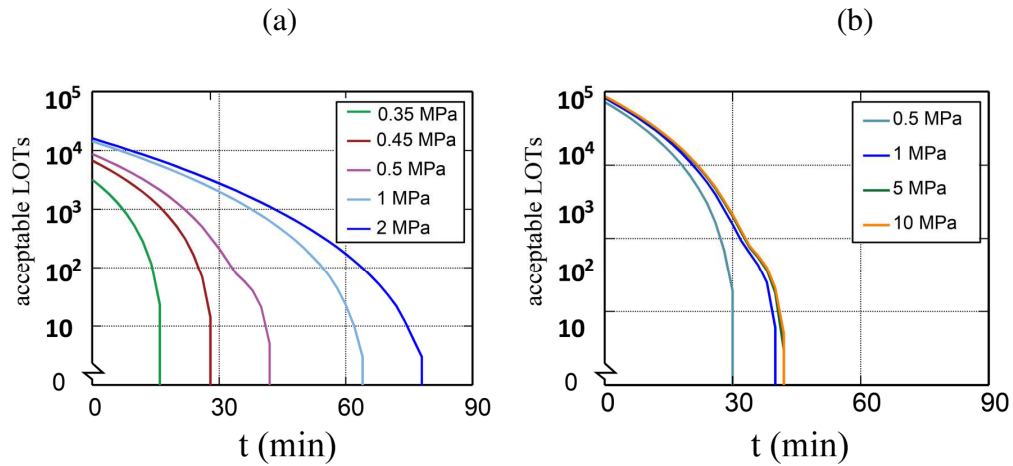
Figure 67 - Calculation of the number of acceptable LOTs adopting the STA 1 when varying (a) the compressive strength of the masonry (f_{cls} = 10 MPa) and (b) the compressive strength of the concrete cap (f_m = 0.5 MPa).

(a)   (b)
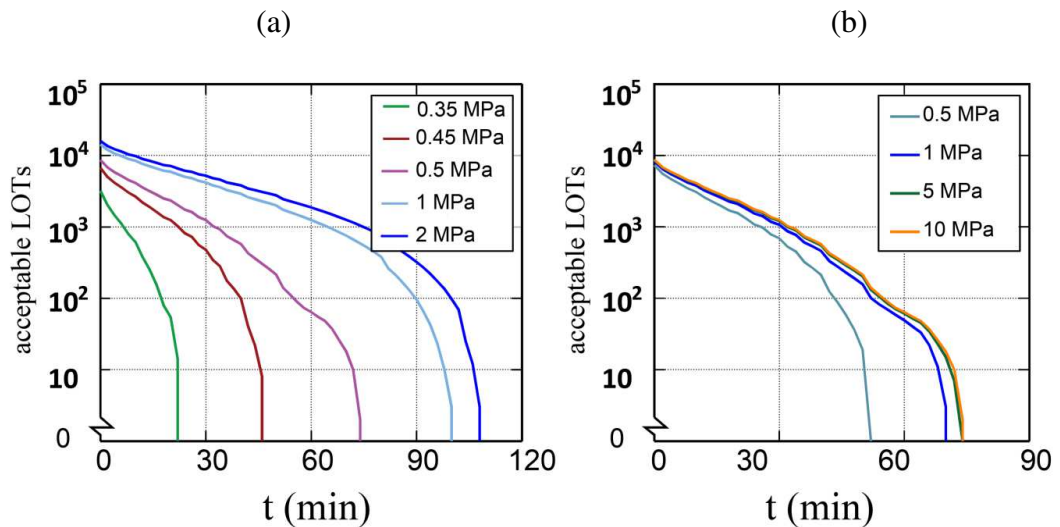
Figure 68 - Calculation of the number of acceptable LOTs adopting the ATA 1 when varying (a) the compressive strength of the masonry (f_{cls} = 10 MPa) and (b) the compressive strength of the concrete cap (f_m = 0.5 MPa).

Thus, assuming $f_{m,20°C}$ = 1.34 MPa and $f_{cls,20°C} \geq$ 10 MPa, the cross-vault is characterized by a fire resistance R $\geq$ 60 min (in the case of STA) or $R \geq$ 90 min (in the case of ATA).

5.5 Main findings

In this chapter, the simplified calculation method, previously introduced in Chapter 3 for barrel vaults, has been improved and the following features were developed:

- − The scope of applicability of the simplified model has been extended from the masonry barrel vaults to the cross-vaults;
- − Both the thermal and the mechanical models have modified to take into account a composite cross-section due to the presence of a second material anchored to the extrados of the vault (namely the concrete shell).
- − The reinforced concrete shell has been conservatively modeled as only-compressive material neglecting any contribution of the steel rebars. The 500°C isotherm method was implemented to for the analyze the concrete shell.

As the materials properties of historical existing structures are generally missing, the application of the simplified model can be finalized to obtain general diagrams, like those of Fig.67 and Fig.68, or table to cover all the possible situations.

Chapter 6

Conclusions

6.1 Main contributions

In the early 2020s, an advanced search on Scopus database using the keywords "Masonry materials", "Arches" and "Fire resistance" was leading to the conclusions that neither experimental data nor numerical models existed. Similarly, the issue of curvilinear masonry structures subject to fire is currently ignored by European codes.

Especially in Italy, where the culture of conservation is predominant over the demolish-and-rebuild strategy, this regulatory vacuum implies considerable difficulties among structural engineers who are generally called to assess the fire resistance of arched elements. The situation is even worse because of the scarce state of knowledge of these structures, for which only the geometric profile is generally known.

Within this context, two approaches to assess existing curvilinear masonry structures under fire are proposed. More precisely, a simplified calculation model (Chapter 3 and Chapter 5) and an advanced numerical model (Chapter 4) were developed.

The simplified numerical model combines the reduced cross-section method with the limit analysis, in order to evaluate masonry arches or barrel vaults (having one axis of symmetry), also subjected to external concentrated or distributed loads. The effect of the fire exposure at the intrados was initially taken into account by

means of the simplified thermal analysis proposed by current standard for the walls. Subsequently, a more refined thermal analysis was implemented by means of a finite difference model. The fire resistance R is calculated as the last period of exposure for which it is possible to define at least one acceptable thrust line.

Conversely, the advanced calculation method, based on the Colonnetti's Theory of the elastic coactions, takes into account the thermal expansion due to the elevated temperatures and additional nonlinearities due to the material properties. Thus, a variable constitutive law was introduced to better predict the behavior of curved structures under fire.

To validate these models, experimental results from direct tests on real-scale masonry barrel vaults were used.

The simplified calculation model has been also extended to the evaluation of a cross-vault in a historical building. In this structure, numerical outcomes have shown that an high level of knowledge can be unnecessary, when low values of R must be achieved. Thus, the simplified numerical model which is less time consuming as well as based on few but essential parameters, is recommended for a practical use.

6.2 Recommendations for Future Research

Future work should be devoted to replicating large-scale experimental tests, focusing on the different forms of arches and vaults commonly found in our architectural heritage, in order to develop new and dedicated computational models (e.g., thrust network method).

Of particular importance are also the so-called vaults n folio which, due to their reduced thickness, most likely constitute a category of structures that would hardly satisfy the fire test.

New tests should be performed acquiring the displacements in many points to better understand the collapse mechanism, characterized by the formation of plastic hinges combined with the degradation of the mechanical properties of the material.

From a practical point of view, the reaching of the collapse of the vaults during the test would be necessary to exactly individuate the fire resistance, and furtherly validate both simplified and advanced numerical models. Special device should also be used to detect the formation of hinges and the crack patterns along the curvilinear

profile. In fact, as reported by experimental evidence, the high temperatures involved, the inaccessibility of the chambers until the end of the cooling phase, and the size of the applied loads, complicate the recognition and quantification of the damage to the structure subjected to fire.

A higher effort is also required for the hot mechanical characterization of historical masonry, in order to confirm the prescriptions of current standards (as temperature limits and reductive coefficients.

Finally, the simplified approach should be extended to all the possible shape of vaults and domes, and to all the possible fire protectives.

References

[1] EN 1996 1-2:2005. Eurocode 6 - Design of masonry structures - Part 1-2: General rules - Structural fire design, European Committee for Standardization: Brussels, Belgium, 2005.

[2] EN 1363-2:1999. Fire resistance tests - Part 2: Alternative and additional procedures, European Committee for Standardization: Brussels, Belgium, 1999.

[3] EN 1996-1-1:2005. Eurocode 6 - Design of masonry structures - Part 1-1: General rules for reinforced and unreinforced masonry structures, European Committee for Standardization: Brussels, Belgium, 2005.

[4] P. Böckh, T. Wetzel, Heat Transfer: Basics and Practice, Springer, Berlin, 2012.

[5] EN 1991 1-2:2002. Eurocode 1: Actions on structures - Part 1-2: General actions - Actions on structures exposed to fire, European Committee for Standardization: Brussels, Belgium, 2002.

[6] EN 1363-1:2020. Fire resistance tests - Part 1: General requirements, European Committee for Standardization: Brussels, Belgium, 2020.

[7] J. Zehfussa, D. Hosserb, A parametric natural fire model for the structural fire design of multi-storey buildings, Fire Saf J 42 (2) (2007) 115–126. https://doi.org/10.1016/j.firesaf.2006.08.004

[8] J. Kubica, A. Kwiecień, Ł. Bednarz, Brick and Block Masonry - From Historical to Sustainable Masonry, Proceedings of the 17th International Brick/Block Masonry Conference (17thIB2MaC 2020), July 5-8 (2020) Kraków, Poland.

[9] EN 1015-11:2019. Methods of test for mortar for masonry - Part 11: Determination of flexural and compressive strength of hardened mortar. European Committee for Standardization: Brussels, Belgium, 2019.

[10] ASTM C109/C109M-20, Standard Test Method for Compressive Strength of Hydraulic Cement Mortars (Using 2-in. or [50-mm] Cube Specimens), American Society for Testing and Materials (ASTM), 2020.

[11] ASTM C349-18, Standard Test Method for Compressive Strength of Hydraulic-Cement Mortars (Using Portions of Prisms Broken in Flexure), American Society for Testing and Materials (ASTM), 2018.

[12] EN 771-1:2011+A1:2016. Specification for masonry units - Part 1: Clay masonry units, European Committee for Standardization: Brussels, Belgium, 2016.

[13] ASTM C67-13, Standard Test Methods For Sampling And Testing Brick And Structural Clay Tile, American Society for Testing and Materials (ASTM), 2013.

[14] EN 1052-1:1998. Methods of test for masonry - Part 1: Determination of compressive strength, European Committee for Standardization: Brussels, Belgium, 1998.

[15] ASTM C1314-14 Standard Test Method for Compressive Strength of Masonry Prisms Edition, American Society for Testing and Materials (ASTM), 2014.

[16] S. Arash, Mechanical Properties Of Masonry Samples For Theoretical Modeling, 15th International Brick and Block Masonry Conference Florianópolis, Brazil, 2012.

[17] S. Jafari, J.G. Rots, R. Esposito, A correlation study to support material characterisation of typical Dutch masonry structures, J. Build. Eng. 45 (2022) 103450. https://doi.org/10.1016/j.jobe.2021.103450

[18] A. Costigan and S. Pavía, Influence of the mechanical properties of lime mortar on the strength of brick masonry, RILEM, Historic Mortars: Characterisation, Assessment and Repair (2012) 359-372.

[19] H.B. Kaushik, D.C. Rai, S.K. Jain, Stress-strain characteristics of clay brick masonry under uniaxial compression, J. Mater. Civ. Eng 19 (9) (2007) 728–739.

[20] R. Bennett, K. Boyd, R. Flanagan, Compressive properties of structural clay tile prisms, J. Struct. Eng. 123 (7) (1997) 920–926.

[21] K.S. Gumaste, K.S.N. Rao, B.V.V. Reddy, K.S. Jagadish, Strength and elasticity of brick masonry prisms and wallettes under compression, Mater. Struct. 40 (2) (2007) 241–253.

[22] D. Liberatore, A. Marotta, L. Sorrentino, Estimation of solid clay brick unreinforced masonry compressive strength based on mortar and unit mechanical parameters, 9th International Masonry Conference At: Guimarães, Portugal, 2014.

[23] H.B. Kaushik; D.C. Rai; S. K. Jain, ASCE, Stress-Strain Characteristics of Clay Brick Masonry under Uniaxial Compression, J. Mater. Civ. Eng. (19) (9) (2007). DOI: 10.1061/(ASCE)0899-1561(2007)19:9(728)

[24] A. Costigan, S. Pavía, O. Kinnane, An experimental evaluation of prediction models for the mechanical behavior of unreinforced, lime-mortar masonry under compression. J. Build. En. 4 (2015) 283–294. DOI: 10.1016/j.jobe.2015.10.001

[25] A. Page, The biaxial compressive strength of brick masonry January 1981 Proceedings of the Institution of Civil Engineers 71 (3) 893-906. DOI:10.1680/iicep.1981.1825

[26] R. Nowak , T. Kania , V. Derkach , R. Orłowicz , A. Halaliuk, E. Ekiert and R. Jaworski, Strength Parameters of Clay Brick Walls with Various Directions of Force, Mater. 14 (2021) 6461. https://doi.org/10.3390/ma14216461

[27] J.C. Almeida, P. B. Lourenço, J. A. Barros, Characterization of brick and brick–mortar interface under uniaxial tension, VII International Seminar on Structural Masonry for Developing Countries, Belo Horizonte, Brasil, 2002.

[28] M.R. Maheri, M.F. Motielahi, M.A. Najafgholipour, The effects of pre and post construction moisture condition on the in-plane and out-of-plane strengths of brick walls, Mater Struct 44 (2011) 541–559. DOI 10.1617/s11527-010-9648-y

[29] S. Hetherington, A Comparative Study Into The Tensile Bond Strength Of The Brick Mortar Interface Of Naturally Hydraulic Lime And Portland Cement Mortars, Masonry International, 28 (2) (2015) 37-43.

[30] A. Maroušková, J. Kubát, Solid Burnt Bricks Tensile Strength, Acta Polytechnica CTU Proceedings 13 (2017) 75–79. doi:10.14311/APP.2017.13.0075

[31] J.A. Thamboo, Material characterisation of thin layer mortared clay masonry, Constr. Build. Mater. 230 (2020), 116932. https://doi.org/10.1016/j.conbuildmat.2019.116932

[32] EN 1052-3:2002 Methods of test for masonry - Part 3: Determination of initial shear strength, European Committee for Standardization: Brussels, Belgium, 2002.

[33] S. Barattucci, V. Sarhosis, A.W. Bruno, A.M. D'Altri, S. De Miranda, G. Castellazzi, An experimental and numerical study on masonry triplets subjected to monotonic and cyclic shear loadings. Constr Build Mater, 254 (2020) 119313. https://doi.org/10.1016/j.conbuildmat.2020.119313

[34] T. Zimmermann, A. Strauss, Variation Of Shear Strength Of Masonry With Different Mortar Properties, Proceedings of the 15th International Brick and Block Masonry Conference, Florianopolis, Brazil, 2012.

[35] M.S. Abrams, Compression strength of concrete at temperatures to 1600 F. Effect of temperature on concrete, Portland Cement Association Research and Development, 1971.

[36] S. Thelandersson, Effect of high temperature on tensile strength of concrete. Division of Structural Mechanics and Concrete Construction, Institute of Technology, Lund, Sweden, 1972.

[37] M. Andreini, A. De Falco, and M. Sassu, Stress–strain curves for masonry materials exposed to fire action, Fire Saf. J. 69 (2014) 43-56. https://doi.org/10.1016/j.firesaf.2014.08.005

[38] M. Andreini, M. Caciolai, S. La Mendola, L. Mazziotti, M. Sassu, Mechanical behavior of masonry materials at high temperatures, Fire Mater. 39 (2014) 41-57. https://doi.org/10.1002/fam.2229

[39] W. Khaliq, M.F. Bashir, High temperature mechanical and material properties of burnt masonry bricks, Mater. Struct. 49 (2016) 5195–5208. DOI 10.1617/s11527-016-0854-0

[40] U. Schneider, Test methods for mechanical properties of concrete at high temperatures. Part 4. Tensile Strength for Service and Accident Conditions, Technical Committee 129-MHT, Rilem (2000).

[41] Y.F. Fu, Y.L. Wong, C.S. Poon, C. Tang, P. Lin, Experimental study of micro/macro crack development and stress–strain relations of cement-based composite materials at elevated temperatures,   Cem.   Concr. Res. 34 (2004) 789–797. https://doi.org/10.1016/j.cemconres.2003.08.029

[42] T. Nguyen, F. Meftah, R. Chammas, A. Mebarki, The behaviour of masonry walls subjected to fire : Modelling and parametrical studies in the case of hollow burnt-clay bricks, Fire Saf. J. 44 (2009) 629–641. https://doi.org/10.1016/j.firesaf.2008.12.006

[43] S. Russo, G. Boscato, F. Sciarretta, Behaviour of a Historical Masonry Structure Subjected to Fire, Mas. Int. 1(1) (2008)1-48.

[44] J.C. Bidoung, P. Pliya, P. Meukam, A. Noumowé, T. Beda, Behaviour of clay bricks from small-scale production units after high temperature exposure, Mater. Struct. 49 (2016) 4991-5006. DOI 10.1617/s11527-016-0838-0

[45] J. Bosnjak, S. Gambarelli, A. Sharma, A. Meskovic, Experimental and numerical studies on masonry after exposure to elevated temperatures, Constr. Build. Mater. 230 (2020), 116926. https://doi.org/10.1016/j.conbuildmat.2019.116926

[46] S. Russo, F. Sciarretta, Experimental and Theoretical Investigation on Masonry after High Temperature Exposure, Exp. Mec. 52 (2012) 341–359. DOI 10.1007/s11340-011-9493-0

[47] V. Pachta, S. Triantafyllaki, M. Stefanidou, Performance of lime-based mortars at elevated temperatures, Constr. Build. Mat. 189 (2018) 576–584. https://doi.org/10.1016/j.conbuildmat.2018.09.027

[48] P. Bamonte, P.G. Gambarova, F. Sciarretta, Thermo-mechanical properties and stress-strain curves of ordinary cementitious mortars at elevated temperatures, Constr. Build. Mat. 267 (2021), 121027. https://doi.org/10.1016/j.conbuildmat.2020.121027

[49] M.S. Cülfik , T. Őzturan, Effect of elevated temperatures on the residual mechanical properties of high-performance mortar, Cem. Concr. Res. 32 (2002) 809–816.

[50] O. Karahan, Residual compressive strength of fire-damaged mortar after post-fire-air-curing, Fire Mater. 35 (2011) 561–567. https://doi.org/10.1002/fam.1074

[51] S. Russo, F. Sciarretta, Masonry exposed to high temperatures: Mechanical behaviour and properties - An overview, Fire Saf. J. 55 (2013) 69–86. https://doi.org/10.1016/j.firesaf.2012.10.001

[52] A. Daware, M.Z. Naser, Fire performance of masonry under various testing methods, Construction and Building Materials 289 (2021) 123183. https://doi.org/10.1016/j.conbuildmat.2021.123183

[53] A. Daware, M.Z. Naser, G. Karaki, Generalized temperature-dependent material models for compressive strength of masonry using fire tests, statistical methods and artificial intelligence, Arch. Struct. Constr. 2 (2022) 223 - 229 https://doi.org/10.1007/s44150-021-00019-4

[54] S. Byrne, Fire resistance of load-bearing masonry walls. Fire Tech. 15(3) (1979) 180–188.

[55] S.J. Lawerence, N. Gnankrishnan, The fire resistance of masonry walls, National Building Technology Centre, Technical Record no. 531 (1988).

[56] G.M. Cooke, P.B. Morgan, Thermal Bowing in Fire and how it Affects Building Design, Building Research Establishment, Information Paper (1988)

[57] T.J. Shields, D.J. O'Connor, G.W.H. Silcock, H.A. Donegan, Thermal bowing of a model brickwork panel, Proceedings of 8th International Brick/Block Masonry Conference, Dublin, Ireland, 2 (1988) 846–856.

[58] D. Laverty, A. Nadjai, D.J. O'Connor, Modelling of thermo-structural response of concrete masonry walls subjected to fire, J. App. Sc. 10 (1) (2001) 3–19.

[59] F. Al Nahhas, R. Ami Saada, G. Bonnet, P. Delmotte, Resistance to fire of walls constituted by hollow blocks: Experiments and thermal modelling. Appl. Therm. Eng. 27 (1) (2007) 258–267. https://doi.org/10.1016/j.applthermaleng.2006.04.017

[60] T.D. Nguyen, F. Meftah, Behaviour of clay hollow-brick masonry walls during fire. Part 1: Experimental analysis, Fire Saf. J. 52 (2012) 55–64. https://doi.org/10.1016/j.firesaf.2012.06.001

[61] T.D. Nguyen, F. Meftah, Behaviour of hollow clay brick masonry walls during fire. Part 2: 3D finite element modelling and spalling assessment, Fire Saf. J. 66 (2014) 35–45. https://doi.org/10.1016/j.firesaf.2013.08.017

[62] F. Rene, R. Ayala, Mechanical properties and structural behaviour of masonry at elevated temperatures, PhD Thesis, School of Mechanical, Aerospace and Civil Engineering, University of Manchester, 2010.

[63] C.F. Rezende, Y. Simoes, F. Rodovalho, G.H. Nalon, Thermo-Structural Modeling Of Clay Units Masonry Walls Under Fire Conditions, XXXVIII Iberian-Latin American Congress on Computational Methods in Engineering, Cilamce, Brazil, 2017. DOI:10.20906/CPS/CILAMCE2017-0685

[64] J. Menegon, A.G. Graeff, L.C.P. Silva Filho, Structural masonry walls exposed to high temperatures with thermal expansion control, Revista ALCONPAT, 10 (1) (2020) 97 – 113.

[65] R. Lopes, J.P.C. Rodrigues, J.M. Pereira, P.B. Lourenço, Experimental research on structural concrete masonry walls subjected to fire, IFireSS - 2nd International Fire Safety Symposium, Naples, Italy, 2017.

[66] G. Prager, G. Poleto, R. Perico de Souza, F. Bolina, Experimental analysis
      of fire resistance of mortar coatings on structural masonry walls, Revista
      de la Construcción 19 (3) (2020) 311-320.
      DOI: 10.7764/RDLC.19.3.311

[67] A. Nadjai, M. O'Garra, F.A. Ali, D. Laverty, A numerical model for the
      behaviour of masonry under elevated temperatures, Fire Mater. 27 (a)
      (2003) 163–82. DOI: 10.1002/fam.824

[68] A. Nadjai, M. O'Garra, F.A. Ali, R. Jurgen, Compartment Masonry Walls
      in Fire Situations, Fire Tech., 42 (2006) 211–231. DOI: 10.1007/s10694-
      006-7509-6

[69] M. Andreini, M. Sassu, Mechanical behaviour of full unit masonry panels
      under fire action, Fire Saf. J. 46 (2011) 440–450.
      https://doi.org/10.1016/j.firesaf.2011.07.004

[70] P. Ravi Prakash, M. Azenha, J.M. Pereira, P.B. Lourenço, Finite element
      based micro modelling of masonry walls subjected to fire exposure:
      Framework validation and structural implications, Eng. Struct. 213 (2020),
      110545.

[71] A. Nadjai, M. O'Garra, F.A. Ali, D. Laverty, Finite element modelling of
      compartment masonry walls in fire, Comput. Struct. 81 (2003) 1923–1930.
      https://doi.org/10.1016/S0045-7949(03)00212-8

[72] R.G. Oliveira, J.P.C. Rodrigues, J.M. Pereira, P.B. Lourenço, R.F.R.
      Lopes, Experimental and numerical analysis on the structural fire
      behaviour of three-cell hollowed concrete masonry walls, Engineering
      Structures 228 (2021), 111439.

[73] E. Donval, D.T. Pham, G. Hassen, P. de Buhan, D. Pallix, Determination
      of the Deformed Shape of a Masonry Wall Exposed to Fire Loading by a
      Homogenization Method, IOP Conf. Series: Mat. Sc. Eng. 1203 (2021),
      032076. DOI:10.1088/1757-899X/1203/3/032076

[74] E. Méry, Sur l' équilibre des voutes en berceau. Annales des Ponts et
      Chaussées, 19 (1840) 50-70.

[75] J. Heyman, "The stone skeleton", Int. J. Solids Struct., vol. 2, no. 2, 249-256, 1966.

[76] A.J.S. Pippard, E.R.J. Ashby, An experimental study of the voissour arch, J. Inst. Civ. Eng., 10 (1936) 383-403.

[77] A.J.S. Pippard, The approximate estimation of safe loads on masonry bridges, Civil Eng. War: Inst. Civ. Eng., 1 (1946) 365-371.

[78] A.J.S. Pippard and J.F. Baker. The analysis of Engineering Structures. 2nD Edition, Edward Arnold, 1953.

[79] S. Huerta, The Analysis of Masonry Architecture: A Historical Approach, Architectural Science Review 51 (4) (2008) 297-328 DOI: 10.3763/asre.2008.5136

[80] H. Alexakis, N. Makris, Limit equilibrium analysis of masonry arches, Arch. App. Mech. 85(2015)1363-1381. DOI 10.1007/s00419-014-0963-6

[81] F. Marmo, ArchLab: a MATLAB tool for the Thrust Line Analysis of masonry arches, Curved and Layer. Struct. 8 (2021) 26–35.

[82] P. Block, J. Ochsendorf, Thrust Network Analysis: A New Methodology For Three-Dimensional Equilibrium, Journal Of The International Association For Shell And Spatial Structures: J. IASS, 48 (3) (2007).

[83] A. Fraddosio, N. Lepore, M. D. Piccioni, Thrust Surface Method: An innovative approach for the three-dimensional lower bound Limit Analysis of masonry vaults, Eng. Struct. 202 (1) 2020, 109846. https://doi.org/10.1016/j.engstruct.2019.109846

[84] K. Bagi, When Heyman's Safe Theorem of rigid block systems fails: Non-Heymanian collapse modes of masonry structures, Int. J. Sol. Struct. 51 (14) (2014) 2696-2705.

[85] A. Tralli, C. Alessandri and G. Milani, Computational Methods for Masonry Vaults: A Review of Recent Results, Open Civ. Eng. J., 8 (2014) 272-287.

[86] C. M, G. Croci, A. Viskovic, The structural behaviour of colosseum over
      the centuries. In: More than two thousand years in the history of
      architecture (2000).

[87] G. Macchi, G. Ruggeri, M. Eusebio, M. Moncecchi, Structural assessment
      of the leaning tower of Pisa. In: IABSE reports. IABSE International
      Association for Bridge (1993) 401–401.

[88] E. Milani, G. Milani, A. Tralli, Limit analysis of masonry vaults by means
      of curved shell finite elements and homogenization, Int. J. Solids Struct.,
      45 (2008) 5258-5288.
      https://doi.org/10.1016/j.ijsolstr.2008.05.019

[89] A. Carini, F. Genna, Stability and strength of old masonry vaults under
      compressive longitudinal loads: Engineering analyses of a case study, Eng.
      Struct., 40 (2012) 218-229.
      https://doi.org/10.1016/j.engstruct.2012.02.028

[90] G. Milani, P.B. Lourenço, 3D non-linear behavior of masonry arch
      bridges, Comput. Struct., 110-111 (2012) 133-150.

[91] A.M. D'Altri, V. Sarhosis, G. Milani, J. Rots, S. Cattari, S. Lagomarsino,
      E. Sacco, A. Tralli, G. Castellazzi, S. De Miranda, Modeling Strategies for
      the Computational Analysis of Unreinforced Masonry Structures: Review
      and Classification, Arch. Comp. Met. Eng. 27 (2020) 1153–1185.
      https://doi.org/10.1007/s11831-019-09351-x

[92] G. M, C. Melbourne, Rigid-block analysis to masonry arches, Struct. Eng.
      72 (1994) 356–61.

[93] A.V. Vermeltfoort, Analysis and experiments of masonry arches. In:
      Lourenço PB, Roca P, editors, Proc. historical constructions. Guimarães,
      Portugal, 2001.

[94] A. Audenaert, P. Fanning, L. Sobczak, H. Peremans, 2-D analysis of arch
      bridges using an elasto-plastic material model, Eng. Struct. 30 (2008) 845–
      55.

[95] N. Gattesco, I. Boem, Review of experimental tests and numerical study on masonry vaults reinforced through fiber-reinforced mortar coating, Bulletin of Earthquake Engineering 17 (2019) 4027–4048. https://doi.org/10.1007/s10518-019-00619-y

[96] P. Faccio, P. Foraboschi, E. Siviero, Masonry vaults reinforced with FPR strips, L'Edilizia 7/8 (1999) 44–50. [in Italian]

[97] S. Baraccani, L. Zauli, D. Theodossopoulos, S. Silvestri, Experimental test on a fibre-reinforced scaled cross vault subjected to in-plane shear displacements at the springings, Constr. Build. Mat. 265 (2020), 120305.

[98] N. Bianchini, N. Mendes, C. Calderini, P. X. Candeias, M. Rossi, P. B. Lourenço, Seismic response of a small-scale masonry groin vault: experimental investigation by performing quasi-static and shake table tests, Bulletin of Earthquake Engineering 20 (2022) 1739–1765.

[99] P. Foraboschi, Masonry structures externally reinforced with FRP strips: tests at the collapse. In: Proc. I Convegno Nazionale ''Sperimentazioni su Materiali e Strutture'', Venice, Italia, 2006. [in Italian]

[100] A. Dell'Endice, A. Iannuzzo, M.J. De Jong, T. Van Mele, P. Block, Modelling imperfections in unreinforced masonry structures: Discrete element simulations and scale model experiments of a pavilion vault. Eng. Struct. 228 (2021), 111499.

[101] P. Foraboschi, Strengthening of Masonry Arches with Fiber-Reinforced Polymer Strips, J. Comp. Constr. (2004).

[102] P. Faccio, P. Foraboschi, Masonry cloist-vault: Collapse behavior and rehabilation with composite materials, Proc. British Masonry Society, 6th Int. Masonry Conf., G. Thompson ed., Society Stoke-on-Trent, Penkhull, UK, 9 121–131.

[103] P. Faccio, P. Foraboschi, E. Siviero, Collapse of masonry arch bridges strengthened using FRP laminates, Proc. 3rd Int. Conf. on ACMBS III, Ottawa, A. G. Razaqpur, ed., Carleton University, Ottawa, Canada, 2020, 505–512.

[104] P. Foraboschi, FRP reinforcement used to upgrade masonry arch bridges to current live loads, Proc. Advanced FRP Materials For Civil Structures. Design, Quality Control and Rehabilitation, Technology Transfer Seminar, Bologna, Italy, 2000, 109–119.

[105] P. Foraboschi, Strength assessment of masonry arch retrofitted using composite reinforcements, J. B. Masonry Soc., 15(1) (2001) 17–25.

[106] P. Foraboschi, On the seismic analysis of masonry arch bridges, Proc. ARCH'01, 3rd Int. Arch Bridges Conference, Paris, France, 2001, 607–613.

[107] P. Foraboschi, C. Blasi, Closure to 'Analytical approach to collapse mechanisms of circular masonry arch', J. Struct. Eng., 122(8) (1996) 979–980.

[108] T.C. Triantafillou, Strengthening of masonry structures using epoxy-bonded FRP laminates, J. Compos. Constr., 2 (2) (1998) 96–104.

[109] M. Daryadel, L. Cunningham, Optimisation of FRP Strengthening Systems for Masonry Arch Bridges. Masonry International, 29 (2) (2017) 61-72.

[110] U. Meier, Advanced solutions with composites in construction, Proc. Int. Conf. Porto, Portugal, 2001, 3–8.

[111] I. Cancelliere, M. Imbimbo, E. Sacco, Experimental tests and numerical modeling of reinforced masonry arches, Eng. Struct. 32 (2010) 776-792. doi:10.1016/j.engstruct.2009.12.005

[112] D.V. Oliveira, I. Basilio, P.B. Laurenco, Experimental Behavior of FRP Strengthened Masonry Arches, J. Comp. Constr., 14 (3) (2010). https://ascelibrary.org/doi/pdf/10.1061/(ASCE)CC.1943-5614.0000086

[113] S. Bati Briccoli, T. Rotunno, L. Rovero, U. Tonietti, Innovative techniques and materials for the reinforcement of historical buildings, Proc., IC-SGECT'04, Mansoura Univ., Mansoura, Egypt, 2004, 635–646.

[114] S. Briccoli Bati, L. Rovero, Consolidamento di archi in muratura con nastri di composito a fibre lunghe di carbonio, Proc., Meccanica delle Structure in Muratura Rinforzate con FRPMaterials; Modellazione,

Sperimentazione, Progetto Controllo, A. Di Tommaso, ed., Edizioni Libreria Cortina, Padova, Italy, 2000, 53–64.

[115] S. Briccoli Bati, L. Rovero, Consolidation of masonry arches with carbon-fiber reinforced plastics, Proc., 12th Int. Brick/ Block Masonry Conf., Polytechnic Univ. of Madrid, Madrid, Spain,2000, 1571–1582.

[116] S. Briccoli Bati, L. Rovero, Experimental validation of a proposed numerical model for the FRP consolidation of masonry arches, Proc., 3rd Int. Seminar on Structural Analysis of Historical Constructions, Guimarães, Portugal, 2001, 1057–1066.

[117] S., Briccoli Bati, L. Rovero, U. Tonietti, Four points bending test on masonry elements reinforced with composite materials, Proc., Composites in Construction, Cosenza, Italy, 2003, 171–176.

[118] S., Briccoli Bati, L. Rovero, U. Tonietti, Strengthening of masonry arches with composite materials." Proc., 1st Int. Conf. on Innovative Materials and Technologies for Construction and Restoration, Napoli, Italy, 2004, 386–402.

[119] N. Simoncello, P. Zampieri , J. Gonzalez-Libreros, C. Pellegrino, Experimental behaviour of damaged masonry arches strengthened with steel fiber reinforced mortar (SFRM), Composites Part B 177 (2019) 107386.

[120] P. Zampieri, N. Simoncello, J. Libreros, C. Pellegrino, Evaluation of the vertical load capacity of masonry arch bridges strengthened with FRCM or SFRM by limit analysis, Eng. Struct., 225 (2020) 111135.

[121] L. Garmendia, P. Larrinaga, R. San-Mateos, J.T. San-José, Strengthening masonry vaults with organic and inorganic composites: An experimental approach, Mat. Des. 85 (2015) 102–114.

[122] V. Alecci, F. Focacci, L. Rovero, G. Stipo, M. De Stefano, Extrados strengthening of brick masonry arches with PBO–FRCM composites: Experimental and analytical investigations, Comp. Struct. 149 (2016) 184–196.

[123] V. Alecci, F. Focacci, L. Rovero, G. Stipo, M. De Stefano, Intrados strengthening of brick masonry arches with different FRCM composites: Experimental and analytical investigations, Comp. Struct. 176 (2017) 898–909.

[124] A.M. D'Altri, S. De Miranda, G. Castellazzi, V. Sarhosis, J. Hudson, D. Theodossopoulos, Historic Barrel Vaults Undergoing Differential Settlements, Int. J. Arch. Her. 14 (8) (2020)1196-1209.

[125] V. Cardinali, B. Pintucchi, M. Tanganelli, F. Trovatelli, Settlement of masonry barrel vaults: an experimental and numerical study, Procedia Structural Integrity 44 (2023) 1252-1259.

[126] N. Grillanda, G. Milani, L. Cantini, S. Della Torre, Settlement analysis of the masonry umbrella vault of the Masegra Castle, Imeko TC-4 International Conference on Metrology for Archaeology and Cultural Heritage Trento, Italy, 2020.

[127] F. Masi, I. Stefanou, V. Maffi-Berthier, Scaling Laws for Rigid-Body Response of Masonry Structures under Blast Loads, J. Eng. Mech. 147 (10) (2021), 04021078. DOI: 10.1061/(ASCE)EM.1943-7889.0001986.

[128] F. Masi, I. Stefanou, V. Maffi-Berthier, P. Vannucci, P., A Discrete Element Method based-approach for arched masonry structures under blast loads, Eng. Struct. 216 (2020) 110721. https://doi.org/10.1016/j.engstruct.2020.110721

[129] B.M. Abou-Zeid, W.W. El-Dakhakhni, A. Razaqpur, S. Foo, Response of Arching Unreinforced Concrete Masonry Walls to Blast Loading, J. Struct. Eng. 137(10) (2011) 1205-1214.   DOI: 10.1061/(ASCE)ST.1943-541X.0000344

[130] C. Melbourne, J. Wang, A. Tomor, G. Holm, M. Smith, Bengtsson PE, et al. Masonry arch bridges background document D4.7. Deliverable D4.7, 2007.

[131] M. Thomas, S. Frankie, A. Bora Gencturk, S. Amr, F. Elnashai, ASCE, Simulation-Based Fragility Relationships for Unreinforced Masonry Buildings, J. Struct. Eng. 139 (3) (2013).

[132] Y. Praticò, J. Ochsendorf, S. Holzer, R.J. Flatt, Post-fire restoration of historic buildings and implications for Notre-Dame de Paris, Nat. Mat. 19 (2020) 810–820. www.nature.com/naturematerials

[133] A. Manuello Bertetto, P. D'Angella, M. Fronterre, Residual strength evaluation of Notre Dame surviving masonry after the fire, Eng. Fail. An. 122 (2021) 105183.

[134] A.P. Fantilli, N.S. Burello, Masonry arches and vaults under fire, J. Build. Eng., 56 (2022) 104740.

[135] A.P. Fantilli, N.S. Burello, Experimental and numerical analyses of curvilinear masonry structures exposed to high temperatures, Int. J. Mas. Res. Inn. 1(1) (2023). DOI: 10.1504/IJMRI.2023.10055405

[136] Vigili del Fuoco, Experimental fire test on a barrel vault, technical report, 2015. http://www.vigilfuoco.it/aspx/download_file.aspx?id=19616 (in Italian)

[137] ISO 834-1:1999, Fire-resistance tests - Elements of building construction — Part 1: General requirements. International Organization for Standardization.

[138] EN 1015-10:1999, Methods of test for mortar for masonry - Part 10: Determination of dry bulk density of hardened mortar, European Committee for Standardization: Brussels, Belgium, 1999.

[139] J. Brulin, E. Blond, E. de Bilbao, A. Rekik, M. Landreau, A. Gasser, Y. Colleville, Methodology for brick/mortar interface strength characterization at high temperature, Constr. Build. Mat. 265 (2020), 120565.

[140] W.J. Harvey, The application of the mechanism method to masonry arch bridges, Struct. Engr. 66 (5) (1988) 77-84.

[141] W.J. Harvey, Stability, strength, elasticity and thrust lines in masonry structures, Struct. Eng. 69 (2001) 181-184.

[142] A. Caporale, R. Luciano, Limit analysis of masonry arches with finite compressive strength and externally bonded reinforcement, Comp. Part B: Eng. 43(8) (2012) 3131-3145.

[143] M. Gilbert, Limit analysis applied to masonry arch bridges: state-of-the-art and recent developments, 5th International arch bridges conference, Funchal, Madeira, Portugal 2007. hms.civil.uminho.pt

[144] A. Brencich, L. Gambarotta, E. Sterpi, Load carrying capacity of masonry arches with stochastic compressive strength, Proc. 10th NAMC, St Louis, U.S.A, Paper 159, 2007.

[145] N. Taylor, P. Mallinder, The brittle hinge in masonry arch mechanisms, Struct. Eng., 71 (20) (1993) 359-366.

[146] O.C. Zienkiewicz, R.L. Taylor, The Finite Element Method for Solid and Structure. Mechanics, sixth ed, Elsevier, Amsterdam, 2005.

[147] DCPREV (2013) Lettera circolare, prot. 0004638, 05/04/2013, Rome. (in Italian)

[148] P. Böckh, Heat Transfer: Basics and Practice, Springer; 2012.

[149] J.L. Randall, Finite Difference Methods for Ordinary and Partial Differential Equations', Society for Industrial and Applied Mathematics, Philadelphia, US, 2007. https://doi.org/10.1137/1.9780898717839

[150] G. Colonnetti, Elastic equilibrium in the presence of permanent set, Quarterly of Applied Mathematics, Vol. VII, No. 4, January, 1950.

[151] J. T. Oden, E.A. Ripperger, Mechanics of Elastic Structures, McGraw-Hill, 2th, New York, 1981.

[152] P. Di Re, D. Addessi, E. Sacco, A multiscale force-based curved beam element for masonry arches, Comp. Struct 208 (2018) 17-31.

[153] P.K. Singh, Matrix Structural Analysis, Dorrance Publishing, Pittsburgh, 2020, ISBN 978-1-6461-0988-3.

[154] DM 3 agosto 2015, Codice di prevenzione incendi, Allegato 1, Ministero dell'Interno Dipartimento dei Vigili del fuoco, del Soccorso pubblico e

della Difesa civile Direzione centrale per la Prevenzione e la Sicurezza tecnica, Rome. (in Italian)

[155] Decreto 17 gennaio 2018 Aggiornamento delle Norme tecniche per le costruzioni. Ministero delle infrastrutture e dei trasporti, Roma. (in Italian)

[156] EN 1990-1-1:2002: Eurocode – Basis of structural design, European Committee for Standardization: Brussels, Belgium, 2002.

[157] P. Block, M. DeJong, J. Ochsendorf, As Hangs the Flexible Line: Equilibrium of Masonry Arches, Nex. Net. J. 8(2) (2006) 13–24.

[158] P. Block, Thrust Network Analysis: exploring three-dimensional equilibrium, Ph.D thesis, Massachusetts Institute of Technology, 2009.

[159] D. Nikolić, V. Stojaković, R. Štulić, Parametric Design of Masonry Vaults Based on Structural Affinity, Nex. Net. J. 21 (2019 109–128. https://doi.org/10.1007/s00004-018-0418-4

[160] EN 1992 1-2:2004. Eurocode 2: Design of concrete structures - Part 1-2: General rules - Structural fire design, European Committee for Standardization: Brussels, Belgium, 2002.

[161] M. Indirli, L.A.S. Kouris, R.P. Borg F.M. Mazzolani, Seismic Damage Assessment of Unreinforced Masonry Structures After The Abruzzo 2009 Earthquake: The Case Study of the Historical Centers of L'Aquila and Castelvecchio Subequo, Int. J. Arch. Her., 7 (2013) 536–578. DOI: 10.1080/15583058.2011.654050

[162] CIRCOLARE 21 gennaio 2019, n. 7 C.S.LL.PP., Istruzioni per l'applicazione dell'«Aggiornamento delle "Norme tecniche per le costruzioni"» di cui al decreto ministeriale 17 gennaio 2018., Ministero Delle Infrastrutture E Dei Trasporti, Roma. (in Italian)